AN ABSTRACT OF THE DISSERTATION OF

Todd A. Schroeder for the degree of
Doctor of Philosophy in Forest Science
presented
on December 6, 2006.
Title: Understanding Changes in Forest Cover and Carbon Storage in Early Successional Forests of the Pacific Northwest Using USDA Forest Service FIA and Multi-temporal Landsat Data.

Abstract approved:

Warren B. Cohen

To effectively study dynamic processes like forest succession over long time periods one must effectively integrate data collected at many different times, locations and spatial scales. The purpose of this research is to integrate forest inventory data collected by the USDA Forest Service's Forest Inventory and Analysis (FIA) Program with multi-temporal satellite data to better understand early successional forest regrowth patterns and carbon storage in western Oregon forests. To detect and characterize continuous changes in early forest succession however, optical satellite images must first be transformed to a common radiometric scale to minimize sun, sensor, view-angle and atmospheric differences among images. We present a comparison of five atmospheric correction methods

used to calibrate a nearly continuous, 20-year Landsat TM/ETM+ image data set (19-images) over western Oregon (path 46 row 29). We found that an automated ordination algorithm called multivariate alteration detection (MAD) (Canty et al., 2004), which statistically locates invariant pixels between a subject and a reference image yielded the most consistent common scale among images. Using the cross-normalized image-series we modeled percent tree cover measurements derived by ground survey and airphoto interpretation to the greater landscape. Developing a series of forest regrowth classes we identified a wide range of successional regrowth pathways 18 years after clearcut harvesting. We observed the propensity for faster regrowth on north facing aspects, shallow slopes and at low elevations. Finally, we utilized two sets of forest inventory data to evaluate a Landsat based curve-fitting model for predicting live forest carbon. At the pixel level, the model tended to over-predict carbon and performed better (i.e., higher correlation, lower RMSE) in the Coast Range ecoregion, likely the result of faster, less variable growth patterns. At the landscape scale, we found that the flux of forest carbon predicted by the curve-fit model was in absolute terms, well within the standard error of the inventory estimates. In the process of evaluating the curve-fit model, we discovered a new method for detecting subtle (i.e., forest to non-forest) land-use shifts with Landsat data. Identifying these types of land-use shifts is critically important to developing a more accurate comprehensive carbon budget from forests. We were also able to identify several potential improvements to estimating live forest carbon with the curve-fitting approach.

Understanding Changes in Forest Cover and Carbon Storage in Early Successional Forests of the Pacific Northwest Using USDA Forest Service FIA and Multi-temporal Landsat Data

by
Todd A. Schroeder

A DISSERTATION

submitted to

Oregon State University

in partial fulfillment of
the requirements for the
degree of

Doctor of Philosophy

Presented December 6, 2006
Commencement June 2007

Doctor of Philosophy dissertation of Todd A. Schroeder
Presented on December 6, 2006.

APPROVED:

Major Professor, representing Forest Science

Head of the Department of Forest Science

Dean of the Graduate School

I understand that my dissertation will become part of the permanent collection of Oregon State University libraries. My signature below authorizes release of my dissertation to any reader upon request.

Todd A. Schroeder, Author

ACKNOWLEDGEMENTS

The author express sincere thanks to the Pacific Northwest Forest Inventory and Analysis program for data access and financial support for this research. In addition, the author wishes to thank Joseph Hill, Winston Rodney, and Harrison Stafford for providing motivational inspiration and spiritual consciousness. Many thanks to my one and only, Kirsten who was there to support me every step of the way. I would like to dedicate this work to my Grandmother Mrs. Mildred Weber.

CONTRIBUTION OF AUTHORS

Dr. Conghe Song assisted with radiometric calibration of satellite data and Dr. Morton J. Canty provided expertise and computer code for multivariate alteration detection used in Chapter 2. Dr. Zhiqiang Yang contributed airphoto interpretation data and helpful suggestions with the forest regrowth modeling in Chapter 3. Dr. Andrew Gray provided a wealth of knowledge and information on calculating biomass with FIA data and Dr. David O. Wallin presented helpful suggestions adding to the improvement of Chapter 4. Dr. Warren B. Cohen provided suggestions, mentoring and input ultimately leading to the successful completion of the entire body of work presented in this dissertation.

TABLE OF CONTENTS

TABLE OF CONTENTS (Continued)

LIST OF FIGURES

LIST OF FIGURES (Continued)

LIST OF FIGURES (Continued)

LIST OF TABLES

Understanding Changes in Forest Cover and Carbon Storage in Early Successional Forests of the Pacific Northwest Using USDA Forest Service FIA and Multi-temporal Landsat Data

Chapter 1 Introduction

The forested landscape of western Oregon is comprised of highly complex matrix of early successional, late seral, and old-growth forest conditions. Each forest condition type has the potential to impact ecological processes, such as nutrient and water cycling, carbon storage potential, wildlife habitat, and trophic interactions. Although knowing a forest stands current state of succession is useful, a clearer understanding of the impact forest change has on the aforementioned ecological processes can be achieved with a more dynamic characterization of the successional process.

Studying forest succession with the growing legacy of temporal data available from satellite sensors like Landsat (1972–present) offers a unique opportunity to analyze continuous forest successional changes over a thirty-two year period (Cohen and Goward, 2004). A key component to using satellite imagery to estimate forest change is successful integration with ground inventory data. In the United States, the USDA Forest Service's Forest Inventory and Analysis (FIA) Program has been using a three-phase, double sample design to collect field measurements of forest attributes for more than 50 years (Frayer and Furnival, 1999). The purpose of this research is to integrate forest inventory and multi-temporal satellite data to better understand early successional forest regrowth patterns and carbon storage in western Oregon forests.

To detect and characterize continuous changes in early forest succession however, optical satellite images must first be transformed to a common radiometric scale which minimize sun, sensor, view-angle and atmospheric differences among images. In Chapter 2 we present a comparison of five atmospheric correction methods (2 relative, 3 absolute) used to calibrate a nearly continuous 20 year Landsat TM/ETM+ image data set (19 images) covering western Oregon (path 46 row 29) to like surface reflectance values (Schroeder et al., 2006). The findings of this work are important for two reasons. Thorough radiometric cross-normalization allows for: 1.) accurate characterization of continuous forest change with satellite imagery and 2.) robust integration with ground measured forest inventory data.

Previous studies have established that forest regrowth after disturbance in western Oregon is highly variable both in terms of revegetation rate (Nesje, 1996; Tappeiner et al., 1997; and Yang et al., 2005) and delay (i.e., time to reach 5% canopy cover). While these studies provide convincing evidence that successional variability in western Oregon is real, their use of ground survey (Tappeiner et al., 1997) and airphoto interpretation (Yang et al., 2005) has limited the number of forest stands available to statistically analyze potential causes of the phenomena. In Chapter 3 we overcome these limitations by scaling percent tree cover measurements derived by ground survey and airphoto interpretation to the greater landscape using 19 cross-normalized Landsat images (1984–2004). Developing a series of forest regrowth trajectory classes (little to no regrowth, slow regrowth,

moderate regrowth and fast regrowth) we observed a wide range of successional regrowth pathways 18 years after clearcut harvesting. Using classification and regression tree (CART) statistical modeling we attempted to predict the developed forest regrowth classes with a suite of climatic and topographic variables.

In Chapter 3 we developed a better understanding of where and why successional variability is occurring on the landscape in western Oregon, thus the final stage of this research was to ascertain a greater understanding of the uncertainty surrounding spatial predictions of aboveground carbon storage made with optical satellite imagery. In Chapter 4 we utilize two sets of FIA forest inventory data to evaluate a Landsat based curve-fitting approach to estimating live forest carbon. We conducted a quantitative assessment of model performance and found that although the curve-fit model had a tendency to over-predict carbon, the flux (or change between inventory periods) estimates were well within the standard error of the inventory estimates. In the process of evaluating the curve-fit model, we discovered a new method for detecting subtle (i.e., forest to non-forest) land-use shifts which are common along the foothills of the Willamette Valley. Identifying these types of land-use shifts is critically important to developing a more accurate comprehensive carbon budget from forests. We were also able to identify several potential improvements to estimating live forest carbon with the curve-fitting approach.

Chapter 2 – Radiometric Calibration of Landsat Data for Characterization of Early Successional Forest Patterns in Western Oregon

Todd A. Schroeder[§], Warren B. Cohen[†], Conghe Song[¥], Morton J. Canty[‡], and Yang Zhiqiang[§]

[§] Department of Forest Science, Forestry Sciences Laboratory, Oregon State University, Corvallis, OR 97331

[†] Forestry Sciences Laboratory, Pacific Northwest Research Station, USDA Forest Service, 3200 SW Jefferson Way, Corvallis, OR 97331

[¥] Department of Geography, University of North Carolina, Chapel Hill, NC, 27599

[‡]Systems Analysis and Technology Evaluation, Jülich Research Center, D-52425 Jülich, Germany

Remote Sensing of Environment
Elsevier - Customer Service Department
6277 Sea Harbor Drive
Orlando, FL 32887-4800 USA
Volume 103, Issue 1

ABSTRACT

Detecting and characterizing continuous changes in early forest succession using multi-temporal satellite imagery requires atmospheric correction procedures that are both operationally reliable, and that result in comparable units (e.g., surface reflectance). This paper presents a comparison of five atmospheric correction methods (2 relative, 3 absolute) used to calibrate a nearly continuous 20 year Landsat TM/ETM+ image data set (19 images) covering western Oregon (path/row 46/29) to like surface reflectance values. In theory, absolute correction of individual images in a time series should effectively minimize atmospheric effects resulting in a series of images that appears more similar in spectral response than the same set of uncorrected images. Contradicting this theory, evidence is presented that demonstrates how linear atmospheric correction algorithms such as Second Simulation of the Satellite Signal in the Solar Spectrum (6S), Modified Dense Dark Vegetation (MDDV), and Dark Object Subtraction (DOS) actually make images in a time series somewhat less spectrally similar to one another. Since the development of meaningful spectral reflectance trajectories is more dependant on consistent measurement of surface reflectance rather than on accurate estimation of true surface reflectance, relative normalization is also tested. The relative methods are variants of an approach referred to as absolute-normalization, which matches images in a time series to an atmospherically corrected reference image using pseudo-invariant features and reduced major axis (RMA) regression. An advantage of absolute-normalization is that all images in the time series are

converted to units of estimated surface reflectance while simultaneously being corrected for atmospheric effects. Of the two relative methods used for absolute-normalization, the first employed an automated ordination algorithm called multivariate alteration detection (MAD) to statistically locate invariant pixels between each subject and reference image, while the second used analyst selected pseudo-invariant features (PIF) common to the entire image set. Overall, relative normalization employed in the absolute-normalization context produced the most consistent temporal reflectance response, with the automated MAD algorithm performing equally as well as the handpicked PIFs. Although both relative methods performed nearly equally in terms of observed error, several reasons emerged for preferring the MAD algorithm. The paper concludes by demonstrating how time series normalization improves (i.e., reduces scatter in) spectral reflectance trajectory models used for characterizing patterns in early forest succession.

1. INTRODUCTION

Landsat has been providing a nearly continuous record of global land surface change since 1972. This record represents one of the most consistent available archives of recent earth history information, and its use has facilitated understanding of earth surface processes across spatial and temporal scales and disciplines (Cohen and Goward, 2004).

In forestry, Landsat imagery has been important in characterizing and mapping frequency and extent of forest fire (Miller and Yool, 2002; and van Wagtendonk et al., 2004), stand replacing disturbance (Cohen et al., 1998; Cohen et al., 2002; and Sader et al., 2003), partial harvest (Franklin et al., 2000; Nilson et al., 2001, and Healey et al., 2006), successional stage (Hall et al., 1991; and Mausel et al., 1993) and vegetation regrowth (Foody et al., 1996; Viedma et al., 1997; and Sabol et al., 2002). Studies focusing on the highly dynamic process of forest succession have generally relied on forest age class information extracted from single image dates to make inferences about successional stage attributes (Fiorella and Ripple, 1993; Peterson and Nilson, 1993; and Jakubauskas, 1996). The difficulty with this approach is that the relationship between forest age and spectral data can be highly variable, especially for young (< 20 year) stands with low canopy cover (Horler and Ahern, 1986). The reasons for this variability are many, but can include differences in site quality and location, site preparation, planting practices (density and spacing), and species composition. Perhaps even more important is that forest age is not directly remotely sensible in any given date of

imagery, as are forest structure and composition, both of which are physically related to forest succession (Cohen et al., 1995).

An alternative use of Landsat for characterizing forest succession is examination of a multi-temporal image series. For any forest stand that has been disturbed since 1972 one could theoretically observe the recovery trajectory, and therefore know both its age and how its structural and compositional attributes have changed. However, as described by Song and Woodcock (2003), factors such as phenology, topography, and illumination and viewing geometry can contribute to variability in multi-temporal spectral responses that may have little to do with forest succession. In any multi-temporal analysis where the spectral signal is not sufficiently strong to minimize the effects of these complicating factors, radiometric calibration is essential to differentiate real change from noise. With adequate calibration it may be possible to examine temporal trajectories of Landsat data for a more dynamic characterization of forest succession.

The objective of this paper is to compare the effectiveness of absolute and relative radiometric calibration procedures with the ultimate goal of producing normalized temporal reflectance trajectories of forests that are recovering from stand replacing disturbance. In the strict sense, full absolute calibration involves both atmospheric correction and application of coefficients for sensor and related parameters to derive estimates of surface reflectance. In this study, however, we are also interested in examining results of the intermediate step in which calibration parameters are applied, but atmospheric effects are not removed; i.e., at-satellite

reflectance. For clarity, we refer to this as partial correction. Relative calibration (commonly referred to as normalization) involves image-to-image radiometric matching, where any number of techniques can be employed to select pseudo-invariant features (PIFs) (Schott et al, 1988), which are subsequently used to empirically calibrate images in a time series. Depending on the application, relative normalization need not include corrections for atmospheric and sensor related parameters and thus derivation of physical units such as reflectance. However, when physical surface units are desirable, it is essential that at least one image receive full absolute calibration, and then other images can be relatively normalized to it. This combined calibration-normalization approach may have certain advantages over use of absolute procedures alone.

The main questions addressed in this paper include: 1) How do absolute and combined absolute-relative calibrations compare when used to produce Landsat temporal reflectance trajectories for coniferous forest stands recovering from disturbance in western Oregon? We compare partial with several full calibration methods and (as suggested in Question 2) two relative methods. 2) Are automated relative calibration procedures based on statistical ordination as effective as those based on analyst selected PIFs? The process of selecting PIFs, if done by the analyst, can be time consuming, particularly if more than two image dates are examined. Thus, an automated procedure could have great merit. The ordination procedure we use is called multivariate alteration detection (MAD). 3) How does temporal calibration/normalization affect the spectral manifestation of forest

succession? As the ultimate purpose of a larger study is to characterize temporal spectral trajectories in relation to forest succession, it is important to determine how the different calibration methods compare in those terms.

2. METHODS

2.1. Data and Study Area

The remote sensing dataset used in this study consists of 16 Landsat 5 TM and 3 Landsat 7 ETM+ images (WRS-2 path 46 row 29) from western Oregon ranging between 1984 and 2004 (Table 2-1). All images were resampled to a 30 m resolution and co-registered using an automated tie-point program (Kennedy and Cohen, 2003) to the 1987 image, which had been orthorectified by the United States Geological Survey. All images were co-registered to the UTM coordinate system (zone 10) with a root mean square error of less than 0.5 pixels per image.

The study area encompasses nearly the full elevation (Figure 2-1) and climatic gradients present in western Oregon. The area also includes a diverse distribution of existing land ownership categories (Cohen et al., 2002), and therefore represents the disturbance and recovery patterns present in the region.

2.2. Calibration and Normalization

In this study we compared the effect of absolute calibration (both full and partial, as described earlier) and combined calibration-normalization on temporal reflectance trajectories of recovering conifer forests. Calibration was a multi-step

process. For the final step, atmospheric correction, several different methods were used and compared.

2.2.1. Calibration

Calibration was a several step process that involved the use of standard equations to convert 8-bit satellite-quantized calibrated digital numbers (DN) to at-satellite reflectance. Landsat 5 images were first converted to at-satellite radiance using Eq. (1),

$$L_{sat} = (DN * G) + B \quad (1)$$

where L_{sat} is band specific at-satellite radiance (W m^{-2} sr^{-1} μm^{-1}), DN is satellite quantized calibrated digital number, B is band specific bias in DN, and G is band-specific gain (m^2 sr μm W^{-1}). The impact of sensor degradation on the gain parameter was accounted for using data published by Thome et al. (1997) and Teillet et al. (2001), while revised gain parameters published by Chander and Markham (2003) were used for images acquired and processed after May 5, 2003. The biases reported by Markham and Barker (1986) were used for all images.

Landsat 7 images were converted to at-satellite radiance using Eq. (2),

$$L_{sat} = ((LMAX_{sat} - LMIN_{sat})/(DNMAX - DNMIN)) * (DN - DNMIN) + LMIN_{sat} \quad (2)$$

where $LMAX_{sat}$ is band-specific spectral radiance scaled to $DNMAX$ (W m^{-2} sr^{-1} μm^{-1}), $LMIN_{sat}$ is band-specific spectral radiance scaled to $DNMIN$ (W m^{-2} sr^{-1} μm^{-1}), $DNMAX$ is maximum quantized calibrated digital number (255), and $DNMIN$ is minimum-quantized calibrated digital number (0 for LPGS data, 1 for NLAPS data). Equation (2) accounts for gain state (i.e. high/low setting) and published LMIN/LMAX values (Landsat 7 Science Data Users Handbook).

After conversion to at-satellite radiance, each image was converted to at-satellite reflectance (assuming a uniform Lambertian surface under cloudless conditions) using Eq. (3),

$$\rho = \frac{\pi(L_{sat} - L_p)}{T_v(E_0 \cos(\Theta) T_z + E_{down})} \quad (3)$$

where ρ is estimated surface reflectance, L_p is path radiance (W m^{-2} sr^{-1} μm^{-1}), T_v is atmospheric transmittance from the target toward the sensor, E_0 is the exoatmospheric solar constant (W m^{-2} μm^{-1}), T_z is atmospheric transmittance in the illumination direction, Θ is solar zenith angle, and E_{down} is downwelling diffuse irradiance (W m^{-2} μm^{-1}). By definition, at-satellite reflectance does not remove atmospheric effects, thus T_z and T_v equal 1.0, and E_{down} and L_p equal zero.

2.2.2. Atmospheric Correction

In the previous steps, all imagery was partially calibrated. For full calibration, at-satellite reflectance was converted to surface reflectance using three different methods for deriving values of T_z, T_v, E_{down} and L_p in Eq. 3. These methods included dark object subtraction (DOS), modified dense dark vegetation (MDDV), and second simulation of the satellite signal in the solar spectrum (6S). These methods range in complexity from a simple image-based correction procedure (DOS) to a detailed, theoretical model based on radiative transfer code (6S).

2.2.2.1. Dark Object Subtraction (DOS)

The DOS method assumes that within a satellite image there exist features that have near-zero percent reflectance (i.e., water, dense forest, shadow), such that the signal recorded by the sensor from those features is solely a result of atmospheric scattering (path radiance), which must be removed (Chavez Jr., 1996). Path radiance, L_p, was estimated using Eq. 4,

$$L_p = G * DN_{dark} + B - 0.01\left[E_0 \cos(\Theta) T_z + E_{down}\right] T_v / \pi \qquad (4)$$

where DN_{dark} is the darkest DN value in each spectral band with at least one thousand pixels (Teillet and Fedosejevs, 1995). The DOS method calculated here is referred to in Song et al. (2001) as DOS3, which estimates T_v as $e^{-\tau_r / \cos(\Theta_v)}$ and T_z as $e^{-\tau_r / \cos(\Theta_z)}$ assuming a Rayleigh atmosphere with no aerosols and one percent

surface reflectance for the dark object. Optical thickness for Rayleigh scattering (τ_r) (Kaufman, 1989) was estimated by,

$$\tau_r = 0.008569\lambda^{-4}(1 + 0.0113\lambda^{-2} + 0.00013\lambda^{-4}) \quad (5)$$

where λ is wavelength in μm. E_{down} for a Rayleigh atmosphere was estimated as zero aerosol optical depth at 550 nm using the 6S radiative transfer code (Vermote et al., 1997). DOS3 was selected for use in this study in lieu of other DOS methods based on its ability to create a consistent common scale as evaluated by change detection and classification accuracy for part of the Landsat scene under investigation (Song et al., 2001).

2.2.2.2. Modified Dense Dark Vegetation (MDDV)

This approach is based on the dense dark vegetation (DDV) method (Liang et al, 1997), which assumes that areas of dense, dark vegetation are present in the satellite image in which to use as dark objects for Landsat bands 1 (blue) and 3 (red). Since longer spectral wavelengths are less affected by atmospheric scattering, Landsat band 7 at-satellite reflectance is assumed equal to its surface reflectance. As in Liang et al. (1997), dark areas were spatially defined for each image where band 7 reflectance was ≤ 0.05 and NDVI was > 0.1. The identified dark areas were used to estimate band 1 and band 3 surface reflectance based on the following relationships with band 7 surface reflectance (Kaufman et al., 1997),

$$\rho_1 = \rho_7 / 4 \qquad \rho_3 = \rho_7 / 2 \tag{6}$$

where the subscripts of ρ are Landsat band numbers. L_p for each image was estimated as the difference between the at-satellite reflectance in bands 1 and 3 and the estimated surface reflectance from Eq. (6). This approach was first used with a "smart moving window" (Liang et al., 1997) to atmospherically correct individual pixels, and was subsequently modified by Song et al. (2001) to a "fixed" window approach for band-wise correction as applied here. The presented MDDV approach derives an appropriate aerosol optical depth by iteratively running 6S radiative transfer code until the output surface reflectance matches the predicted surface reflectance from Eq. (6). Matching aerosol optical depths were then used in 6S to atmospherically correct the subsequent bands of each image.

2.2.2.3. Second Simulation of the Satellite Signal in the Solar Spectrum (6S)

The 6S general radiative transfer code (Vermote et al., 1997) was used to estimate surface reflectance using aerosol optical depth (AOD) data collected at the AERONET site located at the HJ Andrews Experimental Forest in Blue River, Oregon (Figure 2-2). Estimates of aerosol optical depth were acquired at 500 and 670 nm for the day and time closest to satellite overpass for the 1994 through 2004 images (except 2002, no data). To estimate the aerosol optical depth at 550 nm required as input to 6S the relationship $\tau_\lambda = a\lambda^b$ was used, where τ_λ is aerosol

optical depth at wavelength λ (nanometers), and a and b are empirical parameters (Liang et al., 1997). The estimated aerosol optical depth at 550 nm (Table 2-2) was used along with the 6S midlatitude summer atmosphere and continental aerosol model to derive surface reflectance for each image. As optical depth data were only available for 1994 – 2001 and 2003 – 2004, only images from these years could be calibrated with 6S.

2.2.3. Relative Normalization

For relative normalization, one fully calibrated image (1994) was chosen as the reference to which all others were adjusted, using two separate approaches: analyst selection of PIFs and statistical ordination (MAD). This image was selected because of its high radiometric quality and its central location in the time series. Because we used a fully calibrated reference image (6S version) for these procedures, we refer to them as two variants of a calibration-normalization approach.

2.2.3.1. Pseudo-invariant Feature (PIF)

Using the criteria for selecting normalization targets suggested by Eckhardt et al. (1990), the image time series was thoroughly inspected to derive a total of 63 PIFs (the same 33 dark and 30 bright features in each image) for relative normalization. The bright (dune, urban, rock) and dark (water, forest, lava) features were hand-selected to be evenly distributed around the image (Figure 2-2),

and to encompass the full range of spectral brightness values (bright, medium, dark) found. Normalization was accomplished on a band-by-band basis using these "training" PIFs with reduced major axis (RMA) regression (Cohen et al., 2003; Canty et al., 2004). An independent set of PIFs (n = 26) to be used for testing the results of calibration and normalization were also selected (Figure 2-2).

2.2.3.2. Multivariate Alteration Detection (MAD)

Selecting PIFs by hand, as previously described, is a time-consuming task, particularly when the time series consists of several images. An attractive and less subjective alternative for selecting PIFs is to use statistical methods to locate them automatically. One such method, multivariate alteration detection (MAD) (Nielsen et al., 1998; Canty et al., 2004) uses traditional canonical correlation analysis (CCA) (Hotelling, 1936) to find linear combinations between two groups of variables (i.e. the spectral bands of subject and reference images) ordered by correlation, or similarity between pairs. Differences between such ordered pairs are called MAD variates and these are invariant to affine transformations (including linear scaling). This implies that linear atmospheric and instrumental effects will not influence the change/no-change probabilities of the pixels derived from the method. In fact, the sum of squares of the standardized MAD components (the MAD components divided by their standard deviations) is approximately chi-square distributed, enabling no-change thresholds to be set easily. The MAD transformation was used here to locate invariant pixels (chi-square threshold 0.99)

between each image in the time series and the 1994 6S corrected reference. The selected invariant pixels were subsequently used to normalize each image band-by-band to the reference scene using RMA regression.

2.3. Error Analysis

The absolute (full and partial) and relative atmospheric correction methods tested here all use linear adjustments to convert raw image DNs to units of estimated surface reflectance (or top of atmosphere reflectance in the case of partial correction). Thus, each image in the time series (except 6S, applied only to images with available in situ atmospheric data) was converted to estimated surface reflectance using the look up table (LUT) approach described by Song et al. (2001).

After applying atmospheric corrections to the image time series, a 3x3 window was placed over each test PIF (26 in number) and the mean spectral reflectance value for each band of corrected imagery (5 methods x 18 images x 6 spectral bands + 9 6S corrected images x 6 spectral bands = 594 in all) was extracted and compared to the mean PIF spectral reflectance values of the reference image. The difference between corrected PIF reflectance and the reference PIF reflectance is reported as the root mean square error (RMSE). Thus, all relatively normalized images where compared to the 6S corrected 1994 reference image, whereas the absolutely calibrated images were compared to the 1994 reference image corrected with each corresponding calibration method (e.g. DOS3 corrected images were compared to the DOS3 1994 reference). To assess robustness of

calibrating an image time-series, RMSE was calculated by image (across spectral bands), by Landsat band (across images), and overall by calibration/normalization method (across images and spectral bands). A typical RMSE for detailed absolute calibration of Landsat imagery has been previously reported at 0.02 (Moran et al., 1992), therefore 0.02 will serve here as a benchmark for establishing successful calibration/normalization.

2.4. Spectral Reflectance Trajectories

The development of meaningful spectral reflectance trajectories is not solely dependent on the accurate calculation of true surface reflectance, but more on a consistent measurement of surface reflectance among images, which has previously been referred to as "common scale" (Song et al., 2001). The consistency of common scale is based here on the difference in spectral response among the corrected images, relative to the respective reference image over the set of test PIFs. The calibration or normalization method found to have the least amount of spectral difference (lowest RMSE) among test PIFs will be used to derive the spectral reflectance trajectories of recovering conifer forests. If two methods have similarly low RMSEs, the method best lending itself to operational use will be selected for spectral trajectory development.

Forest stands undergoing stand-replacing disturbance between 1986 and 1987 were visually identified using a multi-temporal RGB color composite of spectral band 5. To evaluate the effect of image calibration/normalization on the

spectral manifestation of forest succession, twelve forest stands were hand-selected for spectral reflectance trajectory development. Of the twelve forest stands selected (Figure 2-2), six were located in the Coast Range (CR) and six in the Western Cascades (WC). Stand mean reflectance values were extracted from the normalized and partially corrected image time series and fit with quadratic polynomial curves. These quadratic polynomial curves, or spectral reflectance trajectories were developed for all six Landsat spectral bands, as well as for the tasseled cap transformation (brightness, greenness, wetness) and the normalized vegetation index (NDVI). Standard error (RMSE) and variance explained (R^2) were calculated for each quadratic polynomial model, then averaged across the twelve forest stands to determine whether the trajectory models were improved (i.e. lower RMSE) by image calibration/normalization.

3. RESULTS

3.1. Image Calibration/Normalization

3.1.1. RMSE by Image

To evaluate the consistency of common scale at the image level, RMSE was calculated for each image (across spectral bands) by calibration/normalization method (Figure 2-3). Examining RMSE for the partially calibrated images (Figure 2-3a) reveals the surprisingly consistent spectral response of the image time series even with no atmospheric corrections applied. The consistent nature of the partially corrected time series is expressed by seven of the eighteen images (1984,

1986, 1989, 1992, 1997, 2000 and 2004) having less than 0.02 RMSE, with seven others (1993, 1996, 1998, 1999, 2001, 2002, and 2003) falling just slightly above the 0.02 benchmark. Only four images (1987, 1988, 1991, and 1995) were considered appreciably different than the reference image, with RMSEs nearly equal to or greater than 0.03.

Only nine of the eighteen images in the time series were calibrated with all three absolute calibration methods (Figure 2-3b), thus reducing the number of observations to assess improvements to the common scale of the full time series. Of these nine images, DOS3 had the lowest RMSE in six of the images, compared to three for 6S. The MDDV method yielded the highest RMSE of all the absolute calibration methods in six of these nine images. In order to determine whether common scale was improved by absolute calibration, the partially corrected image time series was used as a standard for comparison. Of the nine images that were corrected by all three absolute methods, only four (1998, 1999, 2000, and 2001) had lower RMSEs than their partially corrected counterparts. Of the four images with improved common scale resulting from absolute calibration, two were corrected with DOS3 and two with 6S. Thus, the least complex DOS3 method proved to be the most effective absolute calibration method. It yielded the lowest RMSE in six of the nine images corrected with all three absolute methods, and slightly lowered RMSE from that which was observed in the partially corrected images. Even so, the common scale of the image time series was not consistently improved by any of the absolute calibration methods.

On the other hand, the image time series normalized with the two relative methods appears consistently improved in terms of common scale (Figure 2-3c). All eighteen images had at least one relative normalization method yield an RMSE of 0.02 or less. Compared to the partially corrected time series, fifteen of the images had lower RMSEs after relative normalization. Overall, it appears that the improved common scale was achieved nearly equally by both the PIF and MAD methods. Though differences in RMSE were slight between the two methods, PIF did have lower RMSEs for eleven of the eighteen images in the full time series.

3.1.2. RMSE by Landsat Band

The consistency of the image time series was also evaluated based on RMSE by Landsat band (across images) (Figure 2-4). Shorter wavelength spectral bands like Landsat bands 1 and 2 are commonly impacted by Rayleigh scattering. Although scattering is likely, bands 1 and 2 do not seem significantly impacted here as both have low (< 0.02) partially corrected RMSEs. On the other hand, band 3 has the highest partially corrected RMSE, which is likely attributed to atmospheric scattering. Longer spectral regions like Landsat bands 4, 5 and 7 are typically influenced by atmospheric absorption, which is likely contributing to the elevated (> 0.02) partially corrected RMSEs observed for these spectral bands.

If the errors detailed above are truly a result of atmospheric scattering and absorption, then it stands to reason that absolute calibration would likely account for some of these effects, serving to lower RMSE from that observed in the

partially corrected images. Quite the opposite is observed however, with all of the absolute methods yielding an increase in RMSE in four (1, 2, 4, and 5) of the six spectral bands. In fact, all of the absolute methods failed to lower RMSE to < 0.02. DOS3 and 6S yielded similar RMSEs in four (1 – 4) of the six spectral bands; two (3 and 4) of which were nearly equal to the error observed in partial correction. On the other hand, MDDV yielded the highest RMSEs of all the methods tested in five (1, 2, 3, 4, and 5) of the six spectral bands. Overall, absolute calibration did not improve the consistency of common scale from that observed in the partially corrected images.

Relative normalization on the other hand significantly improved the image time series from the spectral perspective. Both of the relative methods lowered RMSE from that observed in partial correction. In fact, after relative normalization five of six spectral bands had at least one relative method lower RMSE to < 0.02. In terms of lowering RMSE from partial correction, band 4 seemed least improved by relative normalization whereas band 3 the most. Both of the relative methods performed nearly equally in all six spectral bands.

3.1.3. RMSE by Atmospheric Correction Method

To assess overall effectiveness RMSE was calculated by each atmospheric correction method (across all images and spectral bands) (Figure 2-5). Similar to observations by image and by Landsat band, none of the absolute calibration methods reduced the RMSE below that observed in the partially corrected data.

The MDDV method produced the greatest overall error, with the DOS3 and 6S methods resulting in slight increases in the error observed in the partially corrected images. The relative methods were equally effective, reducing the error observed in the partially corrected images by nearly 25%. The PIF method produced a slightly lower overall RMSE than MAD.

3.2. Spectral Reflectance Trajectories

Although the PIF method yielded slightly less error than MAD, there was very little difference between the two methods in terms of improving the common scale of the image time series. Given the similarity of the two methods, the MAD calibration-normalization approach is preferred here for several reasons (see discussion) including its utility to operational use. As a result, spectral reflectance trajectories were developed using the MAD normalized and partially corrected image time series. The parameters (R^2 and RMSE) of the quadratic polynomial models used to form the spectral reflectance trajectories were averaged across the twelve hand-selected forest stands and are presented in Table 2-3.

The results indicate that on average, MAD spectral reflectance trajectories have less residual scatter (lower mean RMSE across stands) than trajectories created with the uncalibrated time series. Although MAD band 1 and 2 trajectories yield the lowest post-correction errors, they explain a relatively low percentage of variance as expressed by R^2. On the other hand, NDVI spectral reflectance trajectories explain a high percentage of variation found in the temporal data, yet

yield high prediction errors. Ideally, models capturing a high percentage of variation combined with low prediction error would produce the best spectral reflectance trajectories. In this regard, trajectories created with MAD normalized band 7 and the tasseled cap wetness seem promising for characterizing the dynamic process of forest succession.

4. DISCUSSION

4.1. Image Calibration/Normalization

The results indicate that the absolute calibration methods tested here were ineffective at correcting satellite images to a consistent common scale, a finding similarly reported by Song et al. (2001) for a portion of the same Landsat scene. The more complex methods (MDDV and 6S) attempt to estimate aerosol optical depth, which generally rely on various simplifying assumptions. These assumptions have been previously reported as ineffective for improving change detection and classification accuracies (Song et al., 2001) and have not served to improve the common scale of the image time series presented here. Given the relatively stable common scale observed in the partially corrected data, it is not surprising that complex theoretical adjustments reduced the spectral consistency of the image time series. While simple corrections like DOS3 generally worked the best, none of the absolute methods produced a common scale more consistent than observed in the partially corrected images.

The MDDV method was the least effective absolute calibration method, and as reported in other studies, tends to significantly over-estimate aerosol optical depth (Table 2-2). This over-estimation resulted in a disproportionate amount of dark features (water and mature forest) being converted to near zero values in bands 1 and 3, yielding over-corrected water and forest spectral signatures. Based on observations in this study it is likely that the criteria for defining dark areas (band 7 reflectance ≤ 0.05 and NDVI > 0.1) is too liberal. More stringent criteria for defining dark areas may improve the performance of this method, especially in highly vegetated scenes. Furthermore, the partially corrected data also suggests that band 7 may be impacted by atmospheric absorption, perhaps invalidating the MDDV assumption that band 7 apparent reflectance equals band 7 surface reflectance.

Although the most complex method, 6S was slightly less effective than the much simpler DOS3 method at creating a consistent common scale. The AOD data used in 6S were collected at the Western Cascade AERONET site, located at the HJ Andrews Experimental Forest. Since Landsat scene 46/29 lies adjacent to the Pacific Ocean and covers portions of two mountain ranges it is likely, given the highly variable nature of aerosol loadings, that AOD estimates recorded in the western Cascades may differ significantly from those observed elsewhere in the scene. Since accurate AOD data is often difficult to obtain, improving image-based estimates from methods like MDDV warrant further investigation. Determining the

success of 6S as an absolute correction method was further limited by the lack of AOD data for the full image time series.

Whether analyzed by image, by Landsat band, or by calibration/normalization method, relative normalization produced the most consistent common scale for the image time series. This finding is similar to Olsson (1995), who reported that relative normalization was to be preferred to absolute calibration for accurate detection of localized changes in boreal forests. Although the PIF method had a slightly lower overall RMSE, there are several reasons for preferring MAD.

First, MAD is easier and more time efficient to implement than PIF. Although hand-selecting invariant features has been successfully employed in other studies, it is a time consuming process that is often subject to analyst interpretation, and potentially limited by scene location. The MAD method however, has been automated to statistically locate invariant pixels in a small subset or clip (Figure 2-2) taken from the subject and reference images. Tests (not presented) show that the performance of normalization can vary depending on the quality and quantity of invariant pixels selected from different image clips. Selecting clips that contain large, highly stable (i.e. low variance) bright features like sand dunes and stable dark features like water and mature forest should be preferred. Although mature forest is likely to change spectrally from year to year due to phenological differences, it seems capturing this natural variability in the normalization model will facilitate separation of real forest change from noise. A simple test can be

conducted to locate several suitable image clips per Landsat scene for future implementation of MAD. In addition, the MAD program is currently being modified to integrate invariant pixels selected from multiple image clips into one normalization model.

The second advantage to using MAD is that areas of significant change (i.e. disturbance, cloud cover) occurring between the subject and reference images do not need to be accounted for prior to selecting invariant pixels. Other methods for statistically selecting invariant pixels, such as ordination by principal components analysis (PCA) have been previously suggested (Du et al., 2002). While this method has produced favorable results, it typically requires more processing time as PCA is not invariant to linear scaling of input data. Hence, significant areas of change between the subject and reference image (i.e. clouds) must be masked out prior to statistical ordination. PCA can also be significantly weighted by a single image in the time series that has high variance. Since the basis for MAD is CCA, pixels that significantly change between the subject and reference image do not need to be masked out prior to ordination, offering additional time savings when correcting multiple images.

Although atmospheric correction is not required before running MAD, it may be useful to have all the images in the time series normalized to units of surface reflectance. Thus, the third advantage to using MAD is that since it is invariant to linear scaling, all images in a time series can be corrected for atmospheric effects while simultaneously being converted to units of reflectance.

This is best achieved by using the calibration-normalization approach suggested here, where the selected reference scene is first converted to estimated surface reflectance using one of the absolute calibration methods, and then all other images are normalized to it. It is important to note that linear transformations such as sensor gain/bias adjustments and absolute calibration are not necessary prior to running MAD. The same consistency of common scale will be achieved with MAD whether or not images are first calibrated, offering additional savings in processing time depending on user needs.

4.2. Spectral Reflectance Trajectories

The objective of radiometric calibration is not primarily to improve the percentage of variance explained (R^2) by a spectral reflectance trajectory, but rather to reduce the noise associated with multi-date data, thus lowering residual scatter (RMSE). Our results indicate that for all spectral bands and indices evaluated, MAD normalized spectral reflectance trajectories had less residual scatter than trajectories created with the partially corrected images. Although normalization effectively reduced residual scatter, two factors contributed to a less than expected magnitude of improvement. First, images acquired in western Oregon during the summer months already have a high degree of spectral consistency due to seasonally dry conditions. Second, calibration/normalization error is obtained here by comparing atmospherically corrected images to images subjected to partial correction (e.g. sun and view angle effects), likely reducing the magnitude of

improvement derived from a comparison against uncorrected images (e.g. DN). We are currently using MAD to normalize images acquired in more spectrally diverse forest types (i.e. eastern deciduous) to assess the level of improvement normalization can make to those types of spectral reflectance trajectories.

Now that we have determined that calibration-normalization with MAD effectively improves the development of spectral reflectance trajectories, our focus turns to using the spectral reflectance trajectories to analyze spatial patterns of forest succession. Our observations indicate that spectral reflectance trajectories developed with MAD normalized band 7 and tasseled cap wetness seem promising for characterizing continuous attributes of forest succession. It should be noted however, that spectral reflectance trajectories are built here on single variables, while models of successional recovery after disturbance will likely include multiple variables.

5. CONCLUSION

An effective and efficient method for atmospherically correcting an image time series for characterization of forest successional patterns, referred to as calibration-normalization, was presented. This method relatively normalizes all images in a time series to an absolutely calibrated reference image. The benefits of this approach are the reliance on the more dependable relative normalization process to yield an improved temporal common scale, while subsequently converting all images in a time series to units of surface reflectance. The results

demonstrated how converting images in a time series to reflectance using absolute calibration alone tends to decrease the consistency of common scale compared to that observed in the partially corrected images.

Overall, the MDDV method was the least effective absolute method, possibly resulting from the overly lenient spatial definition of dark areas. Although the most complex method, the 6S radiative transfer code performed slightly worse than the much simpler DOS3 method, with possible shortcomings attributed to the extrapolation of point sampled AOD data to the full Landsat scene. The image based DOS3 method did the best job of all the absolute calibration methods at correcting the image time series, supporting the assertion that simpler atmospheric correction methods may be preferred when consistency of common scale is more important than accurate estimation of surface reflectance (Song et al., 2001).

The best normalization results, in terms of RMSE, were achieved nearly equally by both relative methods, with correction based on analyst selected PIFs generating only a slightly more accurate common scale than relative correction based on invariant pixels statistically selected by the MAD algorithm. Although the PIF method generated slightly lower overall errors, several reasons emerged for preferring the MAD based approach to invariant feature selection. These reasons include ease and time efficiency of implementation, invariance to linear scaling effects, and the simultaneous correction of atmospheric effects during the conversion to reflectance. While previously shown to work well in arid environments (Canty et al., 2004), the MAD algorithm has been shown here to

generate a temporally consistent, spectrally diverse range of invariant pixels for successful normalization of a highly forested Landsat time series.

To assess the impact of image normalization on the characterization of recovering conifer forests, spectral reflectance trajectories were developed for twelve hand-selected forest stands undergoing stand replacing disturbance. For all spectral bands and indices evaluated, MAD normalized spectral reflectance trajectories had less residual scatter (lower RMSE) than trajectories created with partially corrected images.

REFERENCES CITED

Canty, M.J., Nielsen, A.A., and Schmidt, M. (2004). Automatic radiometric normalization of multitemporal satellite imagery. *Remote Sensing of Environment*. 91, 3-4, 441–451.

Chander, G., and Markham, B. (2003). Revised Landsat-5 TM radiometric calibration procedures and post-calibration dynamic ranges. *IEEE Transactions on Geoscience and Remote Sensing*. 41, 11, 2674–2677.

Chavez, P.S., Jr. (1996). Image-based atmospheric correction – revisited and improved. *Photogrammetric Engineering and Remote Sensing*. 62, 9, 1025–1036.

Cohen, W.B., Spies, T.A., and Fiorella, M. (1995). Estimating the age and structure of forests in a multi-ownership landscape of western Oregon, U.S.A. *International Journal of Remote Sensing*. 16, 4, 721–746.

Cohen, W.B., M., Fiorella, J. Gray, E. Helmer, and Anderson, K. (1998). An efficient and accurate method for mapping forest clearcuts in the Pacific Northwest using Landsat imagery. *Photogrammetric Engineering and Remote Sensing*. 64, 293–300.

Cohen, W.B., Spies, T.A., Alig, R.J., Oetter, D.R., Maiersperger, T.K., and Fiorella, M. (2002). Characterizing 23 years (1972–95) of stand replacement Disturbance in western Oregon forests with Landsat imagery. *Ecosystems*. 5, 122–137.

Cohen, W.B., Maiersperger, T.K., Gower, S.T., and Turner, D.P. (2003). An improved strategy for regression of biophysical variables and Landsat ETM+ data. *Remote Sensing of Environment*. 84, 561–571.

Cohen, W.B., and Goward, S.N. (2004). Landsat's role in ecological applications of remote sensing. *Bioscience*. 54, 6, 535–545.

Du, Y., Teillet, P.M., and Cihlar, J. (2002). Radiometric normalization of multitemporal high-resolution satellite images with quality control for land cover change detection. *Remote Sensing of Environment*. 82, 123–134.

Eckhardt, D.W., Verdin, J.P., and Lyford, G.R. (1990). Automated update of an irrigated lands GIS using SPOT HRV imagery. *Photogrammetric Engineering and Remote Sensing*. 56, 11, 1515–1522.

Fiorella, M., and Ripple, W.J. (1993). Analysis of conifer forest regeneration using Landsat Thematic Mapper data. *Photogrammetric Engineering and Remote Sensing*. 59, 9, 1383–1388.

Foody, G.M., Palubinskas, G., Lucas, R.M., Curran, P.J., and Honzak, M. (1996). Identifying terrestrial carbon sinks: Classification of successional stages in regenerating tropical forest from Landsat TM data. *Remote Sensing of Environment*. 55, 205–216.

Franklin, S.E., Moskal, L.M., Lavigne, M.B., and Pugh, K. (2000). Interpretation and classification of partially harvested forest stands in the Fundy Model forest using multitemporal Landsat TM digital data. *Canadian Journal of Remote Sensing*. 26, 4, 318–333.

Hall, F.G., Botkin, D.B., Strebel, D.E., Woods, K.D., and Goetz, S.J. (1991). Large-scale patterns of forest succession as determined by remote sensing. *Ecology*. 72, 2, 628–640.

Healey, S., Zhiqiang, Y., Cohen, W.B., and Pierce, D.J. (2006). Application of two regression-based methods to estimate the effects of partial harvest on forest structure using Landsat Data. Remote Sensing of Environment. 101, 115–126.

Horler, D.N.H., and Ahern, F.J. (1986). Forestry information content of Thematic Mapper data. *International Journal of Remote Sensing*. 7, 3, 405–428.

Hotelling, H. (1936). Relations between two sets of variates. *Biometrika*. XXVIII, 321–377.

Jakubauskas, M.E. (1996). Thematic Mapper characterization of lodgepole pine seral stages in Yellowstone National Park, USA. *Remote Sensing of Environment*. 56, 118–132.

Kaufman, Y.J. (1989). The atmospheric effect on remote sensing and its correction. In *Theory and Application of Optical Remote Sensing* (G. Asrar, Ed.), New York, pp. 314ff.

Kaufman, Y.J., Wald, A., Remer, L.A., Gao, B., Li, R., and Flynn, L. (1997). The MODIS 2.1 µm channel – correlation with visible reflectance for use in remote sensing of aerosol. *IEEE Transactions on Geoscience and Remote Sensing*. 35, 1–13.

Kennedy, R.E., and Cohen, W.B. (2003). Automated designation of tie-points for image-to-image coregistration. *International Journal of Remote Sensing*. 24, 17, 3467–3490.

Liang, S., Fallah-Adl, H., Kalluri, S., JaJa, J., Kaufman, Y.J., and Townshend, J.R.G. (1997). An operational atmospheric correction algorithm for Landsat Thematic Mapper imagery over the land. *Journal of Geophysical Research*. 102, 17, 173–17,186.

Markham, B.L., and Barker, J.L. (1986). Landsat MSS and TM post-calibration dynamic ranges, exoatmospheric reflectance and at-satellite temperature. EOSAT Landsat Technical Notes. 3–8.

Mausel, P., Wu, Y., Yinghong, L., Moran, E.F., and Brondizio, E.S. (1993). Spectral identification of successional stages following deforestation in the Amazon. *Geocarto International*. 4, 61–71.

Miller, J.D. and Yool, S.R. (2002). Mapping forest post-fire canopy consumption in several overstory types using multi-temporal Landsat TM and ETM data. *Remote Sensing of Environment*. 82, 481–496.

Moran, M.S., Jackson, R.D., Slater, P.N., and Teillet, P.M. (1992). Evaluation of simplified procedures for retrieval of land surface reflectance factors from satellite sensor output. *Remote Sensing of Environment*. 41, 169–184.

Nielsen, A.A., Conradsen, K., and Simpson, J.J. (1998). Multivariate alteration detection (MAD) and MAF post-processing in multispectral, bitemporal image data: New approaches to change detection studies. *Remote Sensing of Environment*. 64, 1–19.

Nilson, T., Olsson, H., Anniste, J., Lukk, T. and Praks, J. (2001). Thinning-caused change in reflectance of ground vegetation in boreal forests. *International Journal of Remote Sensing*. 22, 14, 2763–2776.

Olsson, H. (1995). Reflectance calibration of Thematic Mapper data for forest change detection. *International Journal of Remote Sensing*. 16, 1, 81–96.

Peterson, U., and Nilson, T. (1993). Successional reflectance trajectories in northern temperate forests. *International Journal of Remote Sensing*. 14, 3, 609–613.

Sabol, D.E., Gillespie, A.R., Adams, J.B., Smith, M.O., and Tucker, C.J. (2002). Structural stage in Pacific Northwest forests estimated using simple mixing models of multispectral images. *Remote Sensing of Environment*. 80, 1–16.

Sader, S.A., Bertrand, M., and Wilson, E.H. (2003). Satellite change detection of forest harvest patterns on an industrial forest landscape. *Forest Science*. 49, 3, 341–353.

Schott, J.R., Salvaggio, C., and Volchok, W.J. (1988). Radiometric scene normalization using pseudoinvariant features. *Remote Sensing of Environment*. 26, 1–16.

Song, C. and Woodcock, C.E. (2003). Monitoring forest succession with multitemporal Landsat images: Factors of uncertainty. *IEEE Transactions on Geoscience and Remote Sensing*. 41, 11, 2557–2567.

Song, C., Woodcock, C.E., Seto, K.C., Pax-Lenney, M., and Macomber, S.A. (2001). Classification and change detection using Landsat TM data: when and how to correct atmospheric effects. *Remote Sensing of Environment*. 75, 230–244.

Teillet, P.M., and Fedosejevs, G. (1995). On the dark target approach to atmospheric correction of remotely sensed data. *Canadian Journal of Remote Sensing*. 21, 375–381.

Teillet, P.M., Barker, J.L., Markham, B.L., Irish, R.R., Fedosejevs, G., and Storey, J.C. (2001). Radiometric cross-calibration of the Landsat-7 ETM+ and Landsat-5 TM sensors based on tandem data sets. *Remote Sensing of Environment*. 78, 39–54.

Thome, K., Markham, B., Barker, J., Slater, P., and Biggar, S. (1997). Radiometric calibration of Landsat. *Photogrammetric Engineering and Remote Sensing*. 63, 853–858.

van Wagtendonk, J.W., Root, R.R., and Key, C.H. (2004). Comparison of AVIRIS and Landsat ETM+ detection capabilities for burn severity. *Remote Sensing of Environment*. 92, 3, 397–408.

Vermote, E.F., Tanre, D., Deuze, J.L., Herman, M, and Morcrette, J.J. (1997). Second simulation of the satellite signal in the solar spectrum, 6S: an overview. *IEEE Transactions on Geoscience and Remote Sensing*. 35, 895–934.

Viedma, O., Meliá, J., Segarra, D., and García-Haro, J. (1997). Modeling rates of ecosystem recovery after fires by using Landsat TM data. *Remote Sensing of Environment*. 61, 383–398.

ACKNOWLEDGMENTS

This research was funded by the U.S. Forest Service Pacific Northwest Forest Inventory and Analysis Program.

FIGURES

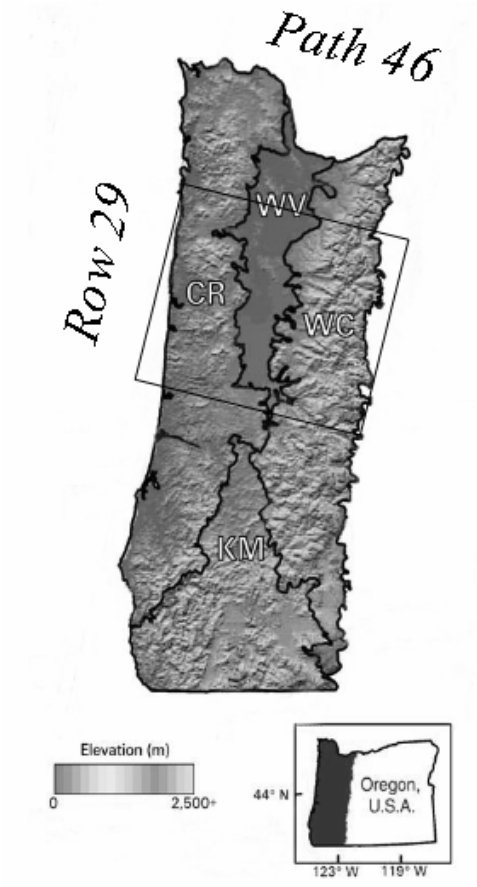

Figure 2-1. Landsat 46/29 study area (adapted from Cohen et al.,2001).

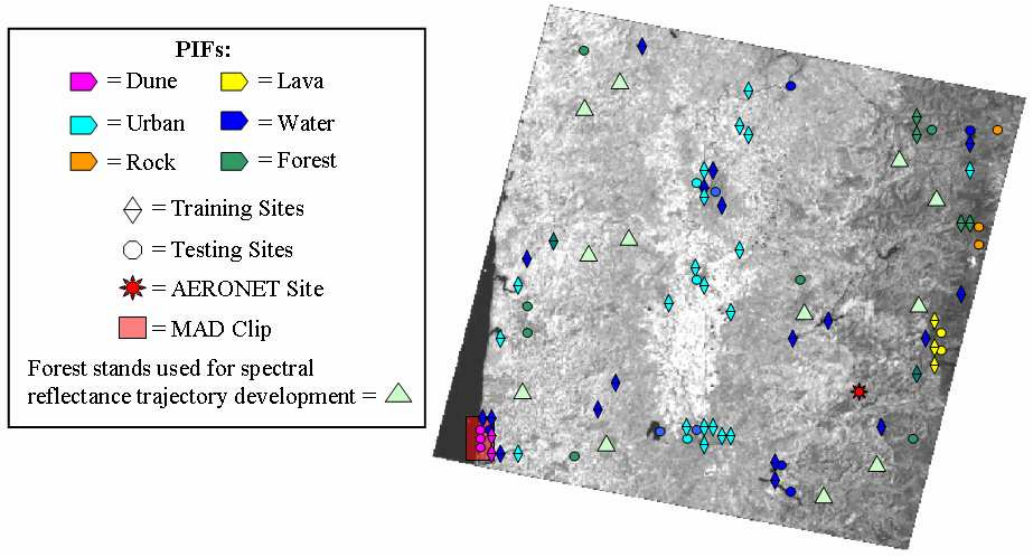

Figure 2-2. Spatial location of hand selected training and testing pseudo-invariant features..

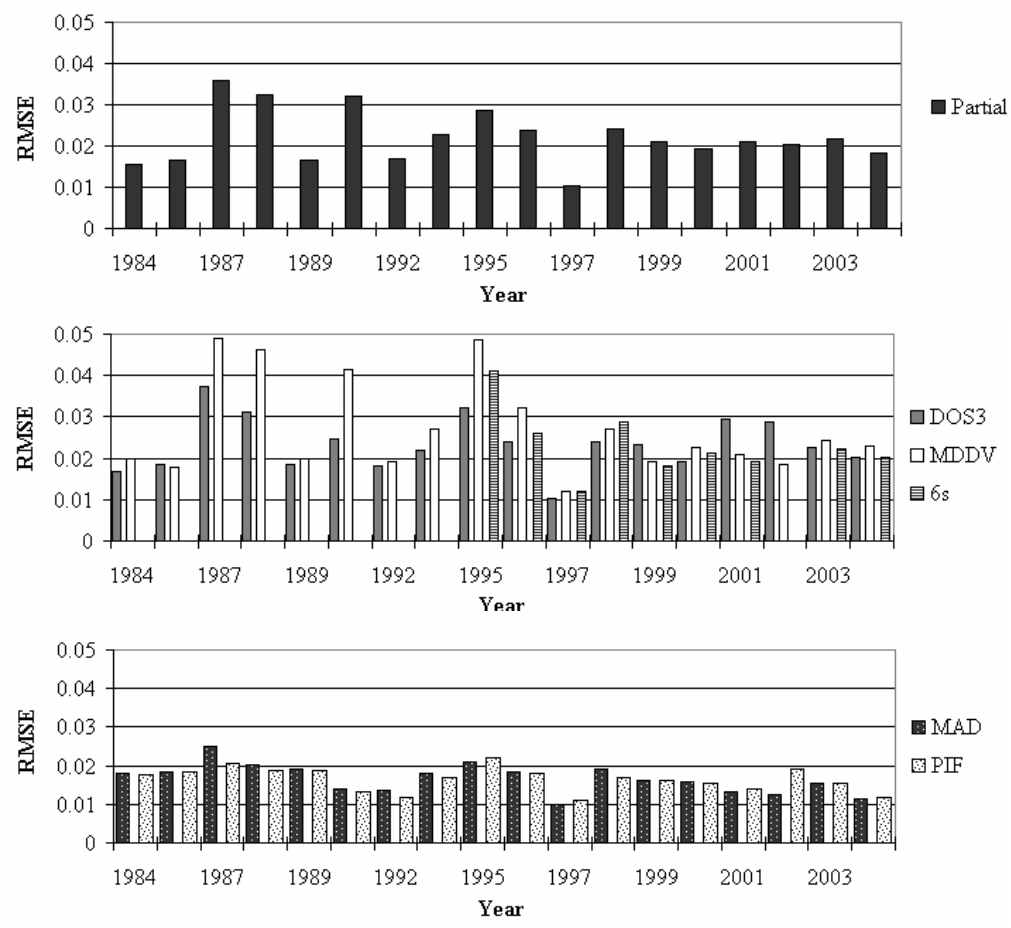

Figure 2-3. RMSE by image (calculated across spectral bands) for a. partial correction b. absolute corrections and c. relative corrections.

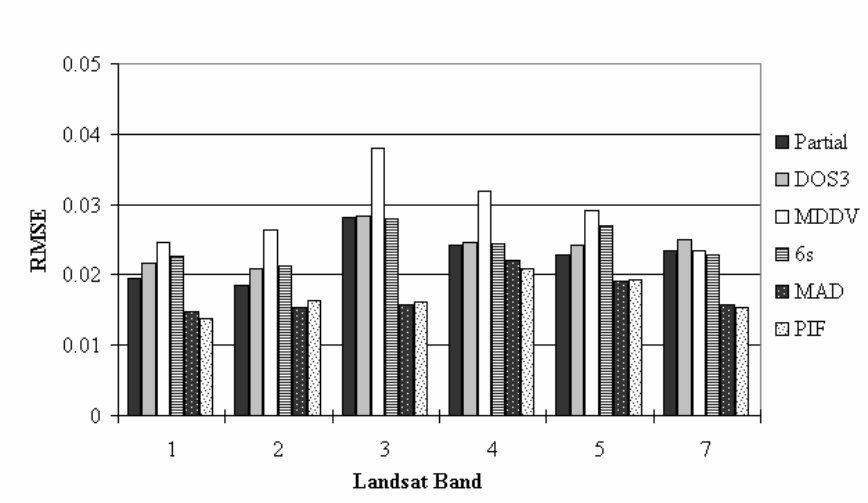

Figure 2-4. RMSE by Landsat band (across images).

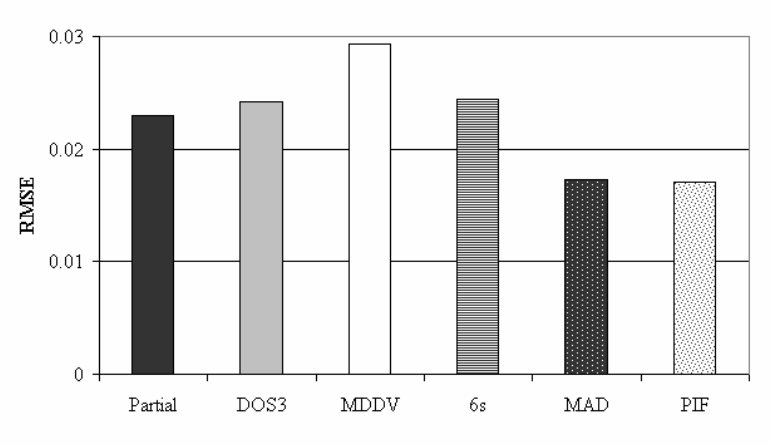

Figure 2-5. RMSE by calibration/normalization method (across images and spectral bands).

TABLES

Table 2-1. Landsat time-series used in this study.

Sensor	Date
TM	8/26/1986
TM	7/12/1987
TM	8/31/1988
TM	9/3/1989
TM	7/7/1991
TM	8/10/1992
TM	8/29/1993
TM	7/31/1994
TM	8/19/1995
TM	8/21/1996
TM	7/23/1997
TM	8/11/1998
TM	8/16/2000
TM	8/25/2003
TM	7/26/2004
ETM+	8/22/1999
ETM+	7/26/2001
ETM+	7/29/2002

Table 2-2. Aerosol optical depth (AOD) obtained from HJ Andrews Aeronet site and AOD estimated by the modified dense dark vegetation (MDDV) absolute calibration method.

Image	MDDV AOD	AERONET AOD
1984	0.240	-
1986	0.230	-
1987	0.380	-
1988	0.370	-
1989	0.110	-
1991	0.400	-
1992	0.140	-
1993	0.090	-
1994	0.150	0.015
1995	0.290	0.010
1996	0.400	0.036
1997	0.110	0.028
1998	0.100	0.008
1999	0.110	0.032
2000	0.130	0.048
2001	0.090	0.029
2002	0.090	-
2003	0.130	0.093
2004	0.070	0.030

Table 2-3. R-square and RMSE of quadratic polynomial models averaged across twelve forest stands recovering from stand replacing disturbance.

		R^2	**RMSE**
		Mean	Mean
Band 1	Partial	0.62	0.0107
	MAD	0.51	0.0057
Band 2	Partial	0.63	0.0088
	MAD	0.56	0.0054
Band 3	Partial	0.77	0.0141
	MAD	0.72	0.0105
Band 4	Partial	0.54	0.0379
	MAD	0.84	0.0255
Band 5	Partial	0.82	0.0217
	MAD	0.77	0.0208
Band 7	Partial	0.90	0.0124
	MAD	0.91	0.0109
Brightness	Partial	0.36	0.0390
	MAD	0.31	0.0254
Greeness	Partial	0.84	0.0226
	MAD	0.91	0.0181
Wetness	Partial	0.92	0.0138
	MAD	0.93	0.0133
NDVI	Partial	0.92	0.0426
	MAD	0.90	0.0410

Chapter 3 – Patterns of Forest Regrowth Following Clearcutting in Western Oregon as Determined From a Landsat Time-Series

Todd A. Schroeder[§], Warren B. Cohen[†], and Zhiqiang Yang[§]

[§] Department of Forest Science, Forestry Sciences Laboratory,

Oregon State University, Corvallis, OR 97331

[†] Forestry Sciences Laboratory, Pacific Northwest Research Station,

USDA Forest Service, 3200 SW Jefferson Way, Corvallis, OR 97331

Forest Ecology and Management
Elsevier - Customer Service Department
6277 Sea Harbor Drive
Orlando, FL 32887-4800 USA
In press

ABSTRACT

The rate at which forest vegetation re-establishes dominance after clearcut harvesting can impact many ecological processes, such as erosion/sedimentation, nutrient and water cycling, carbon storage potential, wildlife habitat, and trophic interactions. Although knowing a forest stand's current state of succession is useful, a clearer understanding of the impact forest harvesting has on the aforementioned ecological processes can be achieved with a more dynamic characterization of the successional process. To more fully model the continuous nature of forest regrowth following clearcut harvesting we extrapolated percent tree cover data collected by the U.S. Forest Service Pacific Northwest Forest Inventory and Analysis program to a cross-normalized Landsat time-series using a date-invariant regression modeling approach. Using three periods of mapped clearcuts we extracted and classified the extrapolated percent tree cover data into four regrowth classes (little to no, slow, moderate and fast). These forest regrowth classes were used to develop frequency distributions describing the landscape patterns of post-harvest forest recovery for two ecological provinces in western Oregon. The patterns of forest regrowth observed over the three clearcut periods indicated a much higher percentage of fast regrowth in the Coastal Range Province and a much higher percentage of little to no regrowth in the Western Cascade Province. For both ecological provinces we observed the propensity for faster regrowth on north facing aspects, shallow slopes and at low elevations. The forest regrowth classes and the frequency distributions indicated that a wide range of

successional stages could be found in both ecological provinces 18 years after clearcutting. The extension of forest regrowth trajectories to the spectral space of Landsat provided an opportunity to use CART statistical analysis to more fully investigate the climatic and topographic drivers influencing the rate of post-harvest forest regrowth. Based on the Kappa statistic, predictions from both CART models were in "fair" to "moderate" agreement with the test samples. Both classification trees yielded ecologically interpretable insights into the environmental attributes influencing forest regrowth rates after clearcutting. In both ecological provinces, elevation followed by potential relative radiation (PRR) explained the largest amount of variation in forest regrowth rates. To gauge the effectiveness of predicting more generalized post-harvest forest regrowth rates we combined the four forest regrowth classes into two general "fast" and "slow" categories. Based on the Tau statistic, the CART models correctly classified 12% (CRP) and 26% (WCP) more combined test samples than classification of the four regrowth classes.

1. INTRODUCTION

There is growing evidence suggesting considerable variability in the rate at which trees re-establish dominance following stand-replacing harvest disturbance in the temperate forests of the Pacific Northwest. This variability in forest regrowth has been observed even among stands with similar abiotic conditions and management prescriptions (Nesje 1996; Tappeiner et al., 1997; Sabol et al., 2002; Yang et al., 2005; and O'Connell et al., unpublished). Re-establishment of forest vegetation after harvest is important because it can influence many ecological processes, such as erosion/sedimentation, nutrient and water cycling, carbon storage potential, wildlife habitat, trophic interactions, and because of the economic value of conifer trees in the region.

Variability in the timing of tree re-establishment is one of the most widely studied phenomenons in forest ecology (Franklin et al., 2002). In western Oregon, ground surveys (e.g., Tappeiner et al., 1997) and interpretation of high-resolution aerial photographs (Nesje 1996; and Yang et al., 2005) have been previously utilized to study tree re-establishment, both of which are time consuming and expensive. Ground surveys are critical in understanding the role of local site factors controlling tree re-establishment, however the number of stands analyzed is often fewer than required to statistically validate relationships between the abiotic and biotic factors influencing forest regrowth. Studies based on the interpretation of high-resolution aerial photographs are useful in that they help establish the spatial and temporal extent over which regrowth variability is occurring, but they do not

readily permit explicit spatial modeling of the phenomenon (Nesje, 1996; and Yang et al., 2005). We seek to overcome these limitations by scaling estimates derived by ground survey and airphoto interpretation to the greater landscape using Landsat data. This synergistic approach should effectively increase the number of stands available for statistical modeling, thus offering an opportunity to advance our understanding of the geographically referenced environmental attributes influencing rates of forest regrowth following clearcutting in western Oregon.

The use of satellite imagery to characterize forest successional processes has mainly focused on estimating forest age from single image dates to make inferences about successional stage condition at one point in time (Fiorella and Ripple, 1993; Peterson and Nilson, 1993; Jakubauskas, 1996; Cohen et al., 2001; and Song et al., 2007). The difficulty with this approach is that the relationship between forest age and spectral data can be highly variable, especially for young (< 20–year) stands with low canopy cover (Horler and Ahern, 1986). A more limited number of studies have taken advantage of multiple images to study the dynamic process of forest succession (Hall et al., 1991; Foody et al, 1996; and Lucas et al., 2002), but have utilized relatively simple techniques such as post-classification comparison to estimate forest change. Although simple to execute, post-classification comparison relies on differencing two or more independently produced image classifications. Thus, its effectiveness at estimating forest change is hindered by the fact that errors inherent to each individual classification combine

multiplicatively as they are overlaid for comparison, resulting in a final change product that contains more error than any of the original classification-based inputs.

An alternative use of satellite imagery for characterizing forest successional processes is through the examination of a multi-temporal image series. A multi-image time-series constructed from the Landsat suite of optical sensors could (at present) theoretically consist of 35 images (1972–2006) per scene, which could be used in a continuous fashion to create "regrowth trajectories" for any forested stand disturbed since 1972. Although in some areas geographic and climatic factors may limit the availability of suitable images required to create useful trajectories of forest regrowth, it is likely the number of images needed to sufficiently capture the landscape disturbance/recovery signal will be fewer than conceptualized in this theoretical example. As forest stands in the Pacific Northwest commonly enter the stem exclusion phase (i.e., closed canopy condition) of successional development within the first 20 years after clearcutting (Franklin et al., 2002) we base our analysis of post-harvest early forest successional patterns on 16 Landsat TM and 3 Landsat ETM+ images covering 18 years. This rapid rate of tree regrowth after disturbance eliminates the need to lengthen the time span of our image series back to the Multi-Spectral Scanner (MSS) system. In addition, the improved 30 m resolution of the post-MSS images better matches the resolution of our ground referenced tree cover data.

We define "trajectory" as a series of states through which a system proceeds over time. Trajectories (or change-curves) are comprised of a series of

mathematical or statistical models fit to repeatedly measured observations, which are used to characterize or quantify various pathways of vegetation response to disturbance. The shape of vegetation regrowth trajectories has long been recognized by field ecologists as a practical means of describing plant community responses to various disturbance types (Armesto and Pickett, 1986; Halpern and Franklin, 1990; and del Moral and Bliss, 1993), as differences in trajectory shape infer differences in the controlling mechanisms of vegetation change. Additionally, the trajectory concept forms the basis of many empirical functions commonly used by foresters to predict theoretical plant growth (Richards, 1959) and stand-level growth based on site-index (Hegler, 1968).

Although the use of repeated observations collected by satellite remote sensing platforms such as Landsat seem particularly well suited to analyzing continuous trends in vegetation via trajectory analysis, only a few examples can be found in the literature (Viedma et al., 1997; and Joyce and Olsson, 1999). One example is presented by Lawrence and Ripple (1999) who derive vegetation change trajectories with estimates of percent green vegetation cover predicted independently from 8 Landsat TM images (covering 15 years). These change trajectories were used to describe and quantify various regrowth pathways following the 1980 volcanic eruption of Mt. St. Helens in southwestern Washington.

Ultimately the success of the trajectory approach in capturing real vegetation change hinges on the successful radiometric calibration of the multi-

temporal image series. Given this importance, we favor the use of a radiometric calibration method which was specifically designed to operationally minimize residual scatter (i.e., lower RMSE) in early forest regrowth trajectories in western Oregon. The method, referred to as "absolute-normalization" (Schroeder et al., 2006), uses statistically selected pseudo-invariant features (see Canty et al., 2004) to relatively normalize an image time-series to an atmospherically corrected reference image (corrected with 6S, Vermote et al., 1997). All images in the multi-temporal Landsat series presented here were normalized to a common radiometric scale (across all images < 0.025 RMSE), while simultaneously correcting for atmospheric and sun/sensor view-angle effects.

Once the images comprising a multi-temporal image series share a common radiometric scale, meaningful regrowth trajectories can be constructed directly from spectral reflectance values, from fraction images derived via spectral mixture analysis (Smith et al., 1990) (e.g., green vegetation, non-photosynthetic vegetation, soil and shade images) or with biophysical estimates predicted from reflectance (e.g., percent tree cover). In this paper we base our forest regrowth trajectories on a date-invariant relationship developed between Landsat spectral data and ground measured tree cover data collected by the U.S. Forest Service Pacific Northwest (PNW) Forest Inventory and Analysis (FIA) program. Although date-invariant regression can be thought of as a form of post classification comparison, the use of a detailed radiometric calibration procedure, continuous versus class based estimates and derivation of change information from multiple image trajectories

improves on the traditional application of the method. For more details on the date-invariant regression approach, referred to as "state model differencing" see Healey et al. (2006).

We aim to address the following three objectives. First, we seek to corroborate the existence of divergent forest regrowth pathways among harvested stands previously identified in western Oregon via airphoto interpretation (Nesje, 1996; and Yang et al., 2005). Second, we compare landscape scale early successional forest regrowth patterns between the two primary forested provinces in the study area (i.e., the moist, warm Coast Range Province and the drier and colder Western Cascade Province). Finally, we use commonly available physical proxies (e.g., aspect, slope, elevation) and plant relevant (e.g., potential relative radiation, temperature, precipitation) explanatory variables to predict early successional forest regrowth patterns in both provinces.

2. METHODS

2.1. Study Area

The study area is comprised of Landsat WRS-2 path 46 row 29, which covers approximately 185 km² of western Oregon (Figure 3-1). The two main forested provinces in the study area are described by Franklin and Dyrness (1988) as the Coast Range Province (CRP) and the Western Cascade Province (WCP). The CRP is characterized in the far west by a Sitka spruce zone a few kilometers wide lying directly adjacent to the Oregon coast. The rest of the CRP and the majority of

the WCP are dominated by conifers common to the Douglas-fir/western hemlock zone, although hardwood species such as red alder, vine maple, big leaf maple, and Pacific dogwood can dominate moist riparian areas and dry valley margins.

In Douglas-fir forests two principal seral groups typically comprise post-disturbance vegetation communities, residuals (members of the original forest community) and invaders (non-forest species that colonize after the disturbance event) (Halpern and Franklin, 1990). Halpern (1989, Table 1) describes six forest understory communities common to Douglas-fir forests. In addition to conifer trees, early seral communities in this region can often be dominated by several grass, herb, shrub (e.g., ceanothus, oceanspray, salal, vine maple, Oregon grape, hazel and sword fern) and non-conifer tree species (bitter cherry, Pacific madrone, and chinkapin). The extent to which of these life forms dominates after disturbance is likely a function of disturbance intensity, initial seed abundance, site condition, stochastic processes (e.g., climate, seed dispersal), and forest management activities. Regardless of life form dominance, a complex mixture of several species is likely to occur until canopy closure is fully achieved.

Overall, the climate of the Pacific Northwest is typified by warm, dry summers and mild, wet winters. The study area encompasses a wide range of elevations, yielding strong physical and climatic gradients. Based on annual averages, the CRP typically receives more precipitation (3000 mm vs. 2300 mm) and is warmer in the winter (5° C vs. -5° C) and cooler in the summer (16° C vs. 23° C) than the WCP. These climatic differences, in concert with differences in

elevation (CRP: 450–750 m vs. WCP: 450–3000 m) and geologic parent materials yield a wide array of growing conditions. The study area also includes a diverse distribution of existing land ownership categories (Cohen et al., 2002), and therefore represents the disturbance and recovery patterns present in the region.

2.2. Data

2.2.1. Multi-temporal Image Series

Our characterization of forest regrowth patterns in western Oregon focuses on the analysis of a multi-temporal image series consisting of 19 summer (e.g., July – September), near anniversary Landsat TM and ETM+ images (WRS-2, path 46 row 29) (Table 3-1). A detailed description of the image selection criteria, as well as the geometric and radiometric corrections applied to the multi-temporal image series can be found in Schroeder et al. (2006). In all, the images comprising the multi-temporal image series were atmospherically corrected and normalized to within 0.025 RMSE of the selected reference image (1994) using the absolute-normalization approach detailed above. For this study the 2005 image was added to the multi-temporal image series using the same geometric and radiometric processing protocols described in Schroeder et al. (2006).

2.2.2. Tree Cover

Three independently collected (1 ground based, 2 photo-interpretation based) tree cover (measured as percent) data sets were utilized in this study. The

ground measured tree cover data set was recorded by line transect method (see pgs. 155 – 162, USDA Forest Service, 1995) during the 1995 periodic forest inventory of western Oregon conducted by the U.S. Forest Service PNW-FIA program. The 2.1 ha FIA plots are coded from 1 to 5 based on the number of different land cover conditions (e.g., forest, water, non-forest) observed on each of the five measured subplots. Thus, a plot labeled 1 (referred to as single condition) would have only 1 dominant land cover condition, whereas a plot labeled 5 would have a different observed land cover condition at each measured subplot. To avoid spectral mixing with unwanted non-forest and water condition classes, we elected to use only the tree cover data collected on the single condition, forested plots (n = 202) falling within the Landsat 46/29 study area. Although this approach required discarding some potentially useable data, our ultimate goal was to minimize the impact of sample heterogeneity on the date-invariant tree cover regression model.

The two airphoto based tree cover data sets, which were used to validate the date-invariant tree cover regression model, were collected by two separate photo-interpreters. Both interpreters estimated percent tree cover over a fixed sample of plots repeatedly over time using an assortment of high-resolution aerial photographs (see Table 3-2 for photo scales and formats). Because we used a date-invariant approach to model tree cover, we elected to use photo-interpreted estimates of tree cover recorded for a given plot, at different points in time, as separate validation samples. Due to the timing of photointerpretation, quantification of interpreter to interpreter bias was not possible.

Interpreter 1 photo-interpreted percent tree cover over 125 of the same 2.1 ha single condition, forested FIA plots that make up the ground based tree cover data set. Several of these plots were re-interpreted at a second point in time, yielding 162 tree cover validation samples (Table 3-2). Interpreter 2 estimated percent tree cover over 153, 1 ha sample plots (see Yang et al., 2005), which including remeasurement yielded 249 tree cover validation samples (see Table 3-2). Overall, the two photo-interpreted tree cover data sets combined to yield a total of 411 tree cover validation samples, spanning 11 years. It is important to note that interpreter 1's photo-interpreted estimates of tree cover were taken solely from plots falling on private forest lands, whereas interpreter 2's were only from national forest lands. Thus, by combining the two data sets we not only maximized the size and temporal span of our validation sample, but also accounted for any potential differences in tree cover based on land ownership.

2.2.3. Explanatory Variables

We are interested in spatially predicting patterns of forest regrowth, thus we compiled 12 geographically referenced explanatory variables (3 physical proxy, 9 plant relevant) for use in Classification and Regression Tree (CART) statistical analysis. The physical proxy variables include transformed aspect (index 0–2) (Beers et al., 1966), slope (%) and elevation (meters), all derived from a 30 m DEM of the study area. Since slope, aspect and elevation are merely correlated with the

moisture and temperature gradients plants commonly respond to, we refer to them as “physical proxies”.

On the other hand, recent advances in the spatial representation of direct resource gradients such as moisture, temperature and soils allowed us to use several “plant relevant” variables in our analysis. These variables include, potential relative radiation (PRR) (Pierce et al., 2005), which is a unit less index at 30 m resolution used to approximate the “potential” incident radiation received by a given surface location during a set window of time (applied here using a 12 month growing season). Here the range of PRR is 985 (e.g., deep, north facing canyon) to 21959 (e.g., open, slightly southern facing hill slope). The highest value (21959) represents the location with the highest probability of receiving incident radiation in the absence of clouds. In addition to PRR, we also use PRISM temperature (Parameter-elevation Regressions on Independent Slopes Model, Daly et al., 1994, http://www.prismclimate.org) – July maximum and January minimum (1 km resolution) in °C, and five CONUS (Conterminous United States) soil layers (Miller and White, 1998, http://www.soilinfo.psu.edu/index.cgi) estimated at a 1 km resolution (sand (%), silt (%), clay (%), soil depth (cm), and field capacity (kg)).

2.3. Date-invariant Regression Modeling

In this study we based our forest regrowth trajectories on estimates of percent tree cover derived from Landsat spectral reflectance data. This was

accomplished by first developing an initial regression model between the ground measured percent tree cover data collected by PNW-FIA and the 1995 Landsat spectral reflectance data. To obtain reflectance data for each of the 202 single-condition, forested FIA plots we took the mean of a 22 pixel mask, (Figure 3-2) which was developed to mimic the size and shape of the FIA ground plot (for details on FIA ground plots see pages 17 – 38 in USDA Forest Service, 1995). As FIA plot coordinates are collected on the southern portion of each plot (i.e., subplot 1), we matched each plot coordinate to the southern portion of our 22-pixel mask (gray shaded pixel in Figure 3-2). Other studies which have extracted Landsat spectral reflectance data for use with FIA data have used similar techniques (Ohmann and Gregory, 2002).

We then employed a standard correlation procedure where the extracted means of the spectral variables (Landsat bands 1-5, and 7), and subsequently derived vegetation indices [Normalized Difference Vegetation Index (NDVI) (Rouse et al., 1973), Normalized Difference Moisture Index (NDMI) (Hardisky et al., 1983; and Jin and Sader, 2005) and Tasseled Cap (Crist and Cicone, 1984)] were evaluated via scatter plot to determine their relationship with tree cover and to explore the need for transformation. This evaluation revealed the need to linearize the Landsat bands using a common square root transformation.

Stepwise multiple regression was then used to identify a preferred (i.e., high R^2, low RMSE) model. Several models were evaluated, however we determined that a three variable model containing Landsat bands 1, 3 and 7 best captured the

variation in the ground measured tree cover data (see discussion). To ensure that the variance observed in our observations was adequately preserved in our predictions we preferred the use of reduced major axis regression (RMA) (Cohen et al., 2003). As in Cohen et al. (2003), we used canonical correlation analysis (CCA) to derive a linear combination of the Landsat bands identified above for use in X on Y RMA regression.

This initial RMA regression model was applied individually to the remaining 18 "absolutely-normalized" Landsat images, which yielded a total of 19 tree cover images. This date-invariant regression approach (Healey et al., 2006) assumes that an effective radiometric calibration procedure has resulted in a common radiometric scale among all images, resulting in an date-invariant relationship between spectral reflectance and the biophysical variable of interest. To test the validity of this assumption, we conducted a leave-one out cross-validation of the initial RMA regression model (n = 202), as well as a temporal accuracy assessment covering 11 different tree cover images using the two airphoto based tree cover data sets (Table 3-2). The date-invariant tree cover estimates falling below 0% and above 100% were rescaled to fall between 0 and 100% to match the scale of the airphoto data. Mean tree cover was calculated for each of the 2.1 ha (interpreter 1) and 1 ha plots (interpreter 2) using each plots coincident tree cover image. The mean plot tree cover estimates (predicted) were then compared with the photo-interpreted tree cover estimates (observed) via linear regression. As we are primarily interested in knowing the accuracy of the percent

tree cover predictions across all images (i.e., those with validation data), we opted to combine all 411 validation samples into one global validation model.

2.4. Stand Disturbance Maps

We are interested in using a trajectory based approach to analyze patterns of forest regrowth following clearcut harvesting. Consequently, we mapped three sets of clearcut harvests which we later use as spatial masks to extract pixel level tree cover estimates from our 19 tree cover images derived via date-invariant regression modeling. We decided on analyzing forest regrowth using three periods of clearcuts for two reasons. First, regrowth patterns are likely to vary from year to year in complex ways, so by including stands clearcut at different times we hoped to capture a broader range of regrowth variability in our analysis. Second, clearcut harvests tend to occur on relatively small (e.g., < 10 ha), scattered blocks over the landscape, so by developing regrowth trajectories over clearcuts occurring in different years we effectively increase the number of stands, as well as the spatial area available for statistical analysis.

The three sets of clearcuts occurring between 1986 – 1987, 1987 – 1988, and 1988 – 1989 (hereafter referred to as periods 1 – 3) were mapped independently using RGB color composite analyses (Coppin et al., 2004) of Landsat band 5 and a minimum distance to means supervised classifier (Lillesand and Kiefer, 2004). As in Cohen et al. (1998), each stand disturbance map was first smoothed using a 7x7 majority filter to rid of unwanted noise (i.e., single pixels

classified as clearcuts). We then used the ERDAS Imagine clump function to identify and group contiguous groups of clearcut pixels, and finally used the ERDAS Imagine sieve function to eliminate all clearcuts less than 2 ha in size. The three stand disturbance maps were then hand-edited using several of the high resolution aerial photographs from Table 3-2 as reference. Areas classified as forest change but were determined not to be clearcuts were removed to ensure a high level of overall quality. Although we did not explicitly evaluate the accuracy of the stand disturbance maps, similar methods for mapping clearcut harvests occurring in Oregon west of the Cascade crest have achieved upwards of 90% accuracy (Cohen et al., 2002).

2.5. Forest Regrowth Class Trajectories

To spatially derive forest regrowth trajectories for the clearcuts identified from the supervised classification we first stacked the geographically referenced tree cover images derived via date-invariant regression modeling into 3 multi-temporal image stacks, one for each period of mapped clearcuts. The first tree cover image in each multi-temporal stack corresponds to the first growing season after each period's mapped harvest disturbances. For period 1, the multi-temporal stack contained a total of 17 tree cover images, the first tree cover image corresponding to 1988. For subsequent periods the multi-temporal tree cover stacks contained 16 and 15 tree cover images respectively. The stand disturbance

maps were then used to mask (i.e., isolate) the pixel level tree cover values from each period's respective tree cover stack.

The extracted time-series of pixel level tree cover estimates were then grouped into 20 individual "regrowth" classes using the ISODATA clustering algorithm in ERDAS Imagine. To facilitate clustering, each period's multi-temporal tree cover stack was clustered separately as each had a different number of tree cover images. Using the statistical measure of transformed divergence (Jensen, 1996) the spectral separability of the 20 "regrowth" classes was evaluated. In general, separability analysis is used in image classification to determine the extent to which clustered class-mean values overlap each other in spectral space. Here separability analysis revealed the need to combine several of the "regrowth" classes as they were not spectrally unique. This process resulted in the creation of 5 statistically discrete forest regrowth classes per period. The four main classes were visually assigned labels based on observed rates of percent tree cover increase, which included little to no regrowth, slow regrowth, moderate regrowth, and fast regrowth. The fifth class, labeled mixed regrowth, was interpreted to contain a highly variable mixture of partially harvested areas, prescribed burns and shadows. These areas commonly have a dark spectral appearance, resulting in a false signal of high initial tree cover immediately following clearcutting. Thus, given its highly variable nature, as well as its limited spatial extent, we exclude the mixed regrowth class from the remainder of the analysis.

2.6. Forest Regrowth Spatial Pattern Analysis

To corroborate the presence of divergent pathways of forest regrowth in western Oregon we summarized the pixel level frequency distribution of the four main forest regrowth classes identified from ISODATA clustering according to area disturbed by clearcut harvest and by topographic position. These distributions were used as a means of describing the landscape scale, forest regrowth signal for both the CRP and WCP. To make meaningful comparisons of forest regrowth between the two ecological provinces we attempted to normalize the differences in harvest area between the CRP and WCP by basing our frequency distributions on the "percent of clearcut area" metric, which we calculated using Eq. 1,

$$\% \text{ of Clearcut Area} = TAFRC \div TACHP \times 100 \quad (1)$$

where, TAFRC is the total area of each forest regrowth class, TACHP is the total area clearcut per harvest period. With three periods of clearcuts available for analysis, we were able to use this metric to characterize the landscape scale forest regrowth patterns occurring in each ecological province. To gain further inference into the patterns of forest regrowth associated with the geographically referenced environmental attributes we also summarized the patterns of forest regrowth in the CRP and WCP according to three relevant topographic variables (i.e., aspect, slope, elevation). For ease of display, the topographic variables were binned into class groupings (e.g., aspect 1° – 33° labeled as N–NE class). For each topographic

class grouping, the distribution of each forest regrowth class was based on “percent of clearcut area” as above, except the mean value observed over all three periods is reported (error bars are across period standard deviations).

2.7. Classification and Regression Tree Modeling

To formulate a better understanding of the environmental attributes influencing forest regrowth following clearcut harvesting in western Oregon we attempted to predict forest regrowth rates for both the CRP and WCP using the aforementioned explanatory variables and CART statistical modeling. We select CART as it is flexible, non-parametric, and robust to complex non-linear relationships (Friedl and Brodley, 1997) and has been previously used to examine changes in vegetation (Lawrence and Ripple, 2000; and Lutz and Halpern, 2006). Since CART modeling is typically data intensive, we decided to combine the three periods of regrowth classes into one spatial layer to maximize the available land area from which to draw our statistical sample. In an attempt to keep training data equal among regrowth classes (Lawrence and Wright, 2001) we used a stratified random design (separately for the CRP and WCP) to select approximately 300 pixels per regrowth class (4 classes) to be used as training samples. An additional ≈300 samples per regrowth class were selected (separately for the CRP and WCP) for the purpose of testing the predictive power of the developed CART models. Overall, a total of 2,375 (1,186 testing, 1,189 training) samples were derived for the CRP and 2,371 (1,183 testing, 1,188) for the WCP. For each sample location, the

explanatory variables were extracted on a per pixel basis for use in statistical modeling.

Using the tree modeling tools in S-plus we developed CART models for both the CRP and WCP. In S-plus, terminal nodes are created either when the total number of observations at the node is less than 10 or the deviance at the node is less than 1% of the total deviance for the entire tree (Venables and Ripley, 1997). Since CART models tend to over-fit the data, it is crucial that they be pruned back to some degree to avoid over-fitting, but not to a point that affects the robustness of the model. To determine an appropriate size for our tree models we elected to use a cross validation procedure (Venables and Ripley, 1997; and Lawrence and Wright, 2001) where each set of training samples is divided into ten equal parts. Trees are fit iteratively for nine of the ten trees, with the tenth being used as validation. After all the trees have been fit, the minimum average deviance suggests a suitable number of nodes for the final tree. Although an analyst may opt to use a smaller size tree than suggested by cross validation, we found the suggested tree sizes to be acceptable for both the CRP and WCP models. The final tree models contained 10 (CRP) and 6 (WCP) terminal nodes and were plotted so that branch size was roughly proportional to the deviance explained by each node.

To assess the accuracy of both CART models we used the test samples to compute standard confusion matrices with overall, producers, and users accuracies, as well as Kappa (Congalton, 1991), and Tau (Ma and Redmond, 1995) statistics. In addition, the accuracy of both CART models was evaluated using an aggregated

approach, where the four regrowth classes were combined to represent “fast” (i.e., combine fast and moderate regrowth classes) and “slow” (i.e., combine little to no and slow regrowth classes) forest regrowth conditions.

3. RESULTS

3.1. Initial Tree Cover Model

Model parameters for the initial tree cover regression model developed using the 202 single condition, forested FIA ground measured field plots and the linear combination of spectral variables (bands 1, 3 and 7) from the 1995 Landsat TM image are found in Table 3-3. Using a leave one out cross-validation procedure (Cohen et al., 2003) we found the RMA regression model to be highly significant both in terms of variance explained ($R^2 = 0.77$) and predicted error (RMSE = 14.15). The predicted (from cross-validation) versus observed tree cover is presented in Figure 3-3. The selection of RMA regression ensured that nearly all the original variation found in our observations was preserved in our tree cover predictions (variance ratio = 1.00). The near zero bias (0.03) indicated that overall there is no over- or under-prediction of tree cover in our initial model.

3.2. Date-invariant Regression

The temporal accuracy of our date-invariant regression approach was assessed using the two airphoto based tree cover data sets which contained coincident measurements with 11 of the 19 tree cover images (Table 3-2). Using

411 airphoto based validation samples we incorporated data from all 11 tree cover images into one global validation model (Table 3-3 for regression model parameters). The scatter plot of predicted (from date-invariant regression) versus observed (airphoto interpreted) tree cover is presented in Figure 3-4. Overall, we found good agreement between the airphoto interpreted measures of percent tree cover and those derived via our date-invariant regression modeling approach. Both the amount of explained variance ($R^2 = 0.68$) as well as the predicted error (RMSE = 16.09) were found to be similar to those observed in the initial tree cover model. The selection of RMA regression ensured that nearly all the variation found in our validation plots was preserved in our tree cover predictions (variance ratio = 1.00). Furthermore, the near zero bias observed in the global validation model indicates that there is no bias in the relationship between date-invariant regression and airphoto based tree cover.

3.3. Forest Regrowth Class Trajectories

Each period's mapped clearcuts were spatially clustered into statistically meaningful forest regrowth classes (i.e., little to no, slow, moderate, fast) using ISODATA clustering. The mean values of each period's forest regrowth classes were fit with third-order polynomial curves, resulting in 3 fitted curves per forest regrowth class (Figure 3-5). These curves, or "mean forest regrowth trajectories" were visually compared for each regrowth class and were found nearly indistinguishable across harvest periods. As a result, we determined that each

period's forest regrowth classes could be used interchangeably in the CART analysis.

3.4. Forest Regrowth Patterns

For the CRP and WCP we used "percent of clearcut area" to summarize forest regrowth at the landscape scale for each clearcut harvest period (Figure 3-6). The consistent patterns of forest regrowth observed over the three clearcut periods indicate a much higher percentage of fast regrowth in the CRP as opposed to a much higher percentage of little to no regrowth in the WCP.

Frequency distributions of forest regrowth were also derived for three topographic variables of interest (aspect, slope, and elevation). Forest regrowth by aspect class is presented in Figure 3-7. For both the CRP and WCP the highest percentage of fast regrowth occurred on north facing aspects (i.e., N–NE, NE, NW, and N–NW), with nearly twice as much fast regrowth being observed on the northern aspects of the CRP then on the WCP. On the other hand, both ecological provinces saw the percentage of little to no and slow forest regrowth classes increase on southern facing aspects (SE, S–SE, S–SW, SW). Although this general trend was observed for south facing aspects in both ecological provinces, the WCP was found to have more than triple the amount of little to no and slow regrowth on southern aspects than the CRP.

Forest regrowth by percent slope class is presented in Figure 3-8. For both ecological provinces, as slope class increased past 10–19% the amount of fast

regrowth tended to decrease. For the WCP, this observed decrease in fast regrowth was more pronounced than for the CRP and was also accompanied by a noticeable increase in the amount of little to no and slow forest regrowth. Other than the observed decrease in fast regrowth with increasing slope, the remaining forest regrowth distributions in the CRP were found to be relatively stable across slope classes.

Forest regrowth by elevation class is presented in Figure 3-9. For both ecological provinces, the percentage of fast regrowth noticeably decreased as elevation increased. This pattern seemed more pronounced for the WCP as clearcut harvesting occurred over a much higher elevation range. Although fast regrowth decreased with elevation in the CRP, at no time did the percentage of little to no regrowth exceed fast regrowth. On the other hand, little to no regrowth significantly exceeded fast regrowth in the WCP at all elevations above 762 m.

3.5. CART Models

Using the 12 explanatory variables we constructed CART classification models to predict the forest regrowth classes of the CRP and WCP ecological provinces. Six of the explanatory variables (elevation, PRR, percent slope, PRISM average annual precipitation, CONUS soil silt, and PRISM July average maximum temperature) were used to construct the final CRP CART model (Figure 3-10), which yielded 10 terminal nodes or classification decision rules. Branch length of the tree indicated that elevation explained the largest percentage of variation in

CRP forest regrowth classes, followed by PRR and percent slope. In the CRP, fast forest regrowth was generally predicted to occur on low elevation sites (< 338 m) and on high elevation sites (> 338 m) with relatively low radiation exposure (PRR < 14262). Little to no forest regrowth was predicted only on high elevation (> 338 m) sites having both high radiation exposure (PRR > 17934) and steep topography (slope % > 32). A variety of other combinations of the 6 explanatory variables resulted in predictions of the moderate and slow forest regrowth classes.

The overall accuracy of the CRP CART model was 46% (Table 3-4). According to Landis and Koch (1977) a Kappa of 27% suggests "fair agreement" between the predicted regrowth classes and test samples. The Tau statistic indicates that 27% more pixels were classified correctly than would be expected by random assignment. Ranging from 17 to 79%, the individual class accuracies (Table 3-4) suggested that the maximum and minimum regrowth classes (i.e., little to no and fast) were predicted with greater accuracy than the classes falling in between (i.e., slow and moderate).

Four of the explanatory variables (elevation, PRR, PRISM July maximum temperature, and PRISM January minimum temperature) were used to construct the final WCP CART model (Figure 3-11), which yielded 6 terminal nodes or classification decision rules. Branch length of the tree indicated that elevation and PRR explained the largest percentage of variation in the WCP forest regrowth classes. In the WCP, fast forest regrowth was generally predicted to occur on low elevation (< 805 m) sites having moderate to high radiation exposure (PRR <

18924) and warm winter minimum temperatures (January min. temp > 0° C). Little to no forest regrowth was predicted to occur on high elevation sites (> 1,014 m) and on moderately high elevation sites (> 805 m and < 1,014 m) with low summer maximum temperatures (July max. temp < 24° C). A variety of other combinations of the 6 explanatory variables resulted in predictions of the moderate and slow forest regrowth classes.

The overall accuracy of the WCP CART model was 47% (Table 3-4). A Kappa of 29% suggests "fair agreement" between the predicted regrowth classes and the test samples (Landis and Koch, 1977). The Tau statistic indicates that 30% more pixels were classified correctly than would be expected by random assignment. Ranging from 29 to 68%, the individual class accuracies (Table 3-4) suggested that the maximum and minimum regrowth classes (i.e., little to no and fast) were predicted with greater accuracy than the classes falling in between (i.e., slow and moderate).

Since the maximum and minimum regrowth classes (i.e., little to no and fast) showed greater predictive potential, we reassessed the accuracy of the CART models using an "aggregated" approach. This was accomplished by combing the fast and moderate regrowth classes to represent "fast" forest regrowth and the little to no and slow regrowth classes to represent "slow" forest regrowth. Using the aggregated approach the CRP model yielded an overall accuracy of 70% (Table 3-5). Landis and Koch (1977) suggest that a Kappa of 39% represents "fair agreement" between the predicted regrowth classes and the test samples. The Tau

statistic indicates that 40% more pixels were classified correctly than would be expected by random assignment. The WCP model improved to an overall accuracy of 78% (Table 3-5). A Kappa of 56% is interpreted by Landis and Koch (1977) as a "moderate agreement" between the predicted regrowth classes and the test samples. The Tau statistic indicates that 56% more pixels were classified correctly than would be expected by random assignment. As expected, both the CRP and WCP overall accuracies improved with the implementation of the aggregated approach. The Tau statistics indicate that when the CART decision rules are used to predict the aggregated "fast" and "slow" forest regrowth classes the resulting classifications yield 12% (CRP) and 26% (WCP) more correctly classified pixels than classification of the four regrowth classes.

4. DISCUSSION

4.1. Date-invariant Regression

Using date-invariant regression to create meaningful forest regrowth trajectories relies heavily on a thorough radiometric calibration of the multi-temporal image series and the creation of a significant initial regression model of the biophysical variable of interest. Although a larger sample of airphoto based tree cover data was available, we opted to develop our initial regression model (Table 3-3, Figure 3-3) with the field measured tree cover data collected by the U.S. Forest Service PNW-FIA program. This decision was based on the fact that photointerpreted percent tree cover often contains significant interpreter bias, which

if extrapolated forward via date-invariant regression could jeopardize the creation of meaningful forest regrowth trajectories. This bias is readily apparent in our airphoto validation of the initial tree cover model shown in Figure 3-3, where Interpreter 1 (filled circles) had a tendency to under predict and Interpreter 2 (open circles) over predict percent tree cover, especially in the 20 to 80% tree cover range. Had both interpreters shared the same directional bias the validation of our initial tree cover model might have been less satisfying. As it stands, our validation model serves as an illustration of why field measured biophysical variables are critically important to the accurate modeling of vegetation with remotely sensed imagery. In addition, use of spectral bands 1 (visible blue, responds to forest type and serves as a measure of overall "brightness"), 3 (visible red, responds to chlorophyll absorption in vegetation) and 7 (short-wave infrared, responds to vegetation shadowing and moisture) in our initial tree cover model demonstrates the utility of multi-wavelength sensors like Landsat at resolving useful spectral information directly pertaining to forested systems (Cohen and Goward, 2004).

Given the wide variation of life forms likely present after clearcutting it is likely that some of the error in our initial tree cover model resulted from the use of total tree cover. Utilizing separate hardwood and softwood tree cover categories could possibly improve both the fit of the initial tree cover regression model, as well as the detail with which the compositional changes associated with post-harvest forest succession could be successfully resolved with an image time-series. Other potential improvements include the use of image transformation methods

such as spectral mixture analysis (Smith et al., 1990), which separates and quantifies sub-pixel scene components such as green foliage, tree bark, and shadow to estimate fractional vegetation cover. Trajectories constructed of fractional images from SMA may help to more fully resolve the complex mixtures of species (deciduous vs. conifer) and vegetation cover (low vs. high) typically found in early successional forests of the Pacific Northwest (Sabol et al., 2002).

Although analysis with multi-temporal image series can be time consuming, one major advantage to their use is that variations from atmospheric effects and vegetation phenology, which can seriously impact change estimates based on year to year image differences are minimized as the overall estimate of change is based on the fitted trajectory curve (or curve class in this case). In this sense, year to year variations are viewed as residuals around each classes fitted trajectory. While residuals resulting from atmospheric effects and vegetation phenology are viewed as "error" in terms of the trajectory model, the overall pattern of regrowth is not assumed to be effected unless the curve fit is unusually low. The lowest R^2 of all four of our forest regrowth class trajectories was .93, indicating minimal year to year impacts from residual error at the class level. At the pixel level, we found a high level of agreement (R^2 = .96, RMSE = 6.05) between average pixel tree cover estimates (selected randomly across all images) and tree cover predicted from the forest regrowth curves (n = 240). The standard deviations of the average pixel tree cover estimates fell within the average across period standard deviations of our forest regrowth trajectories (Figure 3-5), indicating that phenology effects did not

prevent the forest regrowth curves from capturing the response of the original pixel values.

In general, our date-invariant regression approach improves on similar change detection techniques such as post-classification comparison (Coppin et al., 2004) which rely on simple image differencing of two or more independently produced classifications to estimate forest change. Here we derive a more meaningful characterization of continuous forest change after clearcut harvest by employing a robust radiometric calibration procedure specifically designed to reduce the residual scatter in forest regrowth spectral trajectories (Schroeder et al., 2006) and by basing our estimates of forest change on continuous trajectories of percent tree cover. Although here we binned the continuous tree cover trajectories into forest regrowth change classes, the trajectory approach also lends itself to more detailed quantification of forest regrowth information through parameterization of the fitted mean trajectory curves (Figure 3-5) (Lawrence and Ripple, 1999; and Yang et al., 2005).

4.2. Patterns of Forest Regrowth after Clearcut Harvesting

It was presumed that forest succession was initiated in our study by stand-replacing disturbance from clearcut harvesting, after which vegetation communities are thought to shift from ephemeral herbaceous life forms to taller perennial shrubs and finally trees (Franklin et al., 2002). These stages of successional development which are common to western Oregon have been previously classified with percent

tree cover trajectories from repeated airphoto interpretation (Yang et al., 2005), where shrub and herb dominance lasts until roughly 30% tree cover is achieved, at which time semi-closed conditions persist until canopy closure (≥ 70% tree cover). Upon inspection, the endpoints of our forest regrowth class trajectories (Figure 3-5) derived by date-invariant regression seem to coincide well with these previously defined successional stage classes (e.g., little to no forest regrowth class corresponds to open and shrub/herb successional stages; slow forest regrowth class corresponds to the end of shrub/herb successional stage; moderate forest regrowth corresponds to semi-closed forest successional stage; and fast forest regrowth class corresponds to closed canopy forest successional stage). The similarity with which patterns of continuous forest succession can be classified with airphoto and satellite based tree cover trajectories suggests that our date-invariant regression approach has successfully extended the forest regrowth trajectory concept to the spectral space of Landsat.

In terms of forest succession, our forest regrowth classes derived by date-invariant regression indicated that a wide range of successional stages could be found in both the CRP and WCP 18 years after clearcut harvesting. The large difference in tree cover regrowth rates between the little to no (Figure 3-5a) and fast forest regrowth (Figure 3-5d) classes substantiates previous findings that rates of vegetation recovery after disturbance in western Oregon can be highly variable (Halpern, 1988; Myster and Pickett, 1994, Nesje, 1996; and Lutz and Halpern, 2006). Because our forest regrowth classes were explicitly defined in Landsat

spectral space, we were able to summarize the landscape patterns of forest regrowth after clearcut harvesting at the pixel scale using frequency distributions (Figures 3-6 – 3-9) based on the "percent of clearcut area" metric (i.e., area of each forest regrowth class ÷ total area clearcut per harvest period).

Examination of the forest regrowth class distributions in Figure 6 indicate that 18 years after clearcut harvest a much higher proportion of disturbed forest land returned to semi-closed and closed canopy conditions in the CRP (≈70%) than in the WCP (≈50%). Conversely, a much higher proportion of disturbed land persisted in open or semi-closed condition in the WCP (≈34%) than in the CRP (≈10%). Similar distributional patterns of forest regrowth have been previously observed for the CRP and WCP (Yang et al., 2005), and are further substantiated here based on the high degree of distributional consistency observed across three periods of forest clearcuts (Figure 3-6).

As our forest regrowth trajectories were derived in Landsat spectral space, we could further examine the landscape distribution of forest regrowth in relation to several topographic variables thought to influence vegetation growth rates. These distributions revealed several ecologically interpretable patterns in forest regrowth after clearcut harvesting, such as a decrease in fast and increase in slow forest regrowth on southerly aspects (Figure 3-7), on steeper slopes (Figure 3-8) and at higher elevations (Figure 3-9). In general, the rate of forest regrowth seemed most effected by elevation (i.e., as elevation increased rate of forest regrowth tended to get slower) and least affected by steepness of slope (i.e., forest regrowth

classes were distributed somewhat evenly across slope classes). It is possible that spectral variation associated with sun-angle effects could be contributing to the detection of slower regrowth on southern aspects (e.g., more sun on southern exposures will brighten the spectral signal, resulting in the prediction of less tree cover). Using only the FIA plot data (n = 54) we found no statistical difference at the 95% confidence level (ANOVA, F = 1.15, p = 0.30) between mean tree cover of young stands (< 20 yrs of age) located on northern and southern aspects. Given the small sample size, we draw the conclusion that more work is needed to fully understand the effect of sun-angle on the characterization of forest regrowth rates with optical satellite imagery.

Overall, both the forest regrowth class trajectories (Figure 3-5) and the frequency distributions of the forest regrowth classes (Figures 3-6 – 3-9) indicated that forest regrowth rates after clearcut harvesting in western Oregon varied both within and across ecological provinces. At the landscape scale we attributed some of the across province variability in forest regrowth rates to climatic and vegetative differences between the CRP and WCP. With a longer and more favorable growing season (i.e., more annual rainfall and deep, rich soils) the CRP was found to have a larger proportion of fast forest regrowth than observed in the WCP, which is much drier and warmer during the summer growing season (Franklin and Dyrness, 1988). We also observed elevation as a potential limiting factor to forest regrowth (Figure 3-9), which could explain in part the propensity for little to no and slow forest regrowth in the more mountainous WCP. Within-province differences

in forest regrowth after clearcut harvest are likely the result of local site conditions, as well as forest management practices.

4.3. Predicting Rates of Post-harvest Forest Regrowth with CART

The extension of forest regrowth trajectories to the spectral space of Landsat provided the opportunity to more fully investigate the climatic and topographic attributes influencing the rate of forest regrowth following clearcut harvesting in western Oregon. Although the overall accuracies of the CART models were not high in terms of correctly classified test samples (Tables 3-4 and 3-5), the resulting classification decision rules provided interesting insights into the geographically referenced environmental attributes influencing forest succession in both ecological provinces. The CRP CART model (Figure 3-10) had more decision pathways or terminal nodes (10) than the WCP CART model (6) (Figure 3-11), indicating that more favorable growing conditions common to the CRP could possibly result in more complex interactions among plant relevant and physical proxy variables influencing post-harvest forest regrowth. Another possibility is that more subtle environmental gradients influencing forest regrowth may not be detectable with simple dichotomous models like CART. As both physical proxy (aspect, slope and elevation) and plant relevant (precipitation, temperature, soil silt, radiation) explanatory variables were input into the CART models, the relative importance of each type of predictor could be implied based on model inclusion, whereas the relative importance of each selected predictor could be assessed

according to the amount of variance explained (i.e., branch length in Figures 3-10 – 3-11).

The importance of plant relevant predictor variables is apparent as 5 of the 7 predictor variables selected for use in both CART models are known to directly influence forest growth (PRR radiation, PRISM average annual precipitation, PRISM July maximum temperature, PRISM January minimum temperature, and CONUS soil silt). Of the explanatory variables selected, three (elevation, PRR, PRISM July maximum temperature) were used in both the CRP and WCP models. Elevation was found to explain the largest percentage of variation in both forest regrowth models. Although elevation is not known to directly influence forest regrowth, it has been shown to influence air and soil temperatures, length of growing season, amount of damage from wind and snow, and amount of moisture from orographic precipitation (Nesje, 1996). PRR explained the next largest amount of variation in both CART models, indicating that radiation variables such as PRR which integrate annual changes in solar orientation and shading effects from local topography are likely more effective at capturing landscape radiation patterns than commonly used physical proxies (i.e., slope and aspect) (Lookingbill and Urban, 2005; and Pierce et al., 2005). Interestingly the interaction between elevation and radiation has been previously found to be a limiting factor to post-harvest forest successional rates in western Oregon (Cleary et al., 1978). Summer temperature was also used by both CART models, indicating that even at relatively coarse spatial resolutions (1 km) useful climatic patterns can still be resolved.

Since both CART models yielded only “fair agreement” (as measured by Kappa; Landis and Koch, 1977) between the predicted forest regrowth classes and the test samples we combined the four forest regrowth classes into two general “fast” and “slow” categories to gauge the statistical effectiveness of predicting more generalized post-harvest forest regrowth rates. Based on the Tau statistic, the CART models correctly classified a higher percentage of test samples than classification of the four forest regrowth classes, suggesting that more general regrowth classes may be more predictable at the landscape scale.

5. CONCLUSION

The rate at which forest vegetation re-establishes dominance after clearcut harvesting can impact many ecological processes. Although knowing a forest stand’s current state of succession is useful, a more robust characterization can be achieved with the use of continuous trajectories developed with time-series data. A useful methodology was presented which uses a Landsat image time-series to more fully understand the spatial extent, as well as the environmental attributes influencing post-harvest forest regrowth rates in western Oregon forests.

Our methodology required that the Landsat image time-series be transformed to a more meaningful biophysical measure (i.e., percent tree cover). This was accomplished through date-invariant regression, which is the extrapolation of an initial regression model developed between a single Landsat image and ground measured data to a series of cross-normalized images. Here we

extrapolated an initial percent tree cover model to 19 images which had been previously calibrated to a common radiometric scale using the "absolute-normalization" approach of Schroeder et al. (2006). The accuracy of the resulting tree cover estimates were successfully evaluated across time using two sets of photointerpreted tree cover data. Three periods of clearcut harvests were mapped and used to extract tree cover estimates, which were subsequently classified into four main rate classes (little to no, slow, moderate and fast). These forest regrowth rate classes were then used to develop frequency distributions describing the landscape patterns of forest regrowth in western Oregon.

The patterns of forest regrowth observed over the three clearcut periods indicated a much higher percentage of fast regrowth in the CRP and a much higher percentage of little to no regrowth in the WCP. For both ecological provinces we observed the propensity for faster regrowth on north facing aspects, shallow slopes and at low elevations. Overall, the forest regrowth classes and the frequency distributions indicated that a wide range of successional stages could be found in both the CRP and WCP 18 years after clearcut harvesting. This wide range in successional stage classes corroborates previous findings that rates of forest regrowth after disturbance in western Oregon can be highly variable (Halpern, 1988; Myster and Pickett, 1994, Nesje, 1996; and Lutz and Halpern, 2006). The development of forest regrowth trajectories using spectral data from Landsat provided an opportunity to use CART statistical analysis to more fully investigate

the climatic and topographic attributes influencing post-harvest forest regrowth rates in western Oregon.

Both CART models provided ecologically interpretable insights into the environmental attributes influencing forest regrowth rates in both ecological provinces. Elevation followed by relative radiation expressed by PRR explained the largest amount of variation in forest regrowth, substantiating previous findings that elevation and radiation interact to influence local site factors limiting post-harvest successional rates (Cleary et al., 1978). We observed only "fair agreement" (as measured by Kappa; Landis and Koch, 1977) between predicted forest regrowth classes and the test samples, however when combined into two general "fast" and "slow" categories the CART models correctly classified 12% (CRP) and 26% (WCP) percent more test samples than classification of the four regrowth classes. Overall, the CART models yielded ecologically interpretable results regarding the environmental attributes (both physical proxy and plant relevant) influencing landscape scale early forest successional patterns in western Oregon.

ACKNOWLEDGMENTS

We gratefully acknowledge data and financial support provided by the USDA Forest Service Pacific Northwest Research Station's Forest Inventory and Analysis Program. The authors also wish to thank Pacific Northwest Research station's Scott Powell for assistance with the CART statistical modeling and Ken Pierce and Matt Gregory for assistance with PRR calculations.

REFERENCES CITED

Armesto, J.J., and Pickett, S.T.A. (1986). Removal experiments to test mechanisms of plant succession in oldfields. *Vegetatio*. 66, 85–93.

Beers, T.W., Press, P.E., and Wensel, L.C. (1966). Aspect transformation in site productivity research. *Journal of Forestry*. 64, 691–692.

Canty, M.J., Nielsen, A.A., and Schmidt, M. (2004). Automatic radiometric normalization of multitemporal satellite imagery. *Remote Sensing of Environment*. 91, 3-4, 441–451.

Cleary, B, Greaves, R., and Hermann, R. (ed). (1978). Regenerating Oregon's Forests: A Guide for the Regeneration Forester. Oregon State University Extension Service. Corvallis, OR. pp. 7–27.

Cohen, W.B., Fiorella, M., Gray, J., Helmer, E., and Anderson, K. (1998). An Efficient and accurate method for mapping forest clearcuts in the Pacific Northwest using Landsat imagery. *Photogrammetric Engineering and Remote Sensing*. 64, 293–300.

Cohen, W.B., Maiersperger, T.A., Spies, T.A., and Oetter, D.R. (2001). Modeling forest cover as continuous variables in a regional context with Thematic Mapper data. *International Journal of Remote Sensing*. 22, 12, 2279–2310.

Cohen, W.B., Spies, T.A., Alig, R.J., Oetter, D.R., Maiersperger, T.K., and Fiorella, M. (2002). Characterizing 23 years (1972–95) of stand replacement Disturbance in western Oregon forests with Landsat imagery. *Ecosystems*. 5, 122–137.

Cohen, W.B., Maiersperger, T.K., Gower, S.T., and Turner, D.P. (2003). An improved strategy for regression of biophysical variables and Landsat ETM+ data. *Remote Sensing of Environment*. 84, 561–571.

Cohen, W.B., and Goward, S.N. (2004). Landsat's role in ecological applications of remote sensing. *Bioscience*. 54, 6, 535–545.

Congalton, R.G. (1991). A review of assessing the accuracy of classification of remotely sensed data. *Remote Sensing of Environment*. 37, 35–46.

Coppin, P., Jonckheere, I., Nackaerts, K., and Muys, B. (2004). Digital change detection methods in ecosystem monitoring: A review. *International Journal of Remote Sensing*. 25, 9, 1565–1596.

Crist, E.P., and Cicone, R.C. (1984). A physically-based transformation of thematic Mapper data – the TM tasseled cap. *IEEE Transactions on Geoscience and Remote Sensing*. 22, 3, 256–263.

Daly, C., Neilson, R.P., and Phillips, D.L. (1994). A statistical-topographic model for mapping climatological precipitation over mountainous terrain. *Journal of Applied Meteorology*. 33, 140–158.

del Moral, R., and Bliss, L.C. (1993). Mechanisms of primary succession: insights resulting from the eruption of Mount St. Helens, In Advances in Ecological Research (M. Began and A. Fitter, Eds.). Academic, London, Vol. 24, pp. 1–66.

Fiorella, M., and Ripple, W.J. (1993). Determining successional stage of temperate coniferous forests with Landsat satellite data. *Photogrammetric. Engineering and Remote Sensing*. 59, 2, 236–239.

Foody, G. M., Palubinskas, G., Lucas, R. M., Curran, P. J. and Honzak, M. (1996). Identifying terrestrial carbon sinks: classification of successional stages in regenerating tropical forest from Landsat TM data. *Remote Sensing of Environment.* 55, 205–216.

Friedl, M.A., and Brodley, C.E. (1997). Decision tree classification of land cover from remotely sensed data. *Remote Sensing of Environment*. 61, 399–409.

Franklin, J., and Dyrness, C. (1988). Natural Vegetation of Oregon and Washington. Oregon State University Press, Corvallis, OR.

Franklin, J.F., Spies, T.A., Van Pelt, R.V., Carey, A.B., Thornburgh, D.A., Berg, D.R., Lindenmayer, D.B., Harmon, M.E., Keeton, W.S., Shaw, D.C., Bible, K., and Chen, J. (2002). Disturbances and structural development of natural forest ecosystems with silvicultural implications, using Douglas-fir forests as an example. Forest *Ecology and Management*. 155, 399–423.

Hall, F.G., Botkin, D.B., Strebel, D.E., Woods, K.D. and Goetz, S.J. (1991). Large-scale patterns of forest succession as determined by remote sensing. *Ecology*. 72, 2, 628–640.

Halpern, C.B. (1988). Early successional pathways and the resistance and resilience of forest communities. *Ecology*. 69, 1703–1715.

Halpern, C.B. (1989). Early successional patterns of forest species: interactions Of life history traits and disturbance. *Ecology*. 70, 704–720.

Halpern, C.B., and Franklin, J.F. (1990). Physiognomic development of Pseudotsuga forests in relation to initial structure and disturbance intensity. *Journal of Vegetation Science*. 1, 475–482.

Hardisky, M.A., Klemas, V., and Smart, R.M. (1983). The influence of soil salinity, growth form, and leaf moisture on the spectral radiance of *Spartina alterniflora* canopies. *Photogrammetric Engineering and Remote Sensing*. 49, 77–83.

Healey, S.P., Yang, Z., Cohen, W.B., and Pierce, D.J. (2006). Application of two regression-based methods to estimate the effects of partial harvest on forest structure using Landsat data. *Remote Sensing of Environment*. 101, 115–126.

Hegler, L. (1968). A method for constructing site-index curves from stem analysis. *Forestry Chronicles*. 21, 11–15.

Horler, D.N., and Ahern, F.J. (1986). Forestry information content of Thematic Mapper data. *International Journal of Remote Sensing*. 7, 3, 405–428.

Jakubauskas, M.E. (1996). Thematic Mapper characterization of lodgepole pine seral stages in Yellowstone National Park, USA. *Remote Sensing of Environment*. 56, 118–132.

Jensen, J.R. (1996). Introductory digital image processing: A remote sensing perspective. 2nd ed. Englewood Cliffs, NJ. Prentice Hall.

Jin, S., and Sader, S.A. (2005). Comparison of time series tassesled cap wetness and the normalized difference moisture index in detecting forest disturbances. *Remote Sensing of Environment*. 94, 364–372.

Joyce, S. and Olsson, H. (1999). Long-term forest monitoring with temporal-Spectral trajectories from Landsat TM data. IUFRO Div. 4. Rogow, Poland. http://rogow99.sggw.waw.pl/03_poster_session/08/.

Landis, J.R., and Koch, G.G. (1977). The measurement of observer agreement for categorical data. *Biometrics*. 33, 159–174.

Lawrence, R.L., and Ripple, W.J. (1999). Calculating change curves for multitemporal satellite imagery: Mount St. Helens 1980-1995. *Remote Sensing of Environment*. 67, 309–319.

Lawrence, R.L., and Ripple, W.J. (2000). Fifteen years of revegetation of Mount St. Helens: A landscape-scale analysis. *Ecology*. 81, 2742–2752.

Lawrence, R.L., and Wright, A. (2001). Rule-based classification systems using Classification and Regression Tree (CART) Analysis. *Photogrammetric* Engineering and Remote Sensing. 67, 10, 1137–1142.

Lillesand, T.M., Kiefer, R.W., and Chipman, J.W. (2004). Remote sensing and image interpretation. 5th ed. Hoboken, NJ. John Wiley & Sons, Inc.

Lookingbill, T.R., and Urban, D. L. (2005). Gradient analysis, the next generation: towards more plant-relevant explanatory variables. *Canadian Journal of Forest Research*. 35, 1744–1753.

Lucas, R. M., Honzak, M., DO Amaral, I., Curran, P. J. and Foody, G. M. (2002). Forest regeneration on abandoned clearances in central Amazonia. *International Journal of Remote Sensing*. 23, 5, 965–988.

Lutz, J.A., and Halpern, C.B. (2006). Tree mortality during early forest development: A long-term study of rates, causes and consequences. *Ecological Monographs*. 76, 2, 257–275.

Ma, Z and Redmond, R.L. (1995). Tau coefficients for accuracy assessment of classification of remote sensing data. *Photogrammetric Engineering and Remote Sensing*. 61, 4, 435–439.

Miller, D.A., and White, R.A. (1998). A conterminous United States multi-layer soil characteristics data set for regional and climate and hydrology modeling. *Earth Interactions*. 2, 2, 1–26.

Myster, R.W., and Pickett, S.T.A. (1994). A comparison of rate of succession over 18 years in 10 contrasting old fields. *Ecology*. 75, 387–392.

Nesje, A.M. (1996). Spatial patterns of early forest succession in Lookout Creek basin. M.Sc. thesis. Oregon State University, Corvallis, OR.

O'Connell, K.E.B., Acker, S.A., Bruner, H.J., Halpern, C.B., and Harmon, M.E. (unpublished). Carbon dynamics of Douglas-fir forests with different successional rates after timber harvest.

Ohmann, J.L., and Gregory, M.J. (2002). Predictive mapping of forest composition and structure with direct gradient analysis and nearest neighbor imputation in coastal Oregon, U.S.A. *Canadian Journal of Forest Research*. 32, 725–741.

Peterson, U., and Nilson, T. (1993). Successional reflectance trajectories in northern Temperate forests. *International Journal of Remote Sensing*. 14, 3, 609–613.

Pierce, K.B., Lookingbill, T., and Urban, D. (2005). A simple method for estimating potential relative radiation (PRR) for landscape-scale vegetation analysis. *Landscape Ecology*. 20, 137–147.

Richards, F.J. (1959). A flexible growth function for empirical use. *Journal of Experimental Botany*. 10, 290–300.

Rouse, J.W., Haas, R.H., Shell, J.A., and Deering, D.W. (1973). Monitoring vegetation systems in the Great Plains with ERTS-1. In Third Earth Resources Technology Satellite Symposium. Vol. 1, pp. 309–317.

Sabol, D.E., Gillespie, A.R., Adams, J.B., Smith, M.O., and Tucker, C.J. (2002). Structural stage in Pacific Northwest forests estimated using simple mixing models of multispectral images. *Remote Sensing of Environment*. 80, 1–16.

Schroeder, T.A., Cohen, W.B., Song, C., Canty, M.J., and Yang, Z. (2006). Radiometric correction of multi-temporal Landsat data for characterization of early successional forest patterns in western Oregon. *Remote Sensing of Environment*. 103, 1, 16–26.

Smith, M.O., Ustin, S.L., Adams, J.B., and Gillespie, A.R. (1990). Vegetation in deserts: I. A regional measure of abundance from multispectral images. *Remote Sensing of Environment*. 31, 1–26.

Song, C., Schroeder, T.A., and Cohen, W.B. (2007). Predicting temperate conifer forest successional stage distributions with multi-temporal Landsat Thematic Mapper Imagery. *Remote Sensing of Environment*. 106, 228–237.

Tappeiner, J.C., Huffman, D., Marshall, D., Spies, T.A., and Bailey, J.D. (1997). Density, ages, and growth rates in old-growth and young-growth forests in coastal Oregon. *Canadian Journal of Forest Research*. 27, 638–648.

USDA Forest Service. (1995). Field instructions for the inventory of western Oregon 1995–97, http://www.fs.fed.us/pnw/fia/publications/fieldmanuals.shtml.

Venables, W.N., and Ripley, B.D. (1997). Modern Applied Statistics with S-plus. Second Edition, Springer-Verlag, New York, NY. 548p.

Vermote, E.F., Tanre, D., Deuze, J.L., Herman, M, and Morcrette, J.J. (1997). Second simulation of the satellite signal in the solar spectrum, 6S: an overview. *IEEE Transactions on Geoscience and Remote Sensing*. 35, 895–934.

Viedma, O., Meliá, J., Segarra, D., and García-Haro, J. (1997). Modeling rates of ecosystem recovery after fires by using Landsat TM data. *Remote Sensing of Environment*. 61, 383–398.

Yang, Z., Cohen, W.B., and Harmon, M.E. (2005). Modeling early forest succession following clear-cutting in western Oregon. *Canadian Journal of Forest Research*. 35, 1889–1900.

FIGURES

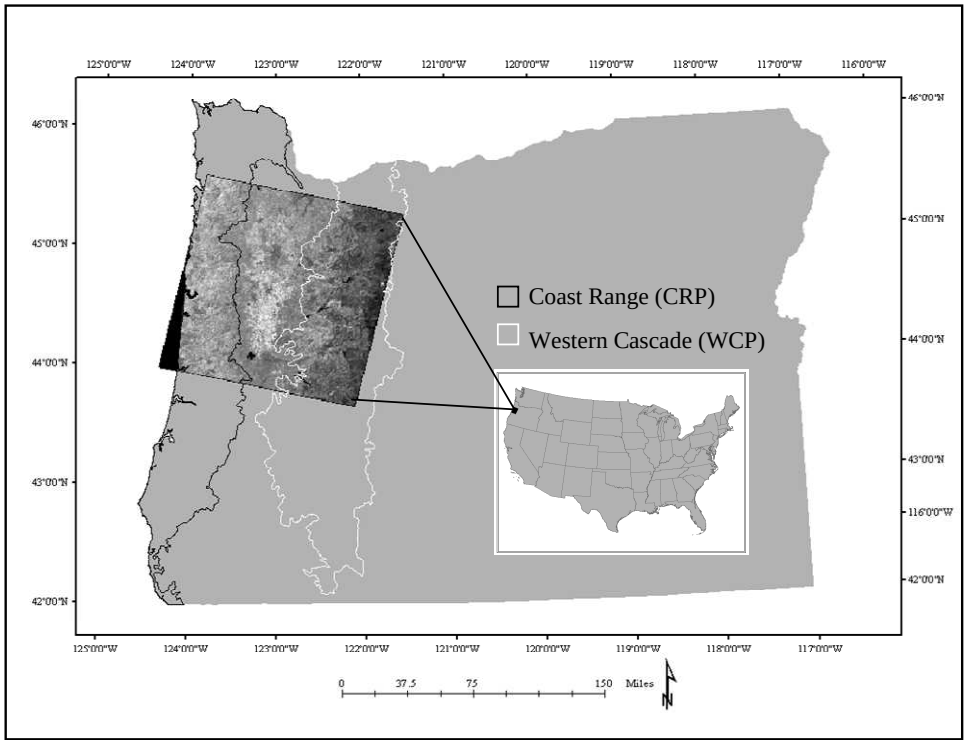

Figure 3-1. Landsat WRS-2, path 46 row 29 study area showing Coast Range (CRP) and Western Cascade (WCP) ecological provinces in western Oregon, U.S.A.

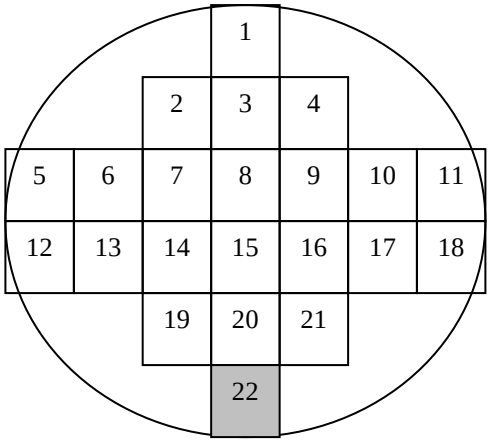

Figure 3-2. Mask used to extract mean Landsat spectral data over FIA plots. Gray shading indicates the anchor pixel matched to each plot coordinate.

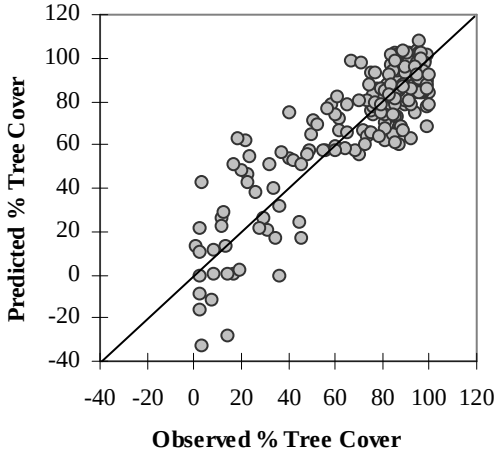

Figure 3-3. Predicted (from cross-validation) versus observed percent tree cover from initial RMA regression model (n = 202). Solid line is 1:1.

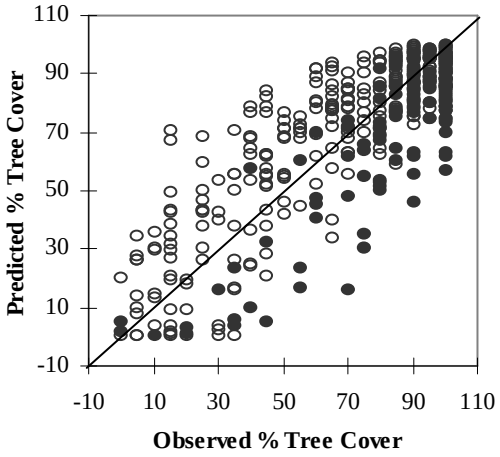

Figure 3-4. Predicted (from date-invariant regression) versus observed percent tree cover from airphoto interpretation data. Filled circles represent interpreter 1 (n=162), open circles interpreter 2 (n = 249). Solid line is 1:1.

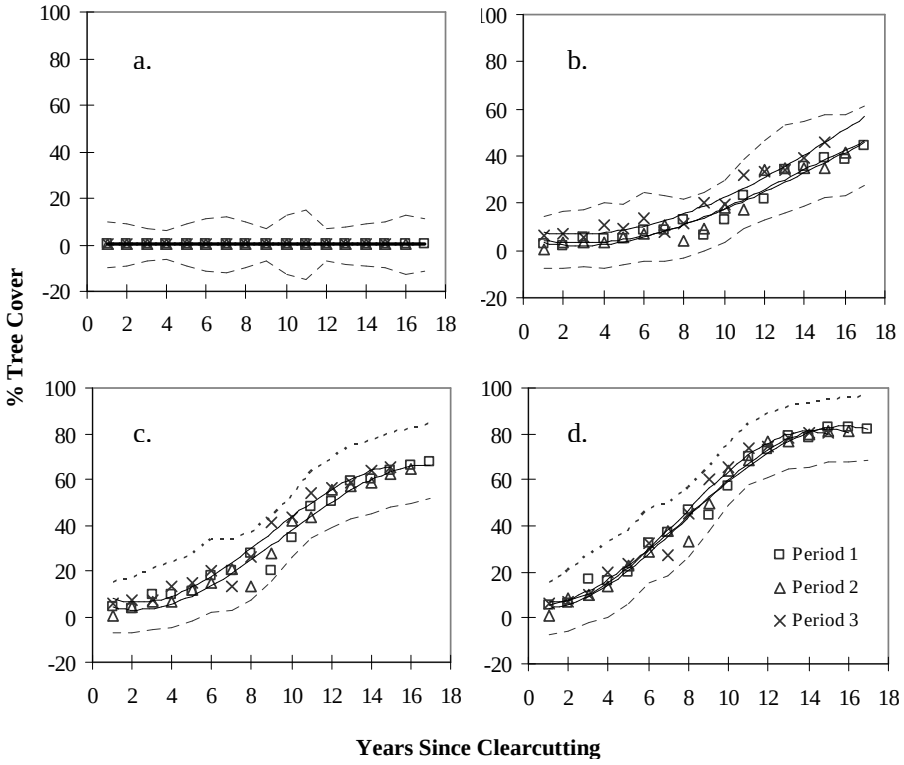

Figure 3-5. Mean forest regrowth trajectories for a. little to no, b. slow, c. moderate, and d. fast regrowth classes. Solid lines are fitted 3rd order polynomial curves; dashed lines are the average across period standard deviations.

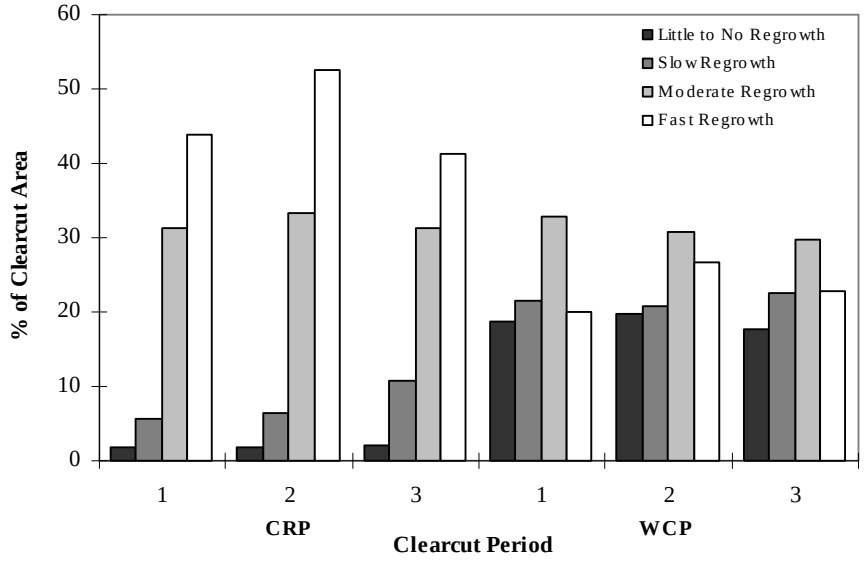

Figure 3-6. Landscape scale forest regrowth patterns based on the percentage of clearcut area (i.e., area of each forest regrowth class ÷ total area clearcut per harvest period). Clearcuts were mapped between 1986 – 1987 (period 1), 1987 – 1988 (period 2), and 1988 – 1989 (period 3).

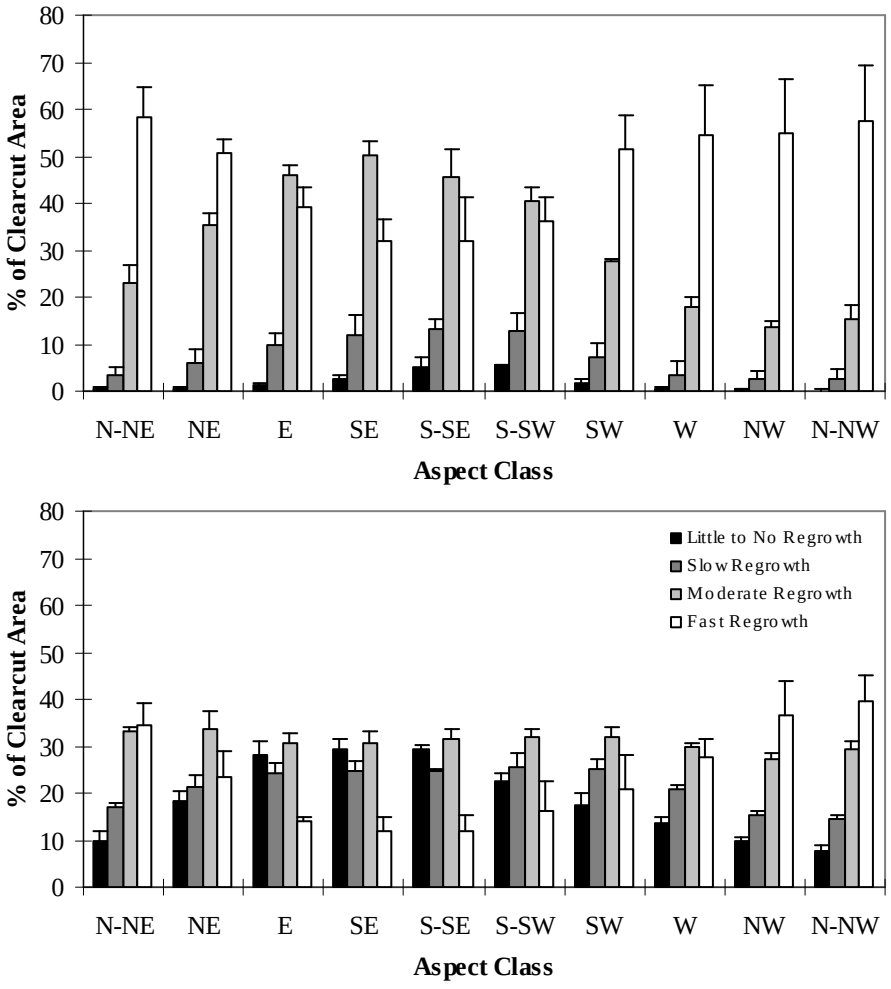

Figure 3-7. Patterns of forest regrowth according to aspect class. Top panel is CRP, bottom panel is WCP. Error bars represent across period standard deviations.

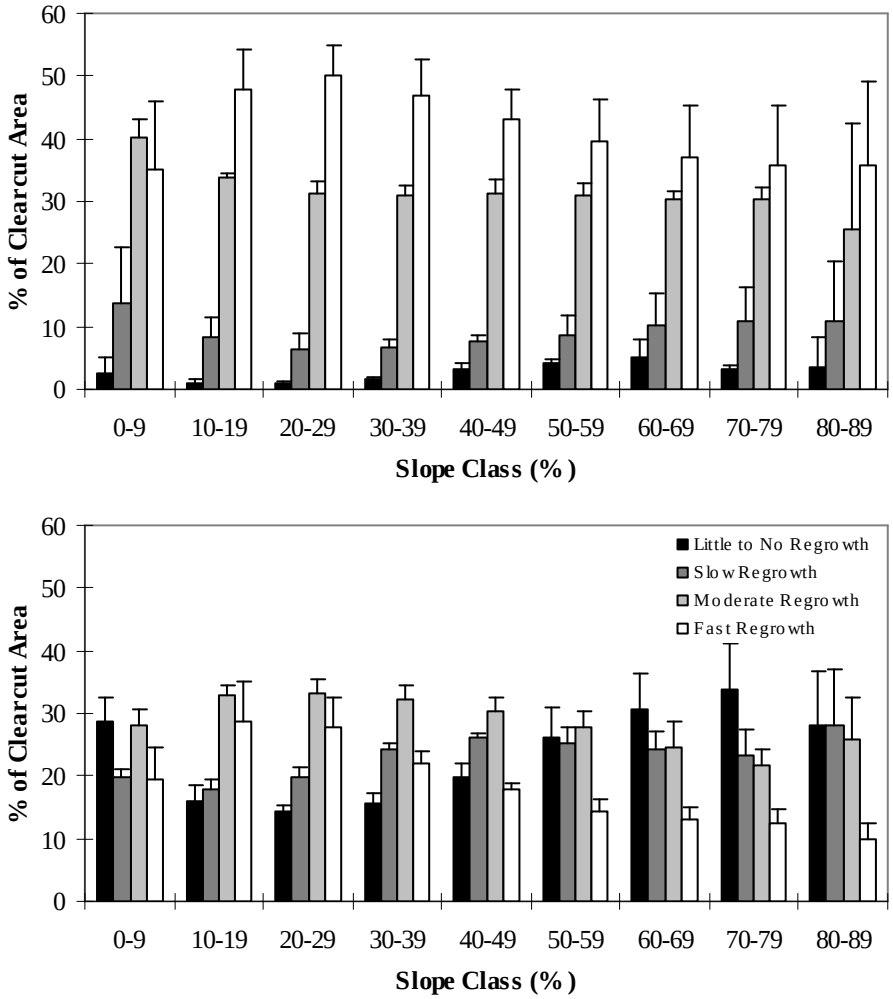

Figure 3-8. Patterns of forest regrowth according to slope class. Top panel is CRP, bottom panel is WCP. Error bars represent across period standard deviations.

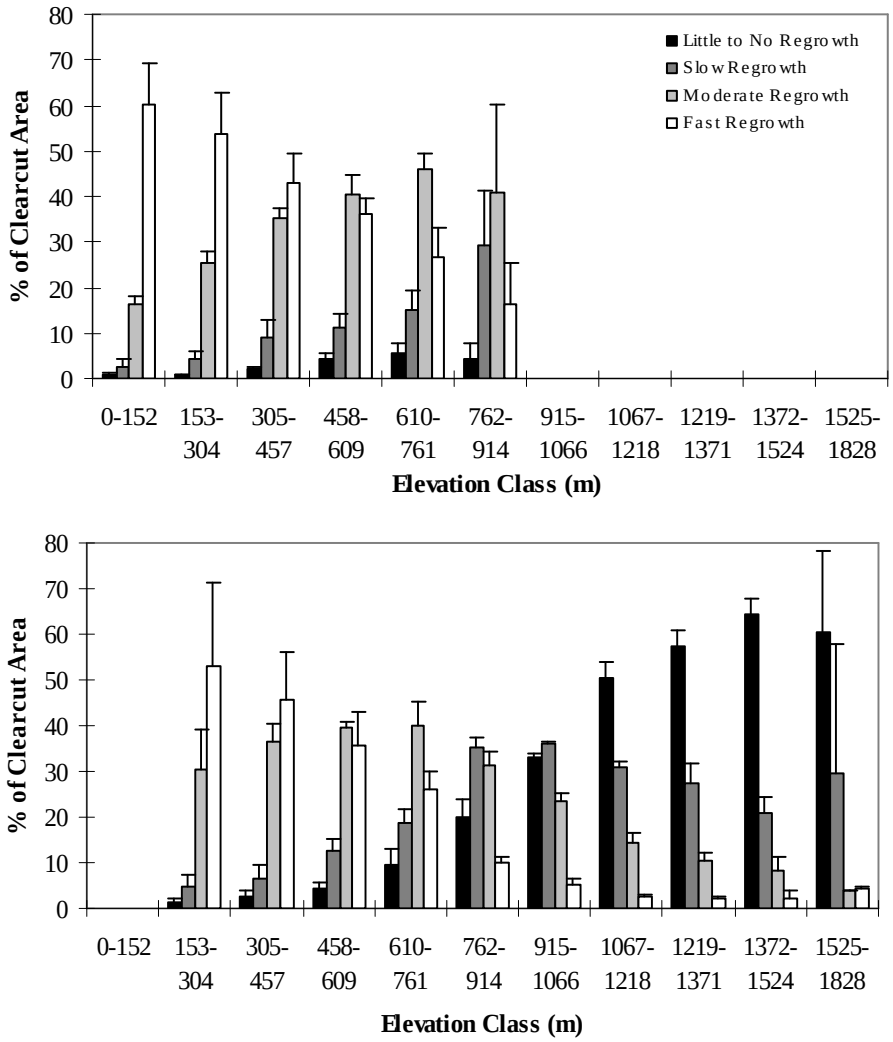

Figure 3-9. Patterns of forest regrowth according to elevation class. Top panel is CRP, bottom panel is WCP. Error bars represent across period standard deviations.

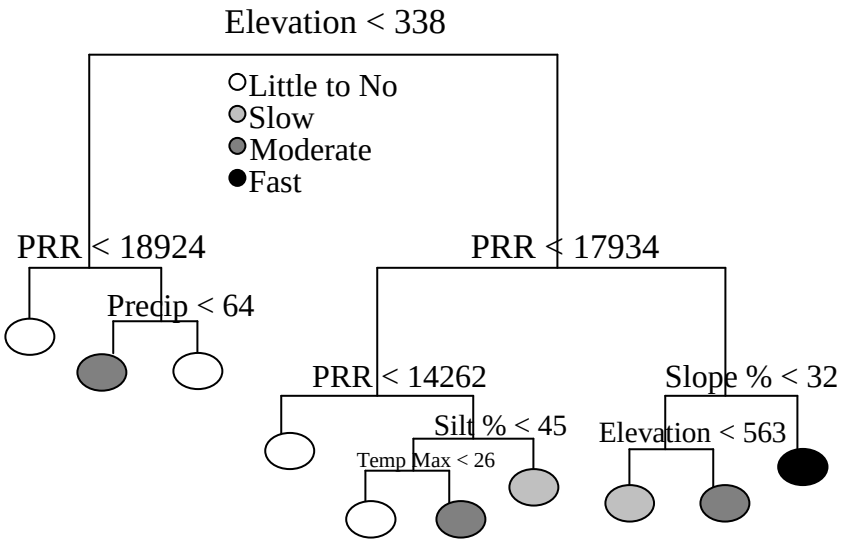

Figure 3-10. CART classification tree model for the CRP.

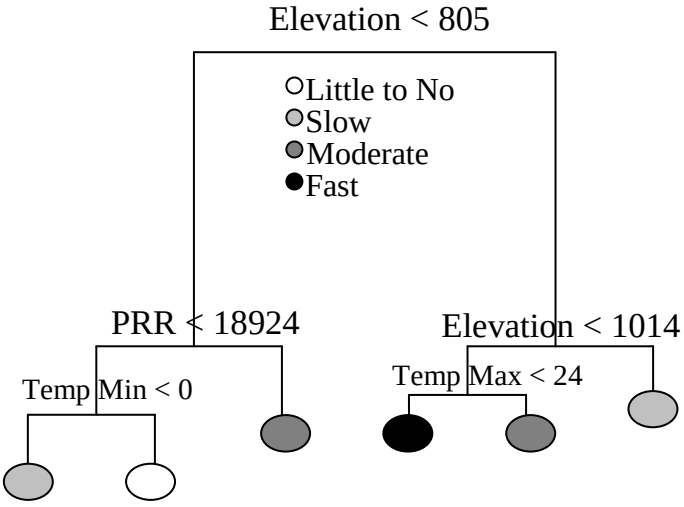

Figure 3-11. CART classification tree model for the WCP.

TABLES

Table 3-1. Landsat path 46 row 29 multi-temporal image series.

Sensor	Date
TM	8/26/1986
TM	7/12/1987
TM	8/31/1988
TM	9/3/1989
TM	7/7/1991
TM	8/10/1992
TM	8/29/1993
TM	7/31/1994
TM	8/19/1995
TM	8/21/1996
TM	7/23/1997
TM	8/11/1998
TM	8/16/2000
TM	8/25/2003
TM	7/26/2004
TM	7/29/2005
ETM+	8/22/1999
ETM+	7/26/2001
ETM+	7/29/2002

Table 3-2. Airphoto based percent tree cover validation data set. BW stands for Black and White.

Year of Photo	Interpreter	Scale	Format	n
1987-1988	2	1 : 40 000	BW	81
1989	2	1 : 12 000	True Color	33
1990-1992	2	1 : 12 000	True Color	18
1993-1995	2	1 : 12 000	True Color	26
1997-1998	2	1 : 12 000	True Color	91
1994	1	1 : 24 000	True Color	125
2000	2	1 : 40 000	BW	37
Total				411

Table 3-3. Regression parameters for the initial percent tree cover and airphoto validation models.

Model	n	Slope	Intercept	Mean	Bias	R^2	RMSE
Initial RMA	202	1.14	-9.66	70.97	0.03	0.77	14.15
Airphoto Validation	411	0.94	3.66	69.38	0.00	0.68	16.09

Table 3-4. Classification error matrices for the CRP and WCP CART models.

CRP	Little to No	Slow	Moderate	Fast	Producers	Users
Little to No	**150**	40	57	34	58%	53%
Slow	70	**50**	101	82	37%	17%
Moderate	30	30	**100**	138	34%	34%
Fast	10	15	40	**242**	49%	79%
WCP	Little to No	Slow	Moderate	Fast	Producers	Users
Little to No	**189**	57	29	3	49%	68%
Slow	136	**93**	60	15	38%	31%
Moderate	51	66	**88**	101	35%	29%
Fast	8	31	71	**190**	61%	63%
	CRP	WCP				
Overall	45.58%	47.14%				
Kappa	27.00%	29.00%				
Tau	27.44%	29.51%				

Table 3-5. Aggregated classification error matrices for the CRP and WCP CART models.

CRP	Slow	Fast	Producers	Users
Slow	**310**	274	78%	53%
Fast	85	**520**	65%	86%
WCP	Slow	Fast	Producers	Users
Slow	**475**	107	75%	82%
Fast	156	**450**	81%	74%
	CRP	WCP		
Overall	69.81%	77.86%		
Kappa	39.25%	55.78%		
Tau	39.60%	55.72%		

Chapter 4 – Estimating Live Forest Carbon with a Landsat Based Curve Fitting Approach

Todd A. Schroeder[§], Andrew Gray[†], Mark E. Harmon[§],
Warren B. Cohen[†] and David O. Wallin[±]

[§] Department of Forest Science, Forestry Sciences Laboratory,

Oregon State University, Corvallis, OR 97331 USA

[†] Forestry Sciences Laboratory, Pacific Northwest Research Station,

USDA Forest Service, 3200 SW Jefferson Way, Corvallis, OR 97331 USA

± Department of Environmental Sciences, Huxley College of the Environment,

Western Washington University, Bellingham, WA, 98225 USA

Forest Science Department
Richardson Hall
Oregon State University
Corvallis, OR 97331

ABSTRACT

No matter the cause, global climate change has prompted an accelerated use of spatially explicit models to study carbon exchange over the terrestrial system. Regardless of modeling strategy it is important that estimates of total carbon flux from terrestrial sources account not only for live carbon stocks, but also for other major component pools such as soils, woody detritus and forest products. Although an integrated approach is required to fully understand the flux of carbon to and from forests, estimates of the living mass are critical for initializing component pools in regional scale models and to form baselines from which to estimate loss from cultivation. Optical satellite imagery has been used to estimate aboveground biomass, however these methods have generally proved ineffective at providing useful estimates for high biomass forests of the Pacific Northwest. Thus, we present an alternative modeling strategy which takes advantage of Landsat's temporal and spectral characteristics to predict live forest carbon through integration of age and site index maps and a set of locally calibrated Chapman-Richards curves. As this curve-fitting approach has been previously used in conjunction with a multi-component model to estimate total carbon flux for western Oregon, we sought a robust evaluation of its ability to estimate live forest carbon at multiple scales. Predictions from the curve-fit model were evaluated at the local (pixel level) and landscape (total carbon and carbon flux) scales for two forested ecoregions (Coast Range Province – CRP and Western Cascade Province – WCP) using two periods of FIA field inventory data. At the pixel level, the curve-fit

model performed better (i.e., higher correlation, lower RMSE) in the CRP than the WCP, likely the result of faster, less variable growth patterns common to the CRP. Model predictions for both ecoregions were observed to have large positive bias statistics, resulting in over-prediction of low to mid-range carbon values and under-prediction of high end carbon values. At the landscape scale, the curve-fit model also over-predicted total study area forest carbon for both inventory periods. Although this over-estimation was significant (average of 138.32 Tg per inventory period) in absolute terms, the flux (i.e., difference between inventory periods) estimated by the curve-fit model was found to be well within the standard error of the inventory estimates. Inventory data is generally considered one of the more reliable means from which to estimate carbon balances over large areas, although for this to be true the sample plots must capture the spatial and temporal changes in land-use patterns occurring on the landscape. To gauge the sense to which the inventory plots captured the forest condition in our study area we compared frequency histograms and stand age chronosequences of Landsat wetness derived for the full study area and for the inventory plots. The study area and inventory based frequency histograms had the same general shape and magnitude of wetness, however the map based stand age chronosequence detected a subtle shift in land-use which was not captured by the inventory sample. Although optical satellite imagery is limited in its ability to directly estimate forest carbon, we found Landsat's temporal (e.g., age maps) and spectral (e.g., wetness chronosequences)

characteristics to be useful inputs to a curve based model which was found to estimate carbon flux from forests within the standard error of inventory estimates.

1. INTRODUCTION

As the global climate continues to warm (Keeling, 2004) and countries around the world are tasked with estimating and reporting changes in terrestrial carbon stocks (e.g., Kyoto protocol) new and innovative techniques must be developed to accurately estimate forest carbon over vast spatial areas. Developing reliable estimates of terrestrial carbon flux is a difficult task as all the major terrestrial carbon pools exhibit considerable variability across space and time (Solomon et al., 1993). Terrestrial carbon fluxes cannot be measured directly, thus at regional and global scales we must rely on estimates derived from models which can be process (Landsberg and Waring, 1997; and Turner et al., 2004) or accounting based (Wallin et al., 1996, Cairns et al., 2000). Regardless of modeling strategy it is important that estimates of total carbon flux from terrestrial sources account not only for live carbon stocks, but also for other major component pools such as soils, woody detritus and forest products (Cohen et al., 1996). Accurately estimating the mass of living material however is critical as it is often used to initialize component pools in regional scale carbon models (Kimball et al., 2000) such as autotrophic respiration and post-disturbance detrital residues (Turner et al., 2004). Optical satellite imagery has been used to directly estimate amount and temporal variability in aboveground biomass (Dong et al., 2003), however these methods are mostly sensitive to green foliage and show an asymptotic relationship with biomass. Thus we seek an alternative method of using optical imagery to estimate live carbon stocks which overcomes these limitations.

A key to accurately estimating live forest carbon is to account for the spatial effects of anthropogenic disturbance, land-use change and site productivity, which can vary considerably by ecoregion or forest type. Moderate resolution satellite data like Landsat are particularly effective at tracking changes in land cover associated with harvest disturbances and land-use change (Cohen et al., 2002) and have recently been used to effectively characterize rates of early successional regrowth after clearcutting in western Oregon (Schroeder et al., in press). As forest growth extends beyond the stem exclusion phase of secondary succession however, the spectral signal recorded by optical sensors such as Landsat shows an asymptotic relationship to biomass (Turner et al., 2004), preventing further growth characterization and limiting direct modeling of biomass for mature forests (Lu, 2005; and Labrecque et al., 2006). Although Landsat is generally less effective at predicting biomass above 50 to 80 megagrams (Mg) per hectare (ha) (Dong et al., 2003), its spatial, spectral and temporal characteristics permit derivation of a variety of other useful products which can be utilized to help predict live forest carbon.

The growing legacy of temporal data available from Landsat (1972 – present) can be used in a "change-detection" context to accurately detect forest disturbances (Cohen et al., 1998; Hayes and Sader, 2001), especially in systems where disturbances are frequently the result of clearcut harvesting. If one takes advantage of the full historical legacy of Landsat (Cohen and Goward, 2004), a variety of disturbance mapping techniques (Cohen et al., 1998; Healey et al., 2006;

and Kennedy et al., in press) can be used to separate undisturbed forests from secondary forests. Once separated, an accurate age can be assigned to younger secondary forest stands which have been disturbed during the Landsat record (≈ 30-years). When these secondary forest age maps are combined with maps of initial vegetation age (from Landsat) and site productivity (e.g., site index) a modeling strategy can be employed to estimate live forest carbon (including foliage, branches, boles, and coarse roots) at the pixel scale through the use of theoretical growth curves like the Chapman-Richards function (Richards, 1959).

Site index curves and associated yield tables have long been used by foresters to predict the productive capacity of forests (Hegler, 1968). Curves are also an effective way of diagramming temporal patterns of forest productivity especially as they relate to carbon sequestration at various spatial scales (Harmon, 2001). Since long term patterns of forest productivity in the Pacific Northwest are generally well understood (Janisch and Harmon, 2002) we can reasonably construct a predictive model using a meta-modeling approach (Law and Kelton, 1991). This involves using a detailed stand-level model to parameterize a simpler set of functions which can more easily be applied to a broader landscape. The approach (referred to here as curve-fit), while simple in nature is extremely useful in that curves, once calibrated, can easily be incorporated into comprehensive models which track carbon through a variety of pools and pathways. In addition, curves offer the potential to be applied in a less computationally intensive manner as some

process driven models and offer potential to estimate more reasonably the upper bounds of carbon storage in mature forests than direct modeling with Landsat data.

This curve-fitting approach to estimating live carbon storage has been previously utilized within the framework of a comprehensive model for estimating total carbon flux from temperate coniferous forests of the Pacific Northwestern United States referred to as Landcarb (Cohen et al., 1996; Wallin et al., 1996; and Wallin et al., in press). A multi-component model, Landcarb spatially tracks exchanges of carbon between the living, detrital and forest products pools for each 25 x 25 meter Landsat pixel, allowing spatial variation resulting from natural and anthropogenic factors to be accounted for over time. Although live carbon estimates from the curve-fit approach have been shown to accurately reflect county level harvest statistics from the Oregon Department of Forestry (ODF) (Wallin et al., in press), a potentially more valuable evaluation of model performance could result from comparison with field measured data. Our aim is to utilize field inventory data collected and compiled by the U.S. Forest Service's Forest Inventory and Analysis (FIA) program to evaluate maps of live carbon produced by the curve-fit model for portions of two forested ecoregions in western Oregon.

FIA has been using a three-phase, double sample design to collect field measurements of forest attributes in the United States since 1928 (Birdsey and Schreuder, 1992). In general the FIA inventory follows a two-phase stratification process (Bechtold and Patterson, 2005), where in the first phase a grid of sample points is classified using aerial photo interpretation or forest/non-forest maps

generated from Landsat imagery. A random or systematic sample of these grid points is then selected for field measurement based on state specific criteria derived from phase one interpretation of forest type, volume class or structural characteristics. The grid points (or plots) selected are then field sampled by a trained field crew and marked for remeasurement in future inventories. Currently the FIA program implements an annual sampling scheme (referred to as annual inventory) where approximately 10% of field plots (for western states) are systematically measured and reported each year. Previously plots were measured non-systematically and reported approximately every 10 to 15 years (referred to as periodic inventory).

Despite changes to the FIA inventory protocol over time, two characteristics of FIA data make them particularly well suited to evaluate the live carbon maps produced by the curve-fit model. First, tree level data measured for each plot can be consistently converted to units of biomass (then to carbon) using national scale allometric equations (Jenkins et al., 2003). Plot level carbon estimates derived from FIA data can be directly compared with mapped based pixel level predictions using scatter plots and regression diagnostics to better understand how well the curve-fit approach performs at a local scale. As data are available from multiple inventories (i.e., annual and periodic), these plot to pixel relationships can be evaluated for performance and consistency over time for each of the forested ecoregions. Second, as the FIA inventory is statistically designed to estimate merchantable bole volume over large areas, plot level estimates of biomass can be

expanded to calculate total live carbon and carbon flux (i.e., difference between inventory estimates), which can be compared to the curve-fit approaches map based estimates for the study area. This two tiered approach to validation allows for robust characterization of both local and landscape scale estimates of carbon dynamics in the region.

Inventory data like those collected by FIA is generally considered one of the most robust ways of estimating carbon dynamics in relation to land-use change and interannual variation in climate. For this to be true however, it necessary that the sample of plots be carefully laid out in order to capture the full range of forested conditions and land-use patterns found in the study area. Satellite sensors like Landsat offer both a synoptic view of the landscape, as well as the spectral capacity to characterize forests in terms of structure and cover using vegetation indices such as the Tasseled Cap (Crist and Cicone, 1984). As Landsat wetness has been found to be an important indicator of maturity and structure in closed canopy forests and is relatively insensitive to cosine of the incidence angle (Cohen and Spies, 1992; and Cohen et al., 1995) we use it here in two ways. First, we evaluate the degree to which the FIA sample plots capture the variability of forest cover in terms of the spectral wetness observed in the study area. Second, substituting space for time, we develop two chronosequences of wetness by stand age class (from the stand age maps and from FIA field estimated stand age) to determine if subtle land-use shifts which may impact the carbon balance are captured by the FIA sample and by the stand age maps.

Overall we aim to address the following two objectives. First, to evaluate predictions of live forest carbon produced by the curve-fit model for image dates corresponding to two FIA field inventories (1995 image for periodic, 2004 image for annual). The predictions of live forest carbon (including foliage, branch, bark, bole, and coarse roots) are evaluated using inventory data at the local (i.e., pixel level) and landscape (study area totals and flux) scales. At the local scale, we evaluate pixel level estimates of forest carbon from the curve-fit model using inventory data collected for two forested ecoregions with known differences in productivity. At the landscape scale, total forest carbon and carbon flux is estimated with field plots from each inventory and the estimates are compared to the curve-fit models map based estimates. Second, Landsat tasseled cap wetness (calculated from the 1995 and 2004 images) is used to investigate the degree to which the FIA plot samples capture the spectral variation in forest conditions found in the study area. This is accomplished by comparing frequency histograms of study area versus inventory plot wetness and by analyzing patterns of forest growth from chronosequences of wetness based on stand age derived from map based and field measured sources.

2. METHODS

2.1. Study Area

The study area is comprised of a 2,140,557 ha forest area determined by a 1988 vegetation map of western Oregon (Cohen et al., 2001). The study area

(Figure 4-1) covers portions of two major forested ecological provinces, which are described by Franklin and Dyrness (1988) as the Coast Range Province (CRP) and the Western Cascade Province (WCP). The CRP is characterized in the far west by a Sitka spruce zone a few kilometers wide lying directly adjacent to the Oregon coast. The rest of the CRP and the majority of the WCP are dominated by conifers common to the Douglas-fir/western hemlock zone, although hardwood species such as red alder, vine maple, big leaf maple, and Pacific dogwood can dominate moist riparian areas and dry valley margins. The climate of the Pacific Northwest is typified by warm, dry summers and mild, wet winters. The study area encompasses a wide range of elevations, yielding strong physical and climatic gradients. Climatic differences, in concert with differences in elevation and geology yield a wide array of growing conditions within the study area. The prevailing winds and rugged topography generally yield warmer, wetter conditions in the CRP and colder and drier conditions in the WCP. The combination of these geographic characteristics in concert with impacts from forest management have led to previous findings that following clearcut harvesting, the CRP typically supports faster forest regrowth than the WCP (Yang et al., 2005; and Schroeder et al., in press).

2.2. Data

2.2.1. Forest Inventory Data

There are several differences between the periodic (data collected between 1993 – 1997) and annual (data collected between 2000 – 2005) FIA inventories, mostly resulting from the switch in 2000 to an "enhanced" inventory design that now collects data on a systematic sample (≈ 10%) of plots within each western state each year. Other differences include plot layout configuration changes (shape and size), number of measured subplots (periodic = 5, annual = 4), and variable vs. fixed radius subplots. In addition, during the periodic inventory FIA only collected plot data on private forest lands in the western U.S., as apposed to the current annual inventory which now collects data on both private and public forest lands. To compensate for this difference we make use of data collected on public lands by the U.S. Forest Service Region 6 (R6) and Bureau of Land Management (BLM). Data collected by all three land management agencies were compiled by the Pacific Northwest FIA program into an Integrated Database (IDB) which uses common formats, definitions, measurement units, column names and table structures (Hiserote and Waddell, 2004). We refer to this data set as IDB periodic and the annual data set collected solely by FIA as FIA annual.

In both the inventories plots are coded based on the number of different land cover conditions (e.g., forest, non-forest, water) observed on each measured subplot. Thus, a plot labeled as 1 (i.e., single condition) would have only 1 dominant land cover condition, whereas a plot labeled as 3 (i.e., multiple condition) would have a different land cover condition on at least 3 of the measured subplots. To minimize spectral heterogeneity it is not uncommon that only single condition,

forested plots are used in studies where plot data are used to directly model forest attributes with remotely sensed imagery (Schroeder et al., in press). Others have used an approach where all condition classes of forested plots are used and a screening process (either visual or statistical) is used to discard plots that are assessed as obvious outliers (Ohmann and Gregory, 2003). FIA plot coordinates are not publicly available, however even when known coordinate locations are used (as in this study) errors in plot coordinate locations and image registration can combine to yield unmeaningful statistical relationships.

2.2.2. Stand Age Maps

Spatial representation of stand age is required as input to the curve-fit carbon model. The process of deriving stand age maps for our western Oregon study area is adapted from the procedure described by Wallin et al. (1996) for use within the Landcarb modeling framework. Briefly the process combines a vegetation age map of western Oregon (Cohen et al., 2001) with a stand disturbance map of timber harvests and wildfires originally produced by Cohen et al. (2002) through 1995; updated with similar change detection techniques through 2002 by Mouer et al., (2005) and through 2004 by Lennartz (2005).

Image classification based on continuous variables (i.e., percent cover) was used to develop the 1988 vegetation map of western Oregon, which included seven classes: open (< 30% green vegetation cover (GVC)), semi-open (30 – 70 % GVC), broadleaf (>70% broadleaf cover (BC)), mixed (>70% GVC, <70% BC and < 70%

conifer cover (CC)), young conifer (>70% CC, < 80 years), mature conifer (>70% CC, 80-200 years) and old-growth conifer (>70% CC, > 200 years). Stand age was only considered for three broad categories (young, mature and old-growth age) when assessing map accuracy, which was reported as 82% overall (Cohen et al., 2001).

Approximated "structural" age classes were assigned to the seven vegetation classes from the 1988 map, these include: open (1-10 years), semi-open (11-20 years), broadleaf/mixed (21-30 years), young (31-80 years), mature (80-200 years) and old-growth (>200 years). For modeling purposes, we assumed the median age was the current stand age in the 1988 vegetation map (old-growth was assigned an age of 225). The stand disturbance map was then used to mask out all stands of known disturbance (fire and timber harvest) occurring between 1972 and 2004 (in roughly 5 (±2) year intervals). We assumed that all disturbances occurred during the median year of each mapped disturbance interval. For example, when creating the 2004 age map all areas of known disturbance were masked from the 1998 vegetation map. If a pixel was labeled as disturbed between 1984 and 1988 its age was estimated as 2004 minus median disturbance age, or 2004 – 1986 = 18 years of age. For all unmasked areas (i.e., undisturbed since 1988), the age from the 1988 vegetation map was added up 16 years to 2004. So if a pixel was labeled as open in 1988, its age was estimated as median age in 1988 (i.e., 5) plus 16 years (2004 – 1988 = 16), which yields an age of 21 years. This procedure was used to "spin-up" an estimated stand age map for both the 1995 and 2004 image dates.

2.2.3. Site Index

To account for variability in forest growth due to climate and soils (i.e., potential productivity) a site index map is used as input to the curve-fit carbon model. Timber companies often keep local data and spatial records of productivity for their land holdings, but consistent regional data are not widely available (Waring et al., 2006). The only known map of site index available for western Oregon and Washington was produced in 1949 by Isaac. The map was produced using field survey and elevation data (Swenson et al., 2005) and has been shown to correspond with known relationships of forest productivity in the region (Wallin et al., in press). As this was the site index map used in the original work involving Landcarb (Cohen et al., 1996; and Wallin et al., 1996), we elect to use it here for further evaluation.

2.2.4. Landsat Imagery

Two cloud free, near anniversary Landsat TM (WRS-2, path 46, row 29) images were used in this study. Both images were radiometrically normalized as part of a 19 image time-series by Schroeder et al. (2006) using statistically selected pseudo-invariant features (see Canty et al., 2004) to relatively normalize all images to an atmospherically corrected reference (corrected with 6S, Vermote et al., 1997). The approach, referred to as absolute-normalization effectively normalized all images to a common radiometric scale (across all images < 0.025 RMSE) while

simultaneously correcting for atmospheric and sun-sensor view-angle effects. Given similar radiometry, the Landsat wetness indices calculated for both images can be compared over time to evaluate the representativeness of the FIA random sample both in terms of wetness frequency and patterns of forest growth derived with the stand age chronosequences.

2.2.5. Inventory Carbon Estimation

2.2.5.1 Per Pixel Carbon

Data derived from both the FIA annual and IDB periodic databases were used to validate both pixel level and total study area predictions of live carbon from the curve-fit model. For the pixel level validation, raw tree data for trees > 2.5 centimeters (cm) diameter at breast height (DBH) from both FIA inventories were converted to aboveground biomass (including branches, bole, bark and foliage) using national-scale allometric equations (Jenkins et al., 2003) of the form of Eq. 1,

$$bm = Exp(\beta_0 + \beta_1 \ln dbh) \quad (1)$$

where bm is biomass per tree in kilograms (kg) per tree, dbh is diameter at breast height (in cm), Exp is an exponential function, ln is natural log base "e", and β_0 and β_1 are parameters based on 10 general species groups (see Jenkins et al., 2003 Table 4 for species group parameters). We favor the use of national scale equations as they are developed over broad areas with large numbers of trees. Coarse root biomass was estimated for trees > 2.5 cm DBH using Eq. 2,

$$ratio = Exp(\beta_0 + \frac{\beta_1}{dbh}) \quad (2)$$

where ratio is the coarse root ratio to total aboveground biomass from Eq. 1. For each plot an adjustment was made to account for seedling biomass based on group count data for trees < 2.5 cm DBH. Tree biomass was expanded to represent plot area (i.e., multiplied by trees per hectare) and summed resulting in a plot estimate of biomass in kg ha^{-1}. Plot biomass was then converted from kg to Mg and finally to Mg C ha^{-1} assuming 50% of living biomass is carbon (Swift et al., 1979).

2.2.5.2. Total Study Area Carbon

To calculate total study area carbon, the tree level data were converted to aboveground biomass as stated above and then expanded by the number of hectares each plot represents in the study area. To derive the area each plot represents in the study area we adjusted the number of hectares each plot represents in each inventory using Eq. 3,

$$Adj\ Fac = \frac{Study\ area\ ha}{Inventory\ \ ha} \quad (3)$$

where Adj Fac is the adjustment factor applied to the plot level expansion factor, Study area ha is the total number of hectares in the study area and Inventory ha is the total number of hectares each collection of plots represents in its respective inventory. After applying the adjustment factor (0.9956 for IDB periodic, 0.9533 for FIA annual) the resulting numbers were used to expand the per plot biomass

estimates, which were then summed across plots to yield the estimate of total live carbon reported in teragrams (Tg).

2.2.6. Curve-fit Carbon Model

Using a look-up table approach (Song et al., 2001), the curve-fit model uses a set of Chapman-Richards curves to estimate aboveground carbon (including foliage, branches, bole, and coarse roots). The curves are defined using Eq. 4,

$$LIVE = LIVEMAX * (1 - e^{(-B_1 * AGE)})^{B_2} \quad (4)$$

where LIVE is the total aboveground carbon store in Mg C ha^{-1}, LIVEMAX is the maximum live aboveground carbon store, B_1 is the rate that determines how quickly live carbon approaches the maximum, B_2 determines how long plant production lags behind the maximum rate, and AGE is the number of years since disturbance. The curve parameters (Table 2-1) are derived from STANDCARB (Harmon et al., 1995), which is a stand-level model that integrates effects of site condition, disturbance severity, tree re-establishment and species composition on forest growth. The maximum carbon storage in aboveground and belowground pools was determined from past field based studies conducted within the region (Grier and Logan, 1977, Harmon et al., 1986, Smithwick et al., 2002). The curves, parameterized using yield tables published for Douglas-fir (Curtis et al., 1982) are presented in Figure 4-2. Live carbon maps were produced for the 1995 and 2004 image dates to correspond with the two FIA inventory periods. The steps of the

curve-fit modeling and validation process are diagramed in the flow chart found in Figure 4-3.

2.2.7. Carbon Model Validation

2.2.7.1. Per Pixel Carbon

To evaluate local scale performance of the curve-fit model we directly compared predictions of forest carbon to those estimated from the FIA data. We elected a conservative approach were we used all multiple condition plots with measured trees, resulting in 1,180 IDB periodic plots (n = 404 CRP, n = 776 WCP) and 403 FIA annual plots (n = 165 CRP, n = 238 WCP) available for analysis. Fewer plots are available from the FIA annual inventory as only 5 years of data (≈ 40%) has been collected since the inception of the new enhanced FIA inventory starting in 2000. For each of the sample plots we derived the pixel level estimates of carbon using the mean value of one of two pixel masks (1. 22-pixel mask for FIA plots in both IDB periodic and FIA annual data sets; 2. 13-pixel mask for BLM and R6 plots in the IDB periodic data set) which were designed to reflect the various sizes, shapes and coordinate measurement locations of the plots collected in the two inventories. Scatter plots for both image dates are developed by ecoregion using the predictions (from the curve-fit model) and observed estimates (from FIA data) of forest carbon. Descriptive statistics (i.e., minimum (min), maximum (max), mean and standard deviation (stdev)) and regression diagnostics (bias, root mean square error (RMSE), variance ratio (VR)) are used to evaluate the carbon

models capacity to locally predict forest carbon in each ecoregion. A small portion of the study area does not fall into either of the forested ecoregions used in the per pixel validation. Thus, for each inventory, the number of plots used in the per pixel validation are slightly less than the total number of plots used to estimate total live carbon for the study area.

2.2.7.2. Total Study Area Carbon

To evaluate the landscape scale performance of the curve-fit model we directly compared the map based predictions of forest carbon to those estimated with a collection of plots from each inventory period (n = 1,450 for IDB periodic, n = 432 for FIA annual). For each inventory period the plots were used to calculate total study area carbon (in Tg), as well as associated standard errors. For the curve-fit model, total study area carbon was calculated for both image dates by summarizing the map based predictions using Eq. 5,

$$Total\ C = \sum_{AB} (AB_P) * (AB_C * 0.0625)) \quad (5)$$

where Total C is the estimated study area carbon (in Tg), *AB* represents the age class bins from the stand age maps, AB_P is the number of pixels in each age class bin, AB_C is the carbon value in Mg C ha^{-1} of each age class bin, and 0.0625 is the number of ha in each 25 x 25 meter Landsat pixel. In addition to total study area forest carbon, we also difference the respective map and inventory based estimates to report the carbon flux occurring between the near decadal point-in-time

estimates. Differences are reported in absolute values (in Tg), relative percentages (i.e., % of initial value) and amount of forest carbon sequestered on a per year basis (based on 9 years between point-in-time estimates, reported in Mg C ha^{-1}).

2.2.8. Landsat Wetness

Landsat wetness was calculated for both the 1995 and 2004 Landsat images using the reflectance based tasseled cap equations of Crist (1985). We use wetness to evaluate the extent to which the FIA sample plots capture the spectral variation of forest conditions found in the study area. This is accomplished by comparing frequency histograms of the wetness values observed across the full study area (i.e., image base) to those captured by the inventory plots used to calculate total study area carbon (n = 1,450 for IDB periodic, n = 432 for FIA annual). The frequency histograms were constructed for both image dates using the mean wetness value from each plots respective pixel mask (described above).

In addition to the frequency histograms, we also develop temporal signatures of forest growth using a chronosequence approach were average wetness values are plotted according to stand age from the Landsat age maps, as well as from age derived from the inventory data. Since the stand age maps were generated to represent forest structural ages at different points in time (e.g., age 12 in 1995 map is age 21 in 2004 map) we summarize wetness from both age maps in one chronosequence. For the inventory based chronosequence, we combined estimated stand age from both sets of FIA inventories into the same age bins used

in the stand age maps. For both chronosequences wetness is reported as average per age bin (error bars are standard deviations). As wetness responds predictably to forest growth, we can use the chronosequences to determine if land-use shifts that might permanently impact the carbon balance can be detected at the landscape scale with the FIA sample and with the stand age maps.

3. RESULTS

3.1. Per Pixel Carbon Validation

Local scale performance of the curve-fit carbon model is based on the descriptive statistics and regression diagnostics presented in Table 4-2. These results indicate that across ecoregions and inventory periods the curve-fit mean predictions are in all cases greater than the mean estimates of the inventory data. In addition, all the curve-fit maximum predictions where less than the maximum estimates of the inventory plot data. The standard deviations of the curve-fit predictions were similar across ecoregions and inventory periods and were observed to be within ± 7 Mg C $ha^{-1}$of the standard deviations of the FIA plot estimates. Scatter plots of predicted (from the curve-fit carbon model) versus observed (from FIA plot data) live forest carbon are presented by ecoregion in Figure 4-4. The scatter plots indicate that across inventory periods the curve-fit model more accurately predicts (i.e., has higher correlation and lower RMSE) live forest carbon in the CRP than in the WCP. The large positive bias statistics suggests the curve-fit model consistently over predicts live forest carbon in both

ecoregions. The variance ratio reveals an inconsistent pattern regarding the amount of observed variation preserved in the curve-fit predictions.

3.2. Total Study Area Carbon Validation

Landscape scale performance of the curve-fit carbon model is based on estimates of total study area carbon found in Table 4-3. For both inventory periods, the curve-fit model estimated on average 138.32 Tg more live forest carbon than was estimated with the inventory plot data (+ 133.76 Tg in 1995, + 142.88 Tg in 2004). When considered in absolute terms, the flux (i.e., difference in inventory estimates) of live forest carbon predicted by the curve-fit model is substantially more (+ 9.12 Tg) than estimates derived with the inventory data. In relative terms however, the flux estimate derived with the curve-fit model is nearly identical to that of the FIA estimate. The results suggest that the flux of carbon estimated by the curve-fit model is well within the standard errors calculated for the inventory estimates (Table 4-3). It should be noted that the higher standard error reported for the FIA annual inventory results from fewer plots being available for total carbon calculation. On a per year basis, the curve-fit model predicted a larger carbon sink (0.47 Mg C ha^{-1}/yr) than estimated with the inventory data

3.3. Frequency Histograms and Stand Age Chronosequences

To gauge a general sense of the forest conditions captured by the inventory sample we derived frequency histograms of Landsat wetness for the full forested

study area and for the inventory plots. The histograms, found in Figure 4-5a and b, show that the inventory plots sample the full range of wetness values observed in the study area. The bell shape of the histograms suggests that for both inventory periods the systematic plot sample captures the observed wetness values with a similar frequency as found within the forested study area. Both the study area and inventory plot histograms have a mean wetness around 0.00. This is not surprising as wetness values approach 0.00 twice during successional development (once during early succession just prior to canopy closure, then again later in succession). Thus, to get a better sense of how well the inventory sample captures more subtle changes in forest condition we re-examine wetness plotted according to stand age using a chronosequence approach (i.e., space for time). The curves (or trajectories) of average wetness plotted by ecoregion (error bars are standard deviations), derived with map and inventory based age classes are found in Figure 4-6a and b.

The curves developed with the age maps show wetness increases steadily from year one, with some evidence after year 6 that average growth in the CRP is faster (i.e., approaches 0.00 more quickly) than in the WCP. This same age range in the inventory based curves shows a similar wetness increase, and the ecoregion pattern, although less clear shows the WCP curve approaching 0.00 more quickly than the CRP curve. In year 12 the map based curves for both ecoregions show a sharp drop in wetness (circled area on Figure 4-6a), which reveals a significant shift away from the normal response of wetness that occurs during the process of stand development. As our age maps are 9 years a part (1995 – 2004) the same shift in

wetness is still present in the map based curves in year 21. This sharp drop in wetness is not captured by either of the inventory based curves.

4. DISCUSSION

4.1. Per Pixel Carbon

At the local scale we evaluated the performance of the curve-fit carbon model using pixel level scatter plots, descriptive statistics and regression diagnostics. The results indicated that the curve-fit model, although simple in form performs quite well considering its somewhat conceptual nature. We caution against strict interpretation of the pixel level results as there are many sources of potential error which have not been accounted for. These sources of error include, but are not limited to allometric equations, plot coordinates, image registration, outliers, age maps, site index map, curve calibration for Douglas-fir and the use of one image date to represent each multi-date inventory period. Nonetheless, evidence suggests that the curve-fit model predicted live forest carbon more accurately (i.e., higher correlation, lower RMSE) in the CRP than in the WCP. It is possible the curve-fit model was able to more accurately predict carbon in the CRP as it tends to support faster, more consistent (i.e., less variable) patterns of forest growth resulting from more favorable growing conditions (Schroeder et al., in press). As evidence of this hypothesis we plotted post-harvest forest regrowth classes (normalized by the % of area clearcut) mapped with trajectories of multi-temporal Landsat imagery (Schroeder et al., in press) by site index class from the

Isaac map (Figure 4-7). These graphs clearly show that regardless of site index there is very little variability in the distribution of forest regrowth classes in the CRP. In the WCP however, there is substantial variability in the distribution of forest regrowth classes, especially for site index classes 2 through 4.

Although the curve-fit model performed better in the CRP, the bias statistics suggested that the model over-predicts forest carbon in both ecoregions. Some of the over-prediction could result from using curves parameterized specifically for one species (Douglas-fir). Another possibility is that the model parameters (from Table 4-1) themselves need to be modified. The scatter plots reveal that the over-prediction tends to occur in the low to middle range of carbon and under-prediction at the high end. Thus, a slight decrease to β_1 (controls how quickly live carbon approaches the maximum value) and a slight increase to β_2 (controls lag of plant production behind the maximum rate) from Eq. 4 might help linearize the predictions of the model in relation to the field measured inventory data. Additional pixel level accuracy could also be achieved by improving the spatial representation of forest productivity (i.e., site index map) used to assign the curve based carbon values.

One option to improve the spatial representation of forest productivity would be to use a more detailed measure predicted by a forest growth process model such as 3-PG (Landsberg and Waring, 1997). Driven by coarse resolution (1 km) satellite data from the MODIS sensor the 3-PG model has predicted Douglas-fir site index from FIA inventory data with reasonable accuracy ($R^2 = 0.55$) for the

state of Oregon (Swenson et al., 2005). Another option to improve predictions in young forests would be to rely on a direct measure of forest growth from time-series data from Landsat. Given its temporal frequency, as well as recent advances in algorithms which extract trajectories of forest regrowth in an automated fashion (Kennedy et al., in press) this seems like a viable option. Although young forests do not store large amounts of carbon, differences in successional rate (fast vs. slow) has been shown to significantly impact the amount of live carbon (120 Mg C ha^{-1} vs. 53 Mg C ha^{-1}) stored in 40-year old plantation forests in western Oregon (O'Connell et al., in preparation).

4.2. Total Study Area Carbon

As the pixel level validation showed that the curve-fit model tended to over-predict forest carbon at the local scale, it is no surprise that total study area forest carbon was also over-predicted in relation to the inventory based estimates. Although this over-estimation is significant (average of 138.32 Tg per inventory period) in absolute terms, the flux (i.e., difference between inventory periods) estimated by the curve-fit model was found to be well within the standard error of the inventory estimates. This finding helps provide additional credibility to the live carbon flux estimates derived in previous studies with the curve-fit model (Cohen et al., 1996; Wallin et al., 1996; and Wallin et al., in press). For a slightly larger (but overlapping) western Oregon study area, Wallin et al. (in press) estimated a sink of live forest carbon of approximately 1.7 Mg C ha/yr between 1991 and 1995.

This estimate is similar in magnitude to our 1.63 Mg C ha/yr sink estimated between 1995 and 2004. As our results suggest a similar size sink to that dating back to 1991, it is possible that the flux of forest carbon in western Oregon could be approaching a balanced state given current forest practices (Cohen et al., 2002) resulting from implementation of the Northwest Forest Plan (FEMAT, 1993).

In addition we note that our carbon estimates for both inventory periods were derived using the same set of national scale allometric equations (Jenkins et al., 2003), thus eliminating unwanted error in our flux calculations due to differences in equation form. FIA inventory regions (i.e., Pacific Northwest, Interior West, Southern, Northern) typically calculate and report biomass data using a variety of different allometric equations, however based on the scale of application we favor the use of national equations like those utilized here so that derived estimates and their associated errors can be compared in similar units regardless of modeling strategy.

4.3. Frequency Histograms and Stand Age Chronosequences

Direct forest inventories like FIA are one of the more reliable methods from which to base regional and national scale carbon budgets (Turner et al., 1995; and Jenkins et al., 2001). For inventories (or any method for that matter) to be truly effective they must capture the spatial and temporal changes in land-use patterns occurring at the landscape scale. This can be a difficult task in complex landscapes where differences can occur between ecosystems currently on the landscape and

those that have been previously cleared (Houghten et al., 2001). Thus, to gauge a general sense of how well the inventory sample plots represent the forest condition present in the study area we utilized the tasseled cap wetness index (Crist, 1985) as it responds predictably over the course of forest development and is nearly insensitive to topographic effects (Cohen and Spies, 1992; and Cohen et al., 1995). The frequency histograms of wetness (Figure 4-5a and b) show that in terms of shape and magnitude of response the inventory plots from both periods well represent the forest condition in terms of spectral wetness found in the study area. As this is a very general measure, we were interested in a more detailed evaluation of the inventory samples representation of the wetness continuum found in the study area.

Since wetness responds predictably to structural changes associated with forest growth, we utilized a chronosequence approach to look for significant deviations away from the normal pattern of forest development that might be captured by the spectral index. A typical wetness trajectory starts at its lowest point (≈ -0.15) immediately after disturbance in year one, increases to around 0.00 as leaf area is accumulated, exceeds 0.00 until it reaches its highest point at canopy closure, falls below 0.00 as scene components other than green foliage start to increase, and finally increases slightly back to around 0.00 in old-growth stands when crowns die back and the presence of epiphytic lichens increases in the upper canopy. In young stands (1 – 15 years, Figure 4-6a and b), the large standard deviations around the mean wetness values characterizes the large amount of

spectral variability that can occur early in forest succession due to differences in productivity and management (Horler and Ahern, 1986). This variability is a common feature associated with stands recovering from clearcutting in western Oregon (Yang et al., 2005; and Schroeder et al., in press). What is not common is the considerable drop in average wetness observed at age class 12 in the chronosequence developed with the map based stand age classes (Figure 4-6a circled area). This pronounced spectral shift away from normal forest development is not seen in the chronosequence developed with age classes from the inventory plot data (Figure 4-6b).

Using the stand age maps (specifically age class 12), multi-temporal Landsat imagery and high resolution aerial photography (1 meter resolution true color photography from National Agriculture Imagery Program, 2005) we have interpreted this shift in wetness response as predominately forest clearing along the Willamette valley margins resulting from urban (e.g., rural homesteads) and agricultural (e.g., crop fields and Christmas tree farms) expansion. As we used a space for time approach using stand ages mapped in 1995 and 2004, the age 12 class bin is represented again as age 21 in the map based chronosequence (Figure 4-6a). At age 21 we see that the curves of average wetness have only increased slightly from age 12, indicating that some of the detected shift away from normal forest development maybe a long term change in land-use. This finding is noteworthy as uncertainties associated with rates of land-use change (especially

conversion of forest to non-forest) contribute more to uncertainty of carbon fluxes than do uncertainties in biophysical variables (Houghten and Goodale, 2004).

Based on the stand age map statistics up to 13,668 ha (or 0.6 % of the study area) could potentially be effected by this shift in land-use. This equals approximately 0.02 Mg C ha^{-1}/yr (based on the average of 5 site index curves for 12 year old stands from Figure 4-2 and a 9 year measurement interval), which is not a large amount in absolute terms. The point however is not about the difference between the amount of carbon present on the landscape (based on land-use shift) and what could be present if these areas where progressing along a track of normal forest development, but rather on the difference between what carbon is present on the landscape (based on land-use shift) and what was there before these areas were disturbed. The later view could have a considerable impact on the long-term carbon balance of the region.

Although we present evidence that the inventory based chronosequence did not detect the subtle shift in land-use we have no real means of determining if this had any impact on the total carbon estimates derived for the study area. Our goal was simply to demonstrate the subtle landscape changes that can be detected with the synoptic view of Landsat. We also note that one of the major weakness of the curve-fit carbon model is that it assumes all disturbed forests eventually grow back to new forests. Clearly this a naïve assumption that must be addressed in future versions of the model, along with other issues raised in this study such as curve prediction bias, site index representation, curves for other species and ecoregion

productivity differences (CRP vs. WCP). Regardless of the method used to estimate forest carbon (e.g., forest inventory, process model, accounting model), it is important that shifts in land-use especially those involving forest to non-forest conversion be robustly accounted for. We hope our Landsat based chronosequence approach can allow for better spatial accounting of these forest to non-forest conversions in future applications of the curve-fit model. Although optical satellite imagery has its limitations regarding the direct estimation of forest carbon, we have demonstrated that Landsat's temporal (e.g., age maps) and spectral (e.g., wetness chronosequences) characteristics can be used as effective inputs to a curve based model which estimates carbon flux from forests within the standard error of inventory estimates.

5. CONCLUSION

Given the uncertainty surrounding the effects of climate change many countries have been tasked with accounting for terrestrial carbon stocks over large areas. Although estimating total carbon flux requires accounting for live carbon, as well as other major component pools (e.g., soils, detritus, and forest products) we focused on prediction of live forest carbon as its estimation is critical to initializing various component pools in regional scale models (Turner et al., 2004) and is often spatially estimated with considerable uncertainty (Houghten et al., 2001). As optical satellite data have been shown to have an asymptotic relationship with biomass we sought a method that could overcome this limitation. The curve-fit

model evaluated here uses a look-up table approach, where a set of Chapman-Richards growth curves are used in combination with forest stand age and site productivity (i.e., site index) maps to spatially predict live forest carbon (including foliage, branches, boles, and coarse roots). We presented an ecoregion specific (CRP vs. WCP) evaluation of the local (i.e., pixel level) and landscape (i.e., total carbon and carbon flux) scale performance of the curve-fit model using two periods of FIA forest inventory data (represented by 1995 and 2004 image dates).

At the pixel level, the curve-fit model performed well considering its conceptual framework. In general, the model performed better (i.e., higher correlation, lower RMSE) in the CRP than the WCP, likely the result of faster, less variable growth patterns which have been previously observed for the CRP (Yang et al., 2005; and Schroeder et al., in press). Model predictions for both ecoregions were observed to have large positive bias statistics, resulting in over-prediction of low to mid-range carbon values and under-prediction of high end carbon values. Prediction based descriptive statistics such as mean forest carbon were likely effected by sources of error from outliers, geo-registration (image and plot), input maps, and for curves calibrated only for Douglas-fir. All the pixel level patterns were consistent across both inventory periods.

As the pixel level evaluation revealed the curve-fit models tendency to over-estimate inventory based forest carbon, it was not surprising to find the total carbon estimates were also over-estimated. Even so, we found that the flux (i.e., change between inventory periods) of forest carbon predicted by the curve-fit

model was, in relative terms nearly identical to the inventory based estimate (7.22% curve-fit, 7.40% inventory). In absolute terms, we found the curve-fit models flux estimate to fall well within the standard error of the inventory estimates. On a per year basis, the curve fit model estimated a carbon sink of 1.63 Mg C ha^{-1}/ yr and the inventory data a sink of 1.16 Mg C ha^{-1}/ yr between 1995 and 2004. Use of national scale allometric equations (Jenkins et al., 2003) to predict carbon for both inventory periods minimized unwanted variation in our flux estimates due to differences in equation form.

We consider data collected by national forest inventories like FIA as one of the more reliable means from which to estimate carbon balances over large areas, although for this to be true the sample of inventory plots must capture the spatial and temporal changes in land-use patterns occurring on the landscape. To gauge the sense to which the inventory plots captured the forest condition in our study area we presented frequency histograms of Landsat wetness derived for the full study area and for the inventory plots. Based on shape and magnitude of the histograms we found that the inventory plots from both periods well represent the forest condition in terms of spectral wetness found in the study area. As this is a very general measure, we also presented stand age chronosequences of wetness developed using age classes developed from the stand age maps and from the inventory data. Since wetness responds predictably to structural changes associated with forest growth, we were able to observe a significant shift away from the normal pattern of forest development using the map based stand ages. This shift,

interpreted as forest to non-forest conversion, was not detected in the chronosequence developed with the inventory based age data.

As subtle land-use changes are difficult to detect with any method, we do not imply the inventory sample does not represent the forest conditions of the study area, but rather that synoptic data from Landsat could be used in more synergistic ways to help assign plot locations that could better capture these fine grained spatial processes. We also noted that our curve-fit models assumption that all disturbed forests eventually grow back to new forests needs to be addressed along with other improvements to minimize curve prediction bias, improve site index representation, and account for species and ecoregion productivity differences (CRP vs. WCP). Although optical satellite imagery is limited in its ability to directly estimate forest carbon, we found Landsat's temporal (e.g., age maps) and spectral (e.g., wetness chronosequences) characteristics to be useful inputs to a curve based model which estimated carbon flux from forests within the standard error of inventory estimates.

ACKNOWLEDGMENTS

We gratefully acknowledge data and financial support provided by the USDA Forest Service Pacific Northwest research Station's Forest Inventory and Analysis Program.

REFERENCES CITED

Bechtold, W.A., and Patterson, P.L. (2005). The enhanced forest inventory and analysis program – National sampling design and estimation procedures. U.S. Forest Service GTR – SRS – 80.

Birdsey, R.A., and Schreuder, H.T. (1992). An overview of the forest inventory and analysis estimation procedures in the eastern United States – with an emphasis on the components of change. General Technical Report RM – 214. USDA Forest Service, Rocky Mountain Forest and Range Experiment Station, Fort Collins, CO, USA.

Canty, M.J., Nielsen, A.A., and Schmidt, M. (2004). Automatic radiometric normalization of multitemporal satellite imagery. *Remote Sensing of Environment*. 91, 3–4, 441–451.

Cohen, W.B., and Spies, T.A. (1992). Estimating structural attributes of Douglas-fir/Western hemlock forest stands from Landsat and SPOT Imagery. *Remote Sensing of Environment*. 41, 1 – 17.

Cohen, W.B., Harmon, M.E., Wallin, D.O., and Fiorella, M. (1996). Two decades of carbon flux from forests of the Pacific Northwest. *BioScience*. 46, 11, 836 – 844.

Cohen, W.B., Fiorella, M., Gray, J., Helmer, E., and Anderson, K. (1998). An efficient and accurate method for mapping forest clearcuts in the Pacific Northwest using Landsat imagery. *Photogrammetric Engineering and Remote Sensing*. 64: 293-300.

Cohen, W.B., Maiersperger, T.A., Spies, T.A., and Oetter, D.R. (2001). Modeling forest cover as continuous variables in a regional context with Thematic Mapper data. *International Journal of Remote Sensing*. 22(12): 2279-2310.

Cohen, W.B., Spies, T.A., Alig, R.J., Oetter, D.R., Maiersperger, T.K., and Fiorella, M. (2002). Characterizing 23 years (1972-95) of stand replacement disturbance in western Oregon forests with Landsat imagery. *Ecosystems*. 5: 122-137.

Cohen, W.B., Maiersperger, T.K., Gower, S.T., and Turner, D.P. (2003). An improved strategy for regression of biophysical variables and Landsat ETM+ data. *Remote Sensing of Environment*. 84: 561-571.

Cohen, W.B., and Goward, S.N. (2004). Landsat's role in ecological applications of remote sensing. *Bioscience*. 54 (6), 535-545.

Crist, E.P., and Cicone, R.C. (1984). A physically-based transformation of Thematic Mapper data – the TM Tasseled Cap. *IEEE Transactions on Geosciences and Remote Sensing*. GE:22, 256 – 263.

Crist, E.P. (1985). A TM tasseled cap equivalent transformation for reflectance factor data. *Remote Sensing of Environment*. 17, 301 – 306.

Curtis, R.O., Clendenen, G.W., Reukema, D.L., and DeMars, D.J. (1982). Yield tables for managed stands of coast Douglas-fir. USDA General Technical Report, GTR-PNW-135, Pacific Northwest Forest and Range Experiment Station, Portland, OR.182 pp.

DeFries, R., Houghton, R.A., Hansen, M.C., Field, C.B., Skole, D., and Townshend, J. (2002). Carbon emissions from tropical deforestation and regrowth based on satellite observations for the 1980s and 1990s. *Proceedings of the National Academy of Sciences*. 99, 22, 14256 – 14261.

Dong, J., Kaufmann, R.K., Myneni, R.B., Tucker, C.J., Kauppi, P.E., Liski, J., Buermann, W., Alexeyev, V., Hughes, M.K. (2003). Remote sensing estimates of boreal and temperate forest woody biomass: Carbon pools, sources and sinks. *Remote Sensing of Environment*. 84, 393 – 410.

Franklin, J., and Dyrness, C. (1988). Natural Vegetation of Oregon and Washington. Oregon State University Press, Corvallis, OR.

Grier, C.C., and Logan, R.S. (1977). Old-growth *Pseudotsuga menziesii* communities of a western Oregon watershed: biomass distribution and production budgets. *Ecological Monographs*. 47, 373 – 400.

Harmon, M.E., Franklin, J.F., Swanson, F.J., Sollins, P., Gregory, S.V., Lattin, J.D., Anderson, N.H., Cline, S.P., Aumen, N.G., Sedell, J.R., Lienkaemper, G.W., Cromack, K.W. (1986). Ecology of coarse woody debris in temperate ecosystems. *Recent Advances in Ecological Research*. 15, 133 – 302.

Harmon, M.E., Marks, B., Hejeebu, R.N. (1995). A users guide to STANDCARB Version 1.0: A model to simulate the carbon stores in forest stands. Pacific Forest Trust. Booneville, CA.

Harmon, M.E. (2001). Carbon sequestration in forests addressing the scale question. *Journal of Forestry*. 99, 4, 24 – 29.

Hayes, D.J., and Sader, S.A. (2001). Comparison of change-detection techniques for monitoring tropical forest clearing and vegetation regrowth in a time series. *Photogrammetric Engineering and Remote Sensing*. 67, 9, 1067 – 1075.

Hiserote, B. and Waddell, K. (2004). The PNW – FIA Integrated Database User Guide Version 1.4. Forest Inventory and Analysis Program, Pacific Northwest Research Station. Portland, OR.

Healey, S.P., Yang, Z., Cohen, W.B., and Pierce, D.J. (2006). Application of two regression-based methods to estimate the effects of partial harvest on forest structure using Landsat data. *Remote Sensing of Environment*. 101: 115-126.

Hegler, L. (1996). A method for constructing site-index curves from stem analysis. *Forestry Chronicles*. 21, 11 – 15.

Horler, D.N.H., and Ahern, F.J. (1986). Forestry information content of Thematic Mapper data. *International Journal of Remote Sensing*. 7, 3, 405–428.

Houghton, R.A., Lawrence, K.T., Hackler, J.L., and Brown, S. (2001). The spatial distribution of forest biomass in the Brazilian Amazon: a comparison of estimates. *Global Change Biology*. 7, 731 – 746.

Houghton, R.A., and Goodale, C.L. (2004). Effects of land-use change on the carbon balance of terrestrial ecosystems, In Ecosystems and Land Use Change (DeFries, R.H., Asner, G.P., Houghton, R.A. Eds.). American Geophysical Union, Washington, D.C.

Isaac, L.A. (1949). Better Douglas-fir forests from better seed. University of Washington Press, Seattle, WA.

Janisch, J.E., and Harmon, M.E. (2002). Successional changes in live and dead wood carbon stores: implications for net ecosystem productivity. *Tree Physiology*. 22, 77 – 89.

Jenkins, J.C., Birdsey, R.A., and Pan, Y. (2001). Biomass and NPP estimation for the Mid-Atlantic region (USA) using plot-level forest inventory data. *Ecological Applications*. 11, 4, 1174 – 1193.

Jenkins, J. C., Chojnacky, D.C., Heath, L.S., and Birdsey, R.A. (2003). National-scale biomass estimators for United States tree species. *Forest Science*. 49, 1, 12 – 35.

Keeling, C.D., and Whorf, T.P. (2005). Atmospheric CO_2 concentrations (ppmv) derived from in situ air samples collected at Mauna Loa Observatory, Hawaii. Scripps Institution of Oceanography (SIO), University of California, La Jolla, CA.

Kennedy, R.E., Cohen, W.B., Schroeder, T.A. (in press). Trajectory-based change detection for automated characterization of forest disturbance dynamics. *Remote Sensing of Environment*.

Kimball, J.S., Keyser A.R., Running, S.W., Saatchi, S.S. (2000). Regional assessment of boreal forest productivity using an ecological process model and remote sensing parameter maps. *Tree Physiology*. 20, 761 – 775.

Labrecque, S., Fournier, R.A., Luther, J.E., and Piercey, D. (2006). A comparison of four methods to map biomass from Landsat-TM and inventory data in western Newfoundland. *Forest Ecology and Management*. 226, 129 – 144.

Landsberg, J.J., and Waring, R.H. (1997). A generalized model of forest productivity using simplified concepts of radiation-use efficiency, carbon balance and partitioning. *Forest Ecology and Management*. 172, 199 – 214.

Law, A.M., and Kelton, W.D. (1991). Simulation modeling and analysis. McGraw-Hill, New York.

Lennartz, S. (2005). Oregon forest land change mapping. Pecora 16 – Global Priorities in Land Remote Sensing. October 23 – 27, 2005. Sioux Falls, SD.

Lu, D. (2005). Aboveground biomass estimation using Landsat TM data in the Brazilian Amazon. *International Journal of Remote Sensing*. 26, 12, 2509 – 2525.

Mouer, M., Spies, T.A., Henstrom, M., Martin, J.R., Alegria, J., Browning, J., Cissel, J., Cohen, W.B., Demeo, T., Healey, S., and Warbington, R. (2005). Status and trend of late-successional and old-growth forest under the Northwest Forest Plan. U.S. Forest Service GTR – PNW – 646. Portland, OR.

Ohmann, J.L., and Gregory, M.J. (2002). Predictive mapping of forest composition and structure with direct gradient analysis and nearest-neighbor imputation in coastal Oregon, USA. *Canadian Journal of Forest Research*. 32, 725 – 741.

Richards, F.J. (1959). A flexible growth function for empirical use. *Journal of Experimental Botany*. 10, 290 – 300.

Schroeder, T.A., Cohen, W.B., Song, C., Canty, M.J., and Yang, Z. (2006). Radiometric correction of multi-temporal Landsat data for characterization of early successional forest patterns in western Oregon. *Remote Sensing of Environment*. 103, 16-26.

Schroeder, T.A., Cohen, W.B., and Yang, Z. (in press). Patterns of forest regrowth following clearcutting in western Oregon determined from multi-temporal Landsat data. *Forest Ecology and Management*.

Smithwick, E.H., Harmon, M.E., Remillard, S.M., Acker, S.A., Franklin, S.F. (2002). Potential upper bounds of carbon stores in forests of the Pacific Northwest. *Ecological Applications*. 12, 1303 – 1317.

Solomon, A.M., Prentice, I.C., Leemans, R., Cramer, W.P. (1993). The interaction of climate and land use in future terrestrial carbon storage and release: *Water, Air and Soil Polllution*. 40, 407 – 418.

Song, C., Woodcock, C.E., Seto, K.C., Pax-Lenney, M., and Macomber, S.A. (2001). Classification and change detection using Landsat TM data: when and how to correct atmospheric effects. *Remote Sensing of Environment*. 75, 230–244.

Swenson, J.J., Waring, R.H., Fan, W., Coops, N. (2005). Predicting site-index with a physiologically based growth model across Oregon, USA. *Canadian Journal of Forest Research*. 35, 1697 – 1707.

Swift, M.J., Heal., O.W., and Anderson, J.M. (1979). Decomposition in terrestrial ecosystems. University of California Press. Berkely, CA.

Turner, D.P, Koerper, G.J., Harmon, M.E., Lee, J.J. (1995). A carbon budget for forests of the conterminous United States. *Ecological Applications*. 5, 421 – 436.

Turner, D.P., Ollinger, S.V., and Smith, J.S. (2004). Integrating remote sensing and ecosystem process models for landscape-to regional-scale analysis of the carbon cycle. *Bioscience*. 54, 6, 573 – 584.

Vermote, E.F., Tanre, D., Deuze, J.L., Herman, M, and Morcrette, J.J. (1997). Second simulation of the satellite signal in the solar spectrum, 6S: an overview. *IEEE Transactions on Geoscience and Remote Sensing*. 35, 895–934.

Wallin, D.O., Harmon, M.E., Cohen, W.B., Fiorella, M., Ferrell, W.K. (1996). Use of Remote sensing to model land use effects on carbon flux in forests of the Pacific Northwest, USA, In The Use of Remote Sensing in the Modeling of Forest Productivity at Scales from the Stand to the Globe (Gholz, H.L., Nakane, K., and Shimoda, H., Eds.) Kluwer Academic Publishers, Dordrecht, pp. 219 – 237.

Wallin, D.O., Harmon, M.E., and Cohen, W.B. (in press). Modeling regional-scale carbon dynamics in Pacific Northwest forests: the LANDCARB model, In Carbon Dynamics of Two Forested Regions: Northwestern Russia and the Pacific Northwest (O. Krankina and M.E. Harmon, Eds.). Springer – Verlag, New York.

Waring, R.H., Milner, K.S., Jolly, W.M., Phillips, L., and McWethy, D. (2006). Assessment of site index and forest growth capacity across the Pacific and Inland Northwest U.S.A. with MODIS satellite-derived vegetation index. *Forest Ecology and Management*. 228, 285 – 291.

Yang, Z., Cohen, W.B., and Harmon, M.E. (2005). Modeling early forest succession following clear-cutting in western Oregon. *Canadian Journal of Forest Research*. 35, 1889 – 1900.

FIGURES

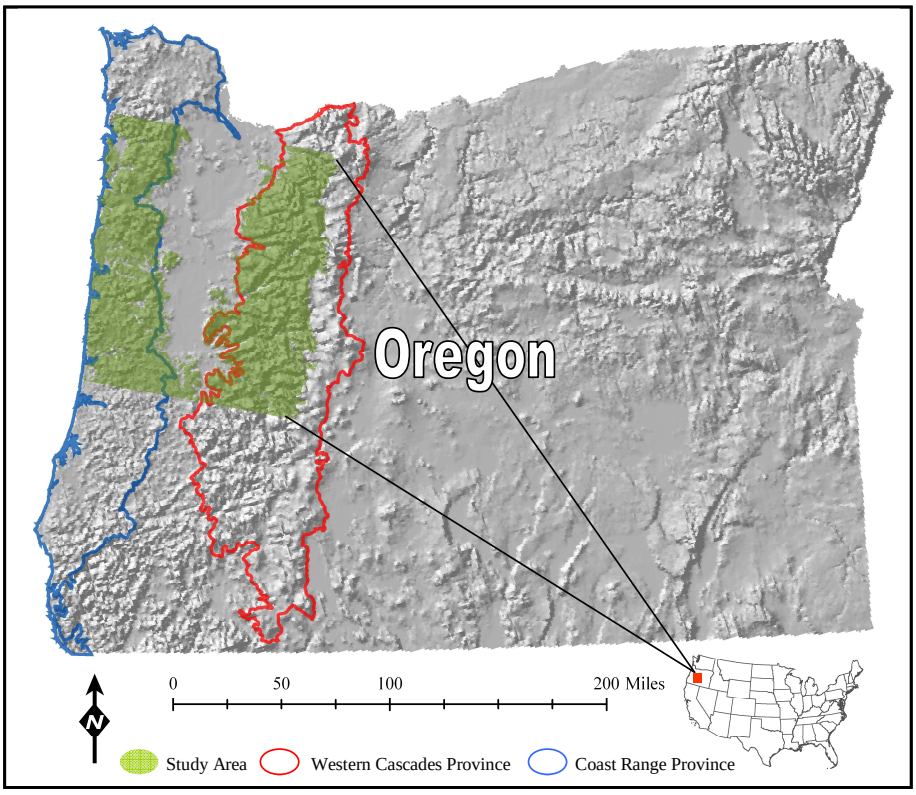

Figure 4-1. The 2,140,557 ha forested study area in western Oregon.

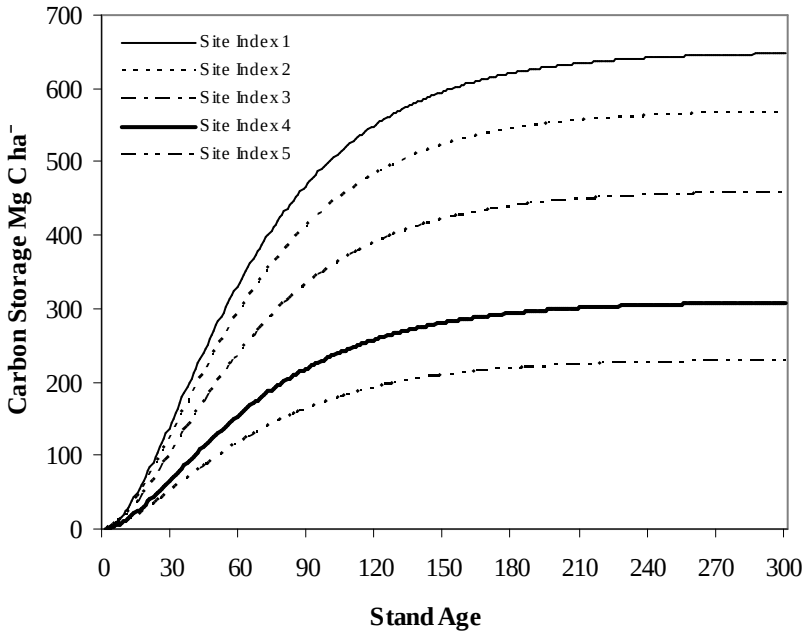

Figure 4-2. Chapman-Richards growth curves used to predict live forest carbon.

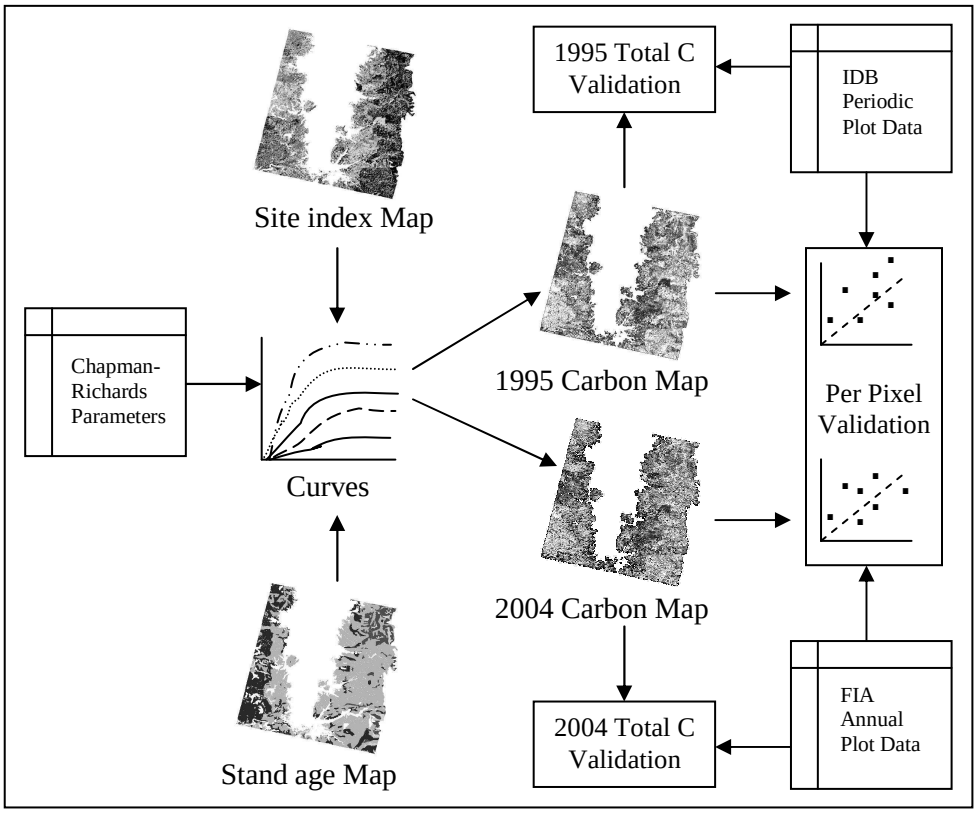

Figure 4-3. The curve-fit carbon modeling and validation process.

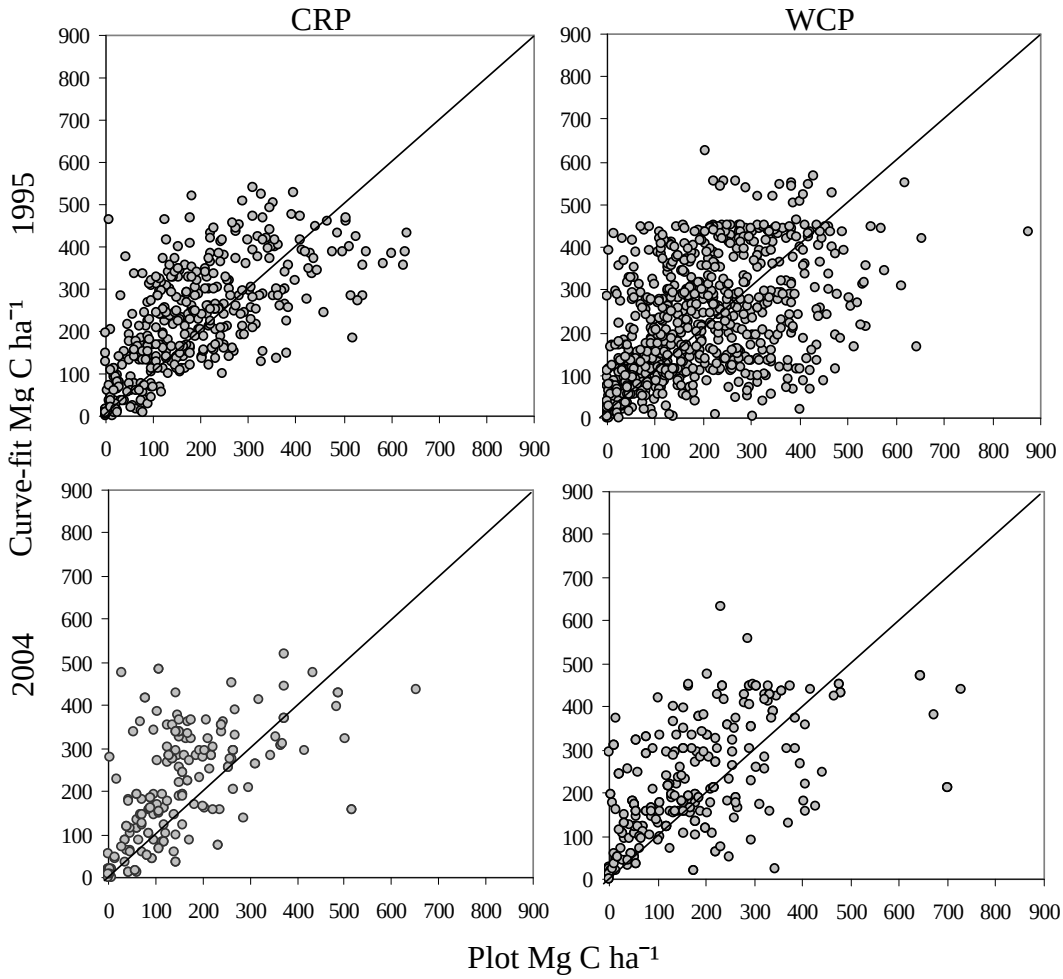

Figure 4-4. Scatter plots of observed (from inventory plots) versus predicted (from curve-fit model) live forest carbon by ecoregion and image date.

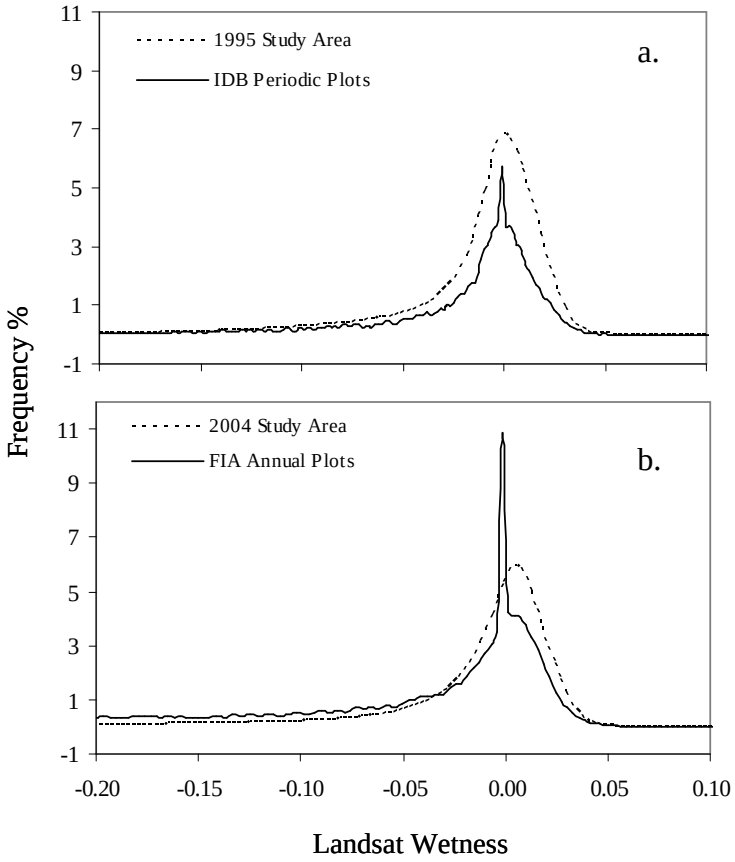

Figure 4-5. Frequency histograms of Landsat wetness for a. 1995 image date and b. 2004 image date. Dashed line is study area wetness, solid line is inventory plot wetness.

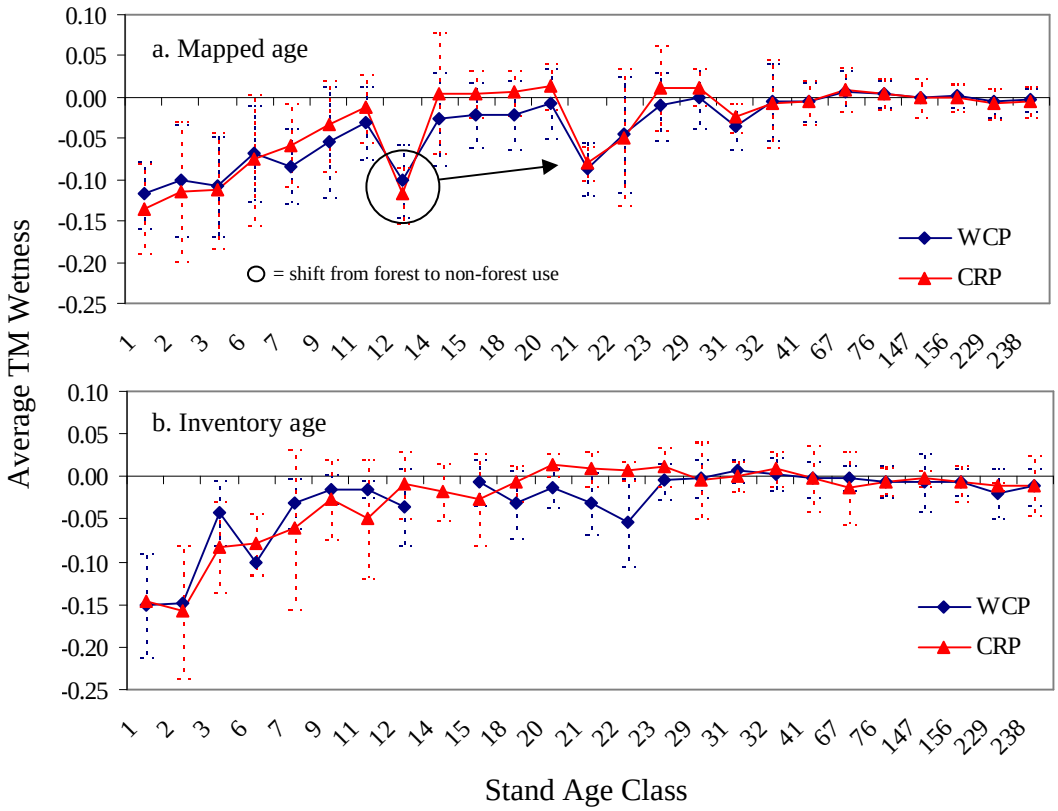

Figure 6. Chronosequences of Landsat wetness according to stand age class from a. stand disturbance maps, b. inventory plots.

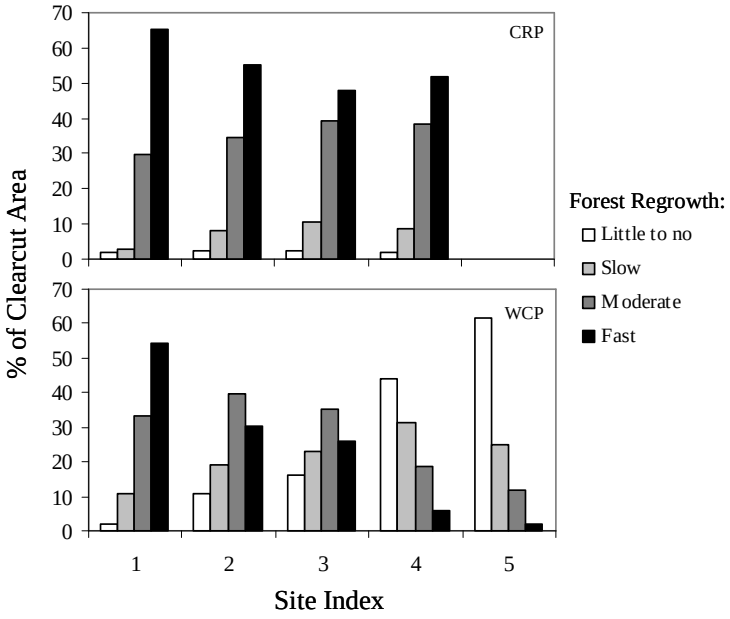

Figure 4-7. Landsat based forest regrowth classes (from Schroeder et al., in press) according to map based site index class (Isaac, 1949). Top graph is for the Coast Range Province (CRP) and bottom graph is for the Western Cascade Province (WCP).

TABLES

Table 4-1. Curve parameters defining Chapman-Richards growth curves from Figure 4-2.

Site index	Live Max (Mg C ha^{-1})	B^1	B^2
1	650	0.02	1.98
2	570	0.02	1.97
3	460	0.02	1.96
4	310	0.02	1.92
5	230	0.02	1.88

Table 4-2. Descriptive statistics and regression diagnostics for pixel level carbon validation.

1995	n	Min*	Max*	Mean*	Stdev*	Bias	RMSE*	VR	r	R^2
CRP	404					41.21	116.03	0.95	0.67	0.45
IDB Plot		0.02	633.71	182.83	136.91					
Landcarb		0.73	541.23	224.04	130.08					
WCP	776					34.28	142.89	1.01	0.50	0.25
IDB Plot		0.01	875.28	190.43	137.90					
Landcarb		1.00	628.15	224.71	139.75					
2004	**n**	**Min***	**Max***	**Mean***	**Stdev***	**Bias**	**RMSE***	**VR**	**r**	**R^2**
CRP	165					52.81	126.87	1.06	0.58	0.33
FIA Plot		0.01	654.09	156.08	121.80					
Landcarb		0.08	518.00	208.88	129.44					
WCP	238					45.75	135.29	0.94	0.57	0.32
FIA Plot		0.03	728.24	179.73	141.22					
Landcarb		1.00	632.54	225.48	132.14					

* units = Mg C ha^{-1}

Table 4-3. Total study area carbon validation statistics.

	n	Total C**	SE**	Absolute**	Relative	Per Year*
Map						
1995 Landcarb	-	435.94	-	31.48	7.22%	-1.63
2004 Landcarb	-	467.42	-			
Plot						
IDB Periodic	1,450	302.18	7.98	22.36	7.40%	-1.16
FIA Annual	432	324.54	15.71			

*units = Mg C ha
**units = Tg C
negative sign denotes C sink

Chapter 5 – Conclusion

The purpose of this research was to integrate forest inventory and multi-temporal satellite data to better understand early successional forest regrowth patterns and carbon storage in western Oregon forests. As many of the data used in this research were collected at different spatial and temporal scales, new and innovative techniques were required to effectively and accurately characterize forest change. Scaling data from large to small spatial scales to answer broad ecological questions often requires a sequential approach which systematically links one scale to the next through common attributes. As such, each chapter presented here builds on the concepts develop in the previous, resulting in significant advancement of our understanding of early successional forest processes in western Oregon forests.

To detect and characterize continuous changes in early forest succession however, optical satellite images must first be transformed to a common radiometric scale to minimize sun, sensor, view-angle and atmospheric differences. In Chapter 2 we presented a comparison of five atmospheric correction methods (2 relative, 3 absolute) used to calibrate a nearly continuous 20-year Landsat TM/ETM+ image data set (19 images) covering western Oregon (path 46 row 29) to like surface reflectance values (Schroeder et al., 2006). We found that an automated ordination algorithm called multivariate alteration detection (MAD) (Canty et al., 2004), which statistically locates invariant pixels between a subject and a series of reference images yielded the most consistent common scale among

all images. Applied in a "absolute-normalization" context, we demonstrated how radiometric calibration with MAD improves (i.e., reduces scatter in) spectral reflectance trajectory models used to characterize patterns of early forest succession. The impact of this research was crucial as thorough radiometric cross-normalization allows for: 1.) accurate characterization of continuous forest change with satellite imagery and 2.) robust integration with ground measured forest inventory data.

Previous studies have established that forest regrowth after disturbance in western Oregon is highly variable both in terms of revegetation rate (Nesje, 1996; Tappeiner et al., 1997; and Yang et al., 2005) and delay (i.e., time to reach 5% canopy cover). While these studies provided convincing evidence that successional variability in western Oregon is real, their use of ground survey (Tappeiner et al., 1997) and airphoto interpretation (Yang et al., 2005) has limited the number of forest stands available to statistically analyze potential causes of the phenomena. In Chapter 3 we overcame these limitations by scaling percent tree cover measurements derived by ground survey and airphoto interpretation to the greater landscape using 19 cross-normalized Landsat images (1984 – 2004). Developing a series of forest regrowth trajectory classes (little to no regrowth, slow regrowth, moderate regrowth and fast regrowth) we observed a wide range of successional regrowth pathways 18 years after clearcut harvesting. These classes showed a higher percentage of fast regrowth in the Coastal Range Province and a much higher percentage of little to no regrowth in the Western Cascade Province. For

both ecological provinces we observed the propensity for faster regrowth on north facing aspects, shallow slopes and at low elevations. In both ecological provinces, elevation followed by potential relative radiation (PRR) (Pierce et al., 2005) explained the largest amount of variation in forest regrowth rates.

As we now had a better understanding of where and why successional variability is occurring on the landscape, the final stage of this research was to ascertain a greater understanding of the uncertainty surrounding spatial predictions of aboveground carbon storage made with optical satellite imagery. In Chapter 4 we utilized two sets of FIA forest inventory data to validate a Landsat based curve fitting model for spatially predicting live forest carbon. We evaluated the performance of the model at the local (pixel level) and landscape (total study area carbon) scales for both the Coast Range and Western Cascade ecological Provinces. At the pixel level we found the curve-fit model performed better (i.e., higher correlation, lower RMSE) in the Coast Range Province than the Western Cascades due to faster, more consistent growth patterns. The model displayed large positive bias statistics indicating a tendency to over-predict carbon in relation to the inventory data. At the landscape scale, the curve-fit model also over-predicted total study area forest carbon for both inventory periods. Although this over-estimation was significant (average of 138.32 Tg per inventory period) in absolute terms, the flux (i.e., difference between inventory periods) estimated by the curve-fit model was found to be well within the standard error of the inventory estimates. To see how well the inventory plots captured the forest conditions

present in the study area we compared frequency histograms and stand age chronosequences of Landsat wetness developed for the full study area and for the inventory plots. The study area and inventory based frequency histograms had the same general shape and magnitude of wetness, however the map based stand age chronosequence detected a subtle shift in land-use which was not captured by the inventory sample. Although optical satellite imagery is limited in its ability to directly estimate forest carbon, we found Landsat's temporal (e.g., age maps) and spectral (e.g., wetness chronosequences) characteristics to be useful inputs to a curve based model which was found to estimate carbon flux from forests within the standard error of inventory estimates.

Taken as a whole, the development of the absolute-normalization approach to image radiometric calibration lead to one of the first continuous characterizations of forest successional change with optical satellite imagery. In addition, our effective cross-normalization procedure has facilitated a new concept of image change detection referred to in this dissertation as "date-invariant" regression. In the process of evaluating an alternative way of using Landsat data to estimate forest carbon we developed a new way to detect subtle land-use shifts (forest to non-forest) from chronosequences of the Landsat wetness index. Overall, the body of work presented here has facilitated a greater understanding of the function and process of western Oregon forests.

Bibliography

Armesto, J.J., and Pickett, S.T.A. (1986). Removal experiments to test mechanisms of plant succession in oldfields. *Vegetatio*. 66, 85–93.

Bechtold, W.A., and Patterson, P.L. (2005). The enhanced forest inventory and Analysis program – National sampling design and estimation procedures. U.S. Forest Service GTR–SRS–80.

Beers, T.W., Press, P.E., and Wensel, L.C. (1966). Aspect transformation in site productivity research. *Journal of Forestry*. 64, 691–692.

Birdsey, R.A., and Schreuder, H.T. (1992). An overview of the forest inventory and analysis estimation procedures in the eastern United States – with an emphasis on the components of change. General Technical Report RM – 214. USDA Forest Service, Rocky Mountain Forest and Range Experiment Station, Fort Collins, CO, USA.

Canty, M.J., Nielsen, A.A., and Schmidt, M. (2004). Automatic radiometric normalization of multitemporal satellite imagery. *Remote Sensing of Environment*. 91, 3–4, 441–451.

Chander, G., and Markham, B. (2003). Revised Landsat-5 TM radiometric calibration procedures and post-calibration dynamic ranges. *IEEE Transactions on Geoscience and Remote Sensing*. 41, 11, 2674–2677.

Chavez, P.S., Jr. (1996). Image-based atmospheric correction – revisited and improved. *Photogrammetric Engineering and Remote Sensing*. 62, 9, 1025–1036.

Cleary, B, Greaves, R., and Hermann, R. (ed). (1978). Regenerating Oregon's Forests: A Guide for the Regeneration Forester. Oregon State University Extension Service. Corvallis, OR. pp. 7–27.

Cohen, W.B., and Spies, T.A. (1992). Estimating structural attributes of Douglas-fir/Western hemlock forest stands from Landsat and SPOT Imagery. *Remote Sensing of Environment*. 41, 1 – 17.

Cohen, W.B., Spies, T.A., and Fiorella, M. (1995). Estimating the age and structure of forests in a multi-ownership landscape of western Oregon, U.S.A. *International Journal of Remote Sensing*. 16, 4, 721–746.

Cohen, W.B., Harmon, M.E., Wallin, D.O., and Fiorella, M. (1996). Two decades of carbon flux from forests of the Pacific Northwest. *BioScience*. 46, 11, 836–844.

Cohen, W.B., M., Fiorella, J. Gray, E. Helmer, and Anderson, K. (1998). An efficient and accurate method for mapping forest clearcuts in the Pacific Northwest using Landsat imagery. *Photogrammetric Engineering and Remote Sensing*. 64, 293–300.

Cohen, W.B., Spies, T.A., Alig, R.J., Oetter, D.R., Maiersperger, T.K., and Fiorella, M. (2002). Characterizing 23 years (1972–95) of stand replacement Disturbance in western Oregon forests with Landsat imagery. *Ecosystems*. 5, 122–137.

Cohen, W.B., Maiersperger, T.K., Gower, S.T., and Turner, D.P. (2003). An improved strategy for regression of biophysical variables and Landsat ETM+ data. *Remote Sensing of Environment*. 84, 561–571.

Cohen, W.B., and Goward, S.N. (2004). Landsat's role in ecological applications of remote sensing. *Bioscience*. 54, 6, 535–545.

Coppin, P., Jonckheere, I., Nackaerts, K., and Muys, B. (2004). Digital change detection methods in ecosystem monitoring: A review. *International Journal of Remote Sensing*. 25, 9, 1565–1596.

Crist, E.P., and Cicone, R.C. (1984). A physically-based transformation of thematic Mapper data–the TM tasseled cap. *IEEE Transactions on Geoscience and Remote Sensing*. 22, 3, 256–263.

Crist, E.P. (1985). A TM tasseled cap equivalent transformation for reflectance factor data. *Remote Sensing of Environment*. 17, 301 – 306.

Curtis, R.O., Clendenen, G.W., Reukema, D.L., and DeMars, D.J. (1982). Yield tables for managed stands of coast Douglas-fir. USDA General Technical Report, GTR-PNW-135, Pacific Northwest Forest and Range Experiment Station, Portland, OR.182 pp.

Daly, C., Neilson, R.P., and Phillips, D.L. (1994). A statistical-topographic model for mapping climatological precipitation over mountainous terrain. *Journal of Applied Meteorology*. 33, 140–158.

DeFries, R., Houghton, R.A., Hansen, M.C., Field, C.B., Skole, D., and Townshend, J. (2002). Carbon emissions from tropical deforestation and regrowth based on satellite observations for the 1980s and 1990s. *Proceedings of the National Academy of Sciences*. 99, 22, 14256–14261.

del Moral, R., and Bliss, L.C. (1993). Mechanisms of primary succession: insights resulting from the eruption of Mount St. Helens, In Advances in Ecological Research (M. Began and A. Fitter, Eds.). Academic, London, Vol. 24, pp. 1–66.

Dong, J., Kaufmann, R.K., Myneni, R.B., Tucker, C.J., Kauppi, P.E., Liski, J., Buermann, W., Alexeyev, V., Hughes, M.K. (2003). Remote sensing estimates of boreal and temperate forest woody biomass: Carbon pools, sources and sinks. *Remote Sensing of Environment*. 84, 393 – 410.

Du, Y., Teillet, P.M., and Cihlar, J. (2002). Radiometric normalization of multitemporal high-resolution satellite images with quality control for land cover change detection. *Remote Sensing of Environment*. 82, 123–134.

Eckhardt, D.W., Verdin, J.P., and Lyford, G.R. (1990). Automated update of an irrigated lands GIS using SPOT HRV imagery. *Photogrammetric Engineering and Remote Sensing*. 56, 11, 1515–1522.

Fiorella, M., and Ripple, W.J. (1993). Analysis of conifer forest regeneration using Landsat Thematic Mapper data. *Photogrammetric Engineering and Remote Sensing*. 59, 9, 1383–1388.

Fiorella, M., and Ripple, W.J. (1993). Determining successional stage of temperate coniferous forests with Landsat satellite data. *Photogrammetric. Engineering and Remote Sensing*. 59, 2, 236–239.

Foody, G.M., Palubinskas, G., Lucas, R.M., Curran, P.J., and Honzak, M. (1996). Identifying terrestrial carbon sinks: Classification of successional stages in regenerating tropical forest from Landsat TM data. *Remote Sensing of Environment*. 55, 205–216.

Franklin, J., and Dyrness, C. (1988). Natural Vegetation of Oregon and Washington. Oregon State University Press, Corvallis, OR.

Franklin, J.F., Spies, T.A., Van Pelt, R.V., Carey, A.B., Thornburgh, D.A., Berg, D.R., Lindenmayer, D.B., Harmon, M.E., Keeton, W.S., Shaw, D.C., Bible, K., and Chen, J. (2002). Disturbances and structural development of natural forest ecosystems with silvicultural implications, using Douglas-fir forests as an example. Forest *Ecology and Management*. 155, 399–423.

Franklin, S.E., Moskal, L.M., Lavigne, M.B., and Pugh, K. (2000). Interpretation and classification of partially harvested forest stands in the Fundy Model forest using multitemporal Landsat TM digital data. *Canadian Journal of Remote Sensing*. 26, 4, 318–333.

Frayer, W.E., and Furnival, G.M. (1999). Forest survey sampling designs: A history. *Journal of Forestry*. 4–9.

Friedl, M.A., and Brodley, C.E. (1997). Decision tree classification of land cover from remotely sensed data. *Remote Sensing of Environment*. 61, 399–409.

Hall, F.G., Botkin, D.B., Strebel, D.E., Woods, K.D., and Goetz, S.J. (1991). Large-scale patterns of forest succession as determined by remote sensing. *Ecology*. 72, 2, 628–640.

Halpern, C.B. (1988). Early successional pathways and the resistance and resilience of forest communities. *Ecology*. 69, 1703–1715.

Halpern, C.B. (1989). Early successional patterns of forest species: interactions Of life history traits and disturbance. *Ecology*. 70, 704–720.

Halpern, C.B., and Franklin, J.F. (1990). Physiognomic development of Pseudotsuga forests in relation to initial structure and disturbance intensity. *Journal of Vegetation Science*. 1, 475–482.

Hardisky, M.A., Klemas, V., and Smart, R.M. (1983). The influence of soil salinity, growth form, and leaf moisture on the spectral radiance of *Spartina alterniflora* canopies. *Photogrammetric Engineering and Remote Sensing*. 49, 77–83.

Harmon, M.E., Franklin, J.F., Swanson, F.J., Sollins, P., Gregory, S.V., Lattin, J.D., Anderson, N.H., Cline, S.P., Aumen, N.G., Sedell, J.R., Lienkaemper, G.W., Cromack, K.W. (1986). Ecology of coarse woody debris in temperate ecosystems. *Recent Advances in Ecological Research*. 15, 133 – 302.

Harmon, M.E., Marks, B., and Hejeebu, R.N. (1995). A users guide to STANDCARB Version 1.0: A model to simulate the carbon stores in forest stands. Pacific Forest Trust. Booneville, CA.

Harmon, M.E. (2001). Carbon sequestration in forests addressing the scale question. *Journal of Forestry*. 99, 4, 24 – 29.

Hayes, D.J., and Sader, S.A. (2001). Comparison of change-detection techniques for monitoring tropical forest clearing and vegetation regrowth in a time series. *Photogrammetric Engineering and Remote Sensing*. 67, 9, 1067–1075.

Hiserote, B. and Waddell, K. (2004). The PNW–FIA Integrated Database User Guide Version 1.4. Forest Inventory and Analysis Program, Pacific Northwest Research Station. Portland, OR.

Healey, S., Zhiqiang, Y., Cohen, W.B., and Pierce, D.J. (2006). Application of two regression-based methods to estimate the effects of partial harvest on forest structure using Landsat Data. Remote Sensing of Environment. 101, 115–126.

Hegler, L. (1968). A method for constructing site-index curves from stem analysis. *Forestry Chronicles*. 21, 11–15.

Heiskanen, J. (2006). Estimating aboveground tree biomass and leaf area index in a mountain birch forest using ASTER satellite data. *International Journal of Remote Sensing*. 27, 6, 1135–1158.

Hese, S., Lucht, W., Schmullius, C., Barnsley, M., Dubayah, R., Knorr, D., Neumann, K., Riedel, T., and Schröter, K. (2005). Global biomass mapping for an improved understanding of the CO_2 balance – the Earth observation mission Carbon-3D. *Remote Sensing of Environment*. 94, 94–104.

Horler, D.N.H., and Ahern, F.J. (1986). Forestry information content of Thematic Mapper data. *International Journal of Remote Sensing*. 7, 3, 405–428.

Hotelling, H. (1936). Relations between two sets of variates. *Biometrika*. XXVIII, 321–377.

Houghton, R.A., Lawrence, K.T., Hackler, J.L., and Brown, S. (2001). The spatial distribution of forest biomass in the Brazilian Amazon: a comparison of estimates. *Global Change Biology*. 7, 731–746.

Houghton, R.A., and Goodale, C.L. (2004). Effects of land-use change on the carbon balance of terrestrial ecosystems, In Ecosystems and Land Use Change (DeFries, R.H., Asner, G.P., Houghton, R.A. Eds.). American Geophysical Union, Washington, D.C.

Isaac, L.A. (1949). Better Douglas-fir forests from better seed. University of Washington Press, Seattle, WA.

Jakubauskas, M.E. (1996). Thematic Mapper characterization of lodgepole pine seral stages in Yellowstone National Park, USA. *Remote Sensing of Environment*. 56, 118–132.

Janisch, J.E., and Harmon, M.E. (2002). Successional changes in live and dead wood carbon stores: implications for net ecosystem productivity. *Tree Physiology*. 22, 77 – 89.

Jenkins, J.C., Birdsey, R.A., and Pan, Y. (2001). Biomass and NPP estimation for the Mid-Atlantic region (USA) using plot-level forest inventory data. *Ecological Applications*. 11, 4, 1174 – 1193.

Jenkins, J. C., Chojnacky, D.C., Heath, L.S., and Birdsey, R.A. (2003). National-scale biomass estimators for United States tree species. *Forest Science*. 49, 1, 12–35.

Jin, S., and Sader, S.A. (2005). Comparison of time series tassesled cap wetness and the normalized difference moisture index in detecting forest disturbances. *Remote Sensing of Environment*. 94, 364–372.

Joyce, S. and Olsson, H. (1999). Long-term forest monitoring with temporal-Spectral trajectories from Landsat TM data. IUFRO Div. 4. Rogow, Poland. http://rogow99.sggw.waw.pl/03_poster_session/08/

Kaufman, Y.J. (1989). The atmospheric effect on remote sensing and its correction. In *Theory and Application of Optical Remote Sensing* (G. Asrar, Ed.), New York, pp. 314ff.

Kaufman, Y.J., Wald, A., Remer, L.A., Gao, B., Li, R., and Flynn, L. (1997). The MODIS 2.1 µm channel – correlation with visible reflectance for use in remote sensing of aerosol. *IEEE Transactions on Geoscience and Remote Sensing*. 35, 1–13.

Keeling, C.D., and Whorf, T.P. (2005). Atmospheric CO_2 concentrations (ppmv) derived from in situ air samples collected at Mauna Loa Observatory, Hawaii. Scripps Institution of Oceanography (SIO), University of California, La Jolla, CA.

Kennedy, R.E., and Cohen, W.B. (2003). Automated designation of tie-points for image-to-image coregistration. *International Journal of Remote Sensing*. 24, 17, 3467–3490.

Kennedy, R.E., Cohen, W.B., Schroeder, T.A. (in press). Trajectory-based change detection for automated characterization of forest disturbance dynamics. *Remote Sensing of Environment*.

Kimball, J.S., Keyser A.R., Running, S.W., Saatchi, S.S. (2000). Regional assessment of boreal forest productivity using an ecological process model and remote sensing parameter maps. *Tree Physiology*. 20, 761 – 775.

Labrecque, S., Fournier, R.A., Luther, J.E., and Piercey, D. (2006). A comparison of four methods to map biomass from Landsat-TM and inventory data in western Newfoundland. *Forest Ecology and Management*. 226, 129–144.

Landis, J.R., and Koch, G.G. (1977). The measurement of observer agreement for categorical data. *Biometrics*. 33, 159–174.

Landsberg, J.J., and Waring, R.H. (1997). A generalized model of forest productivity using simplified concepts of radiation-use efficiency, carbon balance and partitioning. *Forest Ecology and Management*. 172, 199 – 214.

Law, A.M., and Kelton, W.D. (1991). Simulation modeling and analysis. McGraw-Hill, New York.

Lawrence, R.L., and Ripple, W.J. (1999). Calculating change curves for multitemporal satellite imagery: Mount St. Helens 1980-1995. *Remote Sensing of Environment*. 67, 309–319.

Lawrence, R.L., and Ripple, W.J. (2000). Fifteen years of revegetation of Mount St. Helens: A landscape-scale analysis. *Ecology*. 81, 2742–2752.

Lawrence, R.L., and Wright, A. (2001). Rule-based classification systems using Classification and Regression Tree (CART) Analysis. *Photogrammetric* Engineering and Remote Sensing. 67, 10, 1137–1142.

Lennartz, S. (2005). Oregon forest land change mapping. Pecora 16–Global Priorities in Land Remote Sensing. October 23–27, 2005. Sioux Falls, SD.

Liang, S., Fallah-Adl, H., Kalluri, S., JaJa, J., Kaufman, Y.J., and Townshend, J.R.G. (1997). An operational atmospheric correction algorithm for Landsat Thematic Mapper imagery over the land. *Journal of Geophysical Research*. 102, 17, 173–17,186.

Lookingbill, T.R., and Urban, D. L. (2005). Gradient analysis, the next generation: towards more plant-relevant explanatory variables. *Canadian Journal of Forest Research*. 35, 1744–1753.

Lucas, R. M., Honzak, M., DO Amaral, I., Curran, P. J. and Foody, G. M. (2002). Forest regeneration on abandoned clearances in central Amazonia. *International Journal of Remote Sensing*. 23, 5, 965–988.

Lutz, J.A., and Halpern, C.B. (2006). Tree mortality during early forest development: A long-term study of rates, causes and consequences. *Ecological Monographs*. 76, 2, 257–275.

Lu, D. (2005). Aboveground biomass estimation using Landsat TM data in the Brazilian Amazon. *International Journal of Remote Sensing*. 26, 12, 2509 – 2525.

Markham, B.L., and Barker, J.L. (1986). Landsat MSS and TM post-calibration dynamic ranges, exoatmospheric reflectance and at-satellite temperature. EOSAT Landsat Technical Notes. 3–8.

Mausel, P., Wu, Y., Yinghong, L., Moran, E.F., and Brondizio, E.S. (1993). Spectral identification of successional stages following deforestation in the Amazon. *Geocarto International*. 4, 61–71.

Miller, J.D. and Yool, S.R. (2002). Mapping forest post-fire canopy consumption in several overstory types using multi-temporal Landsat TM and ETM data. *Remote Sensing of Environment*. 82, 481–496.

Moran, M.S., Jackson, R.D., Slater, P.N., and Teillet, P.M. (1992). Evaluation of simplified procedures for retrieval of land surface reflectance factors from satellite sensor output. *Remote Sensing of Environment*. 41, 169–184.

Mouer, M., Spies, T.A., Henstrom, M., Martin, J.R., Alegria, J., Browning, J., Cissel, J., Cohen, W.B., Demeo, T., Healey, S., and Warbington, R. (2005). Status and trend of late-successional and old-growth forest under the Northwest Forest Plan. U.S. Forest Service GTR–PNW–646. Portland, OR.

Myster, R.W., and Pickett, S.T.A. (1994). A comparison of rate of succession over 18 years in 10 contrasting old fields. *Ecology*. 75, 387–392.

Nesje, A.M. (1996). Spatial patterns of early forest succession in Lookout Creek basin. M.Sc. thesis. Oregon State University, Corvallis, OR.

Nielsen, A.A., Conradsen, K., and Simpson, J.J. (1998). Multivariate alteration detection (MAD) and MAF post-processing in multispectral, bitemporal image data: New approaches to change detection studies. *Remote Sensing of Environment*. 64, 1–19.

Nilson, T., Olsson, H., Anniste, J., Lukk, T. and Praks, J. (2001). Thinning-caused change in reflectance of ground vegetation in boreal forests. *International Journal of Remote Sensing*. 22, 14, 2763–2776.

O'Connell, K.E.B., Acker, S.A., Bruner, H.J., Halpern, C.B., and Harmon, M.E. (unpublished). Carbon dynamics of Douglas-fir forests with different successional rates after timber harvest.

Ohmann, J.L., and Gregory, M.J. (2002). Predictive mapping of forest composition and structure with direct gradient analysis and nearest neighbor imputation in coastal Oregon, U.S.A. *Canadian Journal of Forest Research*. 32, 725–741.

Olsson, H. (1995). Reflectance calibration of Thematic Mapper data for forest change detection. *International Journal of Remote Sensing*. 16, 1, 81–96.

Peterson, U., and Nilson, T. (1993). Successional reflectance trajectories in northern temperate forests. *International Journal of Remote Sensing*. 14, 3, 609–613.

Pierce, K.B., Lookingbill, T., and Urban, D. (2005). A simple method for estimating potential relative radiation (PRR) for landscape-scale vegetation analysis. *Landscape Ecology*. 20, 137–147.

Richards, F.J. (1959). A flexible growth function for empirical use. *Journal of Experimental Botany*. 10, 290–300.

Rouse, J.W., Haas, R.H., Shell, J.A., and Deering, D.W. (1973). Monitoring vegetation systems in the Great Plains with ERTS-1. In Third Earth Resources Technology Satellite Symposium. Vol. 1, pp. 309–317.

Sabol, D.E., Gillespie, A.R., Adams, J.B., Smith, M.O., and Tucker, C.J. (2002). Structural stage in Pacific Northwest forests estimated using simple mixing models of multispectral images. *Remote Sensing of Environment*. 80, 1–16.

Sader, S.A., Bertrand, M., and Wilson, E.H. (2003). Satellite change detection of forest harvest patterns on an industrial forest landscape. *Forest Science*. 49, 3, 341–353.

Schott, J.R., Salvaggio, C., and Volchok, W.J. (1988). Radiometric scene normalization using pseudoinvariant features. *Remote Sensing of Environment*. 26, 1–16.

Schroeder, T.A., Cohen, W.B., Song, C., Canty, M.J., and Yang, Z. (2006). Radiometric correction of multi-temporal Landsat data for characterization of early successional forest patterns in western Oregon. *Remote Sensing of Environment*. 103, 1, 16–26.

Schroeder, T.A., Cohen, W.B., and Yang, Z. (in press). Patterns of forest regrowth following clearcutting in western Oregon determined from multi-temporal Landsat data. *Forest Ecology and Management*.

Smith, M.O., Ustin, S.L., Adams, J.B., and Gillespie, A.R. (1990). Vegetation in deserts: I. A regional measure of abundance from multispectral images. *Remote Sensing of Environment*. 31, 1–26.

Smithwick, E.H., Harmon, M.E., Remillard, S.M., Acker, S.A., Franklin, S.F. (2002). Potential upper bounds of carbon stores in forests of the Pacific Northwest. *Ecological Applications*. 12, 1303 – 1317.

Solomon, A.M., Prentice, I.C., Leemans, R., Cramer, W.P. (1993). The interaction of climate and land use in future terrestrial carbon storage and release: *Water, Air and Soil Polllution*. 40, 407 – 418.

Song, C., Woodcock, C.E., Seto, K.C., Pax-Lenney, M., and Macomber, S.A. (2001). Classification and change detection using Landsat TM data: when and how to correct atmospheric effects. *Remote Sensing of Environment*. 75, 230–244.

Song, C. and Woodcock, C.E. (2003). Monitoring forest succession with multitemporal Landsat images: Factors of uncertainty. *IEEE Transactions on Geoscience and Remote Sensing*. 41, 11, 2557–2567.

Song, C., Schroeder, T.A., and Cohen, W.B. (2007). Predicting temperate conifer forest successional stage distributions with multi-temporal Landsat Thematic Mapper Imagery. Remote Sensing of Environment. 106, 228–237.

Swenson, J.J., Waring, R.H., Fan, W., Coops, N. (2005). Predicting site-index with a physiologically based growth model across Oregon, USA. *Canadian Journal of Forest Research*. 35, 1697 – 1707.

Swift, M.J., Heal., O.W., and Anderson, J.M. (1979). Decomposition in terrestrial ecosystems. University of California Press. Berkely, CA.

Tappeiner, J.C., Huffman, D., Marshall, D., Spies, T.A., and Bailey, J.D. (1997). Density, ages, and growth rates in old-growth and young-growth forests in coastal Oregon. *Canadian Journal of Forest Research*. 27, 638–648.

Teillet, P.M., and Fedosejevs, G. (1995). On the dark target approach to atmospheric correction of remotely sensed data. *Canadian Journal of Remote Sensing*. 21, 375–381.

Teillet, P.M., Barker, J.L., Markham, B.L., Irish, R.R., Fedosejevs, G., and Storey, J.C. (2001). Radiometric cross-calibration of the Landsat-7 ETM+ and Landsat-5 TM sensors based on tandem data sets. *Remote Sensing of Environment*. 78, 39–54.

Thome, K., Markham, B., Barker, J., Slater, P., and Biggar, S. (1997). Radiometric calibration of Landsat. *Photogrammetric Engineering and Remote Sensing*. 63, 853–858.

Turner, D.P, Koerper, G.J., Harmon, M.E., Lee, J.J. (1995). A carbon budget for forests of the conterminous United States. *Ecological Applications*. 5, 421 – 436.

Turner, D.P., Ollinger, S., Smith, M.L., Krankina, O., and Gregory, M. (2004). Scaling net primary production to a MODIS footprint in support of Earth observing system product validation. *International Journal of Remote Sensing*. 20, 25, 1961–1979.

USDA Forest Service. (1995). Field instructions for the inventory of western Oregon 1995–97, http://www.fs.fed.us/pnw/fia/publications/fieldmanuals.shtml.

van Wagtendonk, J.W., Root, R.R., and Key, C.H. (2004). Comparison of AVIRIS and Landsat ETM+ detection capabilities for burn severity. *Remote Sensing of Environment*. 92, 3, 397–408.

Venables, W.N., and Ripley, B.D. (1997). Modern Applied Statistics with S-plus. Second Edition, Springer-Verlag, New York, NY. 548p.

Vermote, E.F., Tanre, D., Deuze, J.L., Herman, M, and Morcrette, J.J. (1997). Second simulation of the satellite signal in the solar spectrum, 6S: an overview. *IEEE Transactions on Geoscience and Remote Sensing*. 35, 895–934.

Viedma, O., Meliá, J., Segarra, D., and García-Haro, J. (1997). Modeling rates of ecosystem recovery after fires by using Landsat TM data. *Remote Sensing of Environment*. 61, 383–398.

Wallin, D.O., Harmon, M.E., Cohen, W.B., Fiorella, M., Ferrell, W.K. (1996). Use of remote sensing to model land use effects on carbon flux in forests of the Pacific Northwest, USA, In The Use of Remote Sensing in the Modeling of Forest Productivity at Scales from the Stand to the Globe (Gholz, H.L., Nakane, K., and Shimoda, H., Eds.) Kluwer Academic Publishers, Dordrecht, pp. 219–237.

Wallin, D.O., Harmon, M.E., and Cohen, W.B. (in press). Modeling regional-scale carbon dynamics in Pacific Northwest forests: the LANDCARB model, In Carbon Dynamics of Two Forested Regions: Northwestern Russia and the Pacific Northwest (O. Krankina and M.E. Harmon, Eds.). Springer–Verlag, New York.

Waring, R.H., Milner, K.S., Jolly, W.M., Phillips, L., and McWethy, D. (2006). Assessment of site index and forest growth capacity across the Pacific and Inland Northwest U.S.A. with MODIS satellite-derived vegetation index. *Forest Ecology and Management*. 228, 285 – 291.

Yang, Z., Cohen, W.B., and Harmon, M.E. (2005). Modeling early forest succession following clear-cutting in western Oregon. *Canadian Journal of Forest Research*. 35, 1889–1900.